Pacific Marine Environmental Laboratory

Oceanic Internal Waves from Ship, Aircraft, and Spacecraft: A Report on the New York-to-Bermuda Remote Sensing Experiment

U. S. DEPARTMENT OF COMMERCE
NATIONAL OCEANIC AND ATMOSPHERIC ADMINISTRATION
ENVIRONMENTAL RESEARCH LABORATORIES
SEATTLE, WASHINGTON

OCEANIC INTERNAL WAVES FROM SHIP, AIRCRAFT, AND SPACECRAFT:

A REPORT ON THE NEW YORK-TO-BERMUDA REMOTE SENSING EXPERIMENT

John R. Proni
John R. Apel*
H. Michael Byrne*
Ronald L. Sellers
Fred C. Newman

Ocean Remote Sensing Laboratory
Atlantic Oceanographic and Meteorological Laboratories
Environmental Research Laboratories
National Oceanic and Atmospheric Administration
Miami, Florida 33149

*Present address:

Pacific Marine Environmental Laboratory
Environmental Research Laboratories
National Oceanic and Atmospheric Administration
Seattle, Washington 98105

CONTENTS

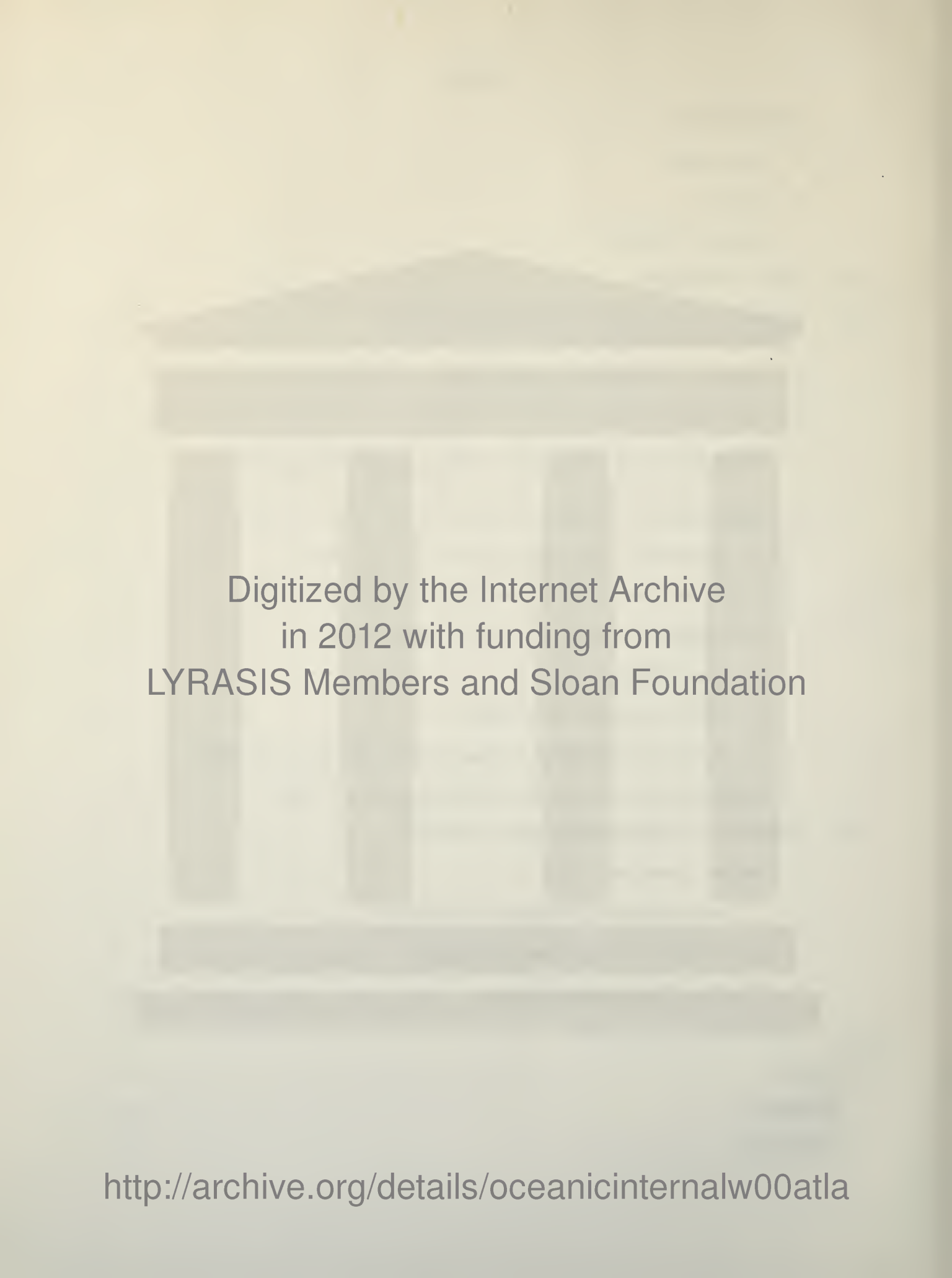

I. INTRODUCTION

A. Background

The Ocean Remote Sensing Laboratory (ORSL) has been studying internal waves using remote sensing techniques employing three different types of observational platforms: ships, aircraft, and spacecraft (Apel et al., 1975a; Proni and Apel, 1975; Apel et al., 1975b). Internal waves and their manifestations have been observed using the following techniques:

(1) Satellite multispectral scanning imagers (principally in the visible and near-infrared);

(2) Radar--both coherent imaging radar and standard meteorological radar (all from aircraft);

(3) Hand-held visible photography (from spacecraft, aircraft, and ship;

(4) Ship-towed thermistors;

(5) STD and XBT casts.

The first internal wave observations made by ORSL were those obtained using Landsat-1 (formerly Erts-1) images. The internal waves manifested themselves through their ocean surface signatures which were detectable using digitally or photographically enhanced images. Apel et al. (1975a, figs. 2 and 3) show very early unenhanced and enhanced Landsat-1 images in the area of the New York continental shelf. The standard Landsat-1 data presentation is not designed for the study of oceanographic effects. It was discovered early on that enhancement of contrast in the intensity range of the ocean image brings out subtle surface features, such as internal-wave signatures (Apel et al., 1976). Apel et al. (1975a and 1976) present a discussion of some enhancement techniques investigated in this laboratory. These two references and the reference to Apel et al. (1975b) are appended to this report. The study of enhancement techniques is continuing at a special image-processing laboratory constructed at the Pacific Marine Environmental Laboratory, NOAA.

Several facts emerged from the early Landsat-1 observations:

(1) The internal waves were being detected as a consequence of their surface signature, which is apparently a modulation of the surface optical reflectivity.

(2) The internal waves occurred in groups or packets. Along the U.S. continental shelf the surface signature of these packets consists of several oscillations with individual wavelength 200-1000 m, the total packet width being 3-5 km.

(3) Along the U.S. continental shelf the packets are separated by distances that are on the order of either 15 or 30 km, which, together with the estimated speed of propagation, suggests either semidiurnal or diurnal origin.

(4) As the group progresses up the continental shelf, there is evidence of a continued lengthening of the waves, especially at the front of the packet.

(5) Of the four spectral bands on Landsat-1, bands 5 (0.6-0.7 μm) and 6 (0.7-0.8 μm) have proven most useful in identifying internal wave signatures.

After these early deductions were made concerning the existence and characteristics of internal waves, it became clear that a "sea-truth" experiment was necessary in order to prove the wave hypothesis. It was, after all, an assumption that the periodic features seen in Landsat-1 images were basically surface slicks associated with an underlying field of internal waves, as described, for example, by Lafond (1962). (Examples of earlier ship and aircraft observations of internal waves are shown by Apel et al., 1975a, fig. 1.) It was decided to undertake a research cruise to verify that indeed an internal-wave field underlay the satellite-observed signatures.

B. Purpose

The New York-to-Bermuda Remote Sensing Experiment (NYBERSEX) had as its prime objective the verification of the internal-wave interpretation of periodic

features observed in Landsat-1 imagery. Specific observational conclusions from the Landsat-1 imagery were drawn regarding internal-wave characteristics. The characteristics to be verified by shipboard observations follow:

(1) The presence of an oceanic internal-wave field underlying a satellite-observed periodic surface signature.

(2) Change in surface-wave structure (e.g., the presence of "slicks") discernable from shipboard occurs with the passage of an internal-wave field.

(3) The accuracy with which internal-wave characteristics were mirrored in the Landsat-1 observations. Characteristics of the internal waves include the following:

(a) Internal waves occur in discreet, well-delineated packets;

(b) Wavelengths present in the packets are on the order of 200-1000 m;

(c) Lateral dimensions of a packet are on the order of 2-4 km in the direction of propagation and on the order of tens of kilometers or more in the direction along the crests (i.e., perpendicular to the direction of propagation and in the plane of the ocean's surface);

(d) Interpacket separation is appropriate for either diurnal or semidiurnal excitation, or both;

(e) Wavelength decreases with distance from the front to the back of the wave packet;

(f) Orientation of constant phase surfaces--i.e., a crest or trough--is roughly parallel to the local isobaths (i.e., topographic orientation).

(4) In addition to these well-defined satellite data verification goals, additional basic research goals were formulated. These included the following:

(a) Determination of the wave amplitude distribution underlying a group of satellite-detected slicks;

(b) Determination of time and location of origin of the wave groups;

(c) Determination of whether high-frequency internal waves exist as packets in the deep ocean and, if so, whether they generate a surface slick signature;

(d) Determination of the basic physical characteristics of the water column, such as the vertical density profile, in order to determine the speeds expected for internal waves. These same data will be used to establish the basic internal-wave mode structure present.

Of course allowance was made for the possibility of unexpected or unanticipated data or events, and the chief scientist was given the freedom to pursue events of significance at his discretion.

C. Method of Attack

The most obvious requirement for verification of satellite data is that a ship be present within the satellite viewing area (or scene) gathering sea-truth data while the satellite records its multispectral scanner data.

The near-polar orbit of Landsat-1 was such that, after completing 14-13/18 orbits every 24 hours, its viewing area shifted 1.42° to the west. This slow westward drift thus allowed a ship to proceed westward synchronously with the spacecraft and be in its field of view once each day. A description of the Landsat-1 orbits and swath widths is given in Section II.

In order to present as many opportunities as possible for the sea-truth ship to be within the satellite viewing area, it was decided that the vessel

should begin at Bermuda and proceed northwestward at such a rate as to remain within each subsequent day's Landsat-1 overpass viewing area.

Because one of the major in-water instruments to be used for mapping the internal-wave field at depth was a high-frequency acoustic echo-sounder, it was decided that a sailing vessel would be useful because of lower noise environment. A calculation indicated that 12- to 15-dB increase in signal-to-noise ratio at 20 kHz could be expected under sail as compared with being underway on engine; this increase subsequently proved to be 22 dB, as the data below show. While a sailing ship is somewhat subject to the vagaries of wind, an auxiliary-powered vessel can circumvent much of those troubles. Therefore, a 30-m auxiliary staysail schooner, the RV Westward, was chartered for a 6-week interval. The Westward appeared capable of meeting a schedule that began with a Landsat-1 overpass of the New York Bight on June 12, 1974, followed by two successive 8-day drifts from Bermuda to New York, each a part of the fundamental 18-day Landsat-1 repeat cycle.

Two different towed devices were used to gather data on the subsurface internal-wave field: a thermistor and an acoustic echo-sounder. These instruments provided two continuous data records of the internal-wave field of quite different characteristics. The single thermistor utilized could, of course provide information only on the temperature at the depth at which it was situated. The acoustic device provided data at different depths (in principle, at any depth at which a sufficient concentration of acoustic reflectors existed) and gave a direct measure of internal-wave amplitude, encounter frequency, and packet length.

Non-towed instrumentation included expendable bathythermographs (XBT's) which recorded the water-column vertical temperature profile, salinity-temperature-depth (STD) records which enabled the construction of water-column density profiles, and water-surface temperatures. Hand-held cameras were also utilized,

including a Hasselblad 70-mm remote-sensing camera, a 16-mm movie camera, and a 35-mm reflex camera.

In addition to Landsat-1 and the Westward, a final platform included was a NASA U-2 which had been scheduled to operate on July 18 and 19, 1974, but because of heavy overcast weather conditions did not fly until July 21. The U-2 provided 70-mm, four-channel Vinton visible and near-infrared photography with filters identical to those on the Landsat-1 multispectral scanner and also five-channel multispectral scanner data from a Nimbus G prototype instrument. The planned objective was for the U-2 to obtain data from similar instruments at aircraft (20,000 m) and satellite (900 km) altitudes simultaneously, and, at the same time, for the Westward to provide in-situ sea truth. This objective was not achieved because of the delay in the overflight mentioned above.

II. CRUISE CHRONOLOGY

The New York-to-Bermuda Remote Sensing Experiment began on June 11, 1974, and terminated on July 21, 1974. The cruise was divided into two legs: Leg 1 with John R. Apel as chief scientist and Leg 2 with John R. Proni as chief scientist. The track of the ship for Leg 1 is shown in figures 1-4. After departing Woods Hole on June 11, the vessel proceeded to the head of the Hudson Canyon and was present in the Landsat-1 viewing area on June 12 and 13. A failure of the main generator precluded gathering any acoustic or thermistor data, however, and forced the return of the Westward to Woods Hole. However, useful XBT and photographic data were obtained, and Landsat yielded imagery showing internal-wave slicks on June 12. On June 13, a strong northeast breeze eradicated surface signs of the waves at both deck height and satellite altitude.

The vessel departed Woods Hole again on June 14 and proceeded to Bermuda, taking an XBT section along 71°W in the process. After a 3-day layover at Bermuda, the Westward departed for New York. Plans called for the vessel to proceed along a northwesterly course at a speed that would maintain the ship within the Landsat-1 viewing area for a series of 8 consecutive days. Figure 2 shows the actual course of the Westward from Bermuda to New York from June 24 through July 1. The circles indicate the location of the ship at the time of the satellite overpass for each day. The series of sloping rectangles shows the satellite viewing area on the day indicated in the lower left-hand corner of each rectangle. The Westward encountered unavoidable delays due to weather and equipment problems that prevented it from keeping the schedule with the Landsat-1 overflights until near the end of Leg 1. The loss of synchronism resulted in ship data that were gathered nearly simultaneously or concurrently with Landsat-1 only on June 30 and July 1; tracks for these two days are shown in figures 3 and 4, respectively.

An important series of shipboard measurements on an internal-wave packet took place during a maneuver executed between 1700 and 1950 UT on June 30. This consisted of three nearly parallel traverses through the same internal-wave packet that yielded data discussed in detail below. The location of these runs is indicated in figure 3. On July 1, 1974, a triangle maneuver and an on-station experiment on a wavepacket took place. The locations of these events are shown in figure 4. Data from these two days proved to be of considerable value in supporting the internal-wave interpretation.

Leg 2 began with the departure of the RV Westward from Floyd Bennett Field on July 4, 1974. The vessel proceeded directly to Bermuda, gathered some acoustic data along the way, and arrived on July 9. Leg 2 was designed to be a repeat of Leg 1, with the Westward again attempting to be within the field of view of Landsat-1. Figure 5 shows the ship's course from Bermuda to New York from July 12 through July 19, 1974. Again, circles indicate the position of the ship at the time of the satellite overpass for each day, and the series of sloping rectangles gives the satellite viewing area on the day indicated in the lower left-hand corner of each rectangle. Note that the ship was within the satellite viewing area on July 17, 18, and 19. Unfortunately, cloud coverage was very high and most of the satellite pictures could not be used.

The data gathered on July 17 have proven to be useful; they provide nearly simultaneous satellite and sea-truth data. The ship tracks for July 17, 18, and 19 are shown in detail in figure 6. A final stretch of data was gathered on July 20 and 21 as the ship went from New York to Woods Hole, and this track is also shown in figure 6. The arrival of the Westward at Woods Hole on July 22, 1974, completed the seagoing phase of NYBERSEX.

III. INTERNAL-WAVE AND GULF STREAM OBSERVATIONS FROM SHIP AND SATELLITE

A. Landsat-1 Images for June 12 and 13, 1974

On June 12, Westward was in the vicinity of the Hudson Canyon during the Landsat-1 overpass (see fig. 1) and observed weakly developed, somewhat incoherent slick patterns; the satellite images for this date are shown in figures 7 and 8 and illustrate the same features. The ship was in the area shown in the Landsat image, figure 8. Little supporting data were obtained from the ship because of the generator failure mentioned earlier; however, the widths and intervals between slicks were timed for a few of the more coherent groups. A histogram for slick widths observed during passage through an internal wave group is given in figure 9. Note that there is a definite upper limit of order 125 m observed for the slicks' widths. Such a limit is expected to exist if these slicks are indeed produced by an underlying internal-wave field. More will be said on this matter in Section IV.

On June 13 no slicks were observed at the time of the Landsat-1 overpass because of the presence of a fresh, 7-8 m/s northeast breeze. The concurrent satellite image is shown in figure 10a and 10b, and the effects of the wind are clearly visible on the photographs. Only a small area south of eastern Long Island, a lee shore, shows any hint of internal-wave slicks.

However, by approximately 2100 UT (1700 EDT) the wind had decreased to near-calm conditions and in 30-45 minutes periodic slicks began to reappear. By sunset, extraordinarily uniform bands were observed as the ship proceeded parallel to the south shore of Long Island on its return to Woods Hole for repairs. This observation, together with the more quantitative data presented below, suggests that internal waves on the shelf can generate a surface signature within two or three periods of oscillation.

B. Ship Data for June 20, 1974

An interesting series of data was gathered approximately 100 nmi from Bermuda at 33°40'N, 65°20'W as the ship was proceeding toward that island at a speed of approximately 3.5 m/s. The acoustic echo-sounder revealed the presence of both short-wavelength and long-wavelength oscillations in the upper layers of the water column. The short-wavelength oscillations appeared to be centered near a depth range of about 20 m. The short oscillations occurred in narrow bursts, with a burst length of about 2000 m and a wavelength typically on the order of 100-200 m. The acoustic record is shown in figure 11a.

At 0530 GMT, a series of oscillations of extremely large amplitude was encountered, as shown in figure 11b. These were the largest internal waves detected on the entire cruise, with a peak-to-trough range of approximately 35 m. Their wavelength was about 500 m, and they were concentrated in an isolated packet whose extent as projected along the ship path was nearly 7 km. Little activity (outside of the short-wavelength oscillations above) was observed either before or after this packet was encountered. Because these data were taken at night, it was not possible to determine if surface slicks accompanied the packet. It may be noted that there is a distinct asymmetry between the widths of the "crests" and of the "troughs." This wave group is discussed at greater length in Section IV, where use is made of certain general features of the wavepackets to expand upon the interpretation here.

C. Observations of the Northwest Wall of the Gulf Stream from Ship and Satellites on June 29 and 30, 1974

Between approximately 0900 and 1100 UT on June 29, RV Westward traversed the Gulf Stream front from southeast to northwest as evidenced by XBT, towed thermistor, and echo-sounder data; the location of the maximum geostrophic tilt was approximately 37°42'N, 69°50'W. Traces from XBT's Nos. 76-79 are

shown in figure 12 (a,b,c,d). These data are plotted as isotherm depth contours along the ship track in figure 13a. The 18°C isotherm at 200 m depth may be taken as the position of the Gulf Stream boundary; it was passed at about 0830 UT.

Figure 13b illustrates the echo-sounder record for a portion of the same time period; the sloping acoustic reflecting layers are quite visible. If it is assumed that the reflectors are biological in origin and tend to accumulate along constant density surfaces at a given time of day, then the slopes of the reflecting layers may be taken to be the same as the slopes of the isopycnal surfaces at the Gulf Stream boundary. Using this interpretation for the interval between 1100 and 1150 UT, the acoustic data yield a cross-stream (normal) slope,

$$\left(\frac{\partial \eta}{\partial n}\right)_{\text{acoustic}} \simeq 9.4 \times 10^{-3} ,$$

where η = depth of an isopycnal and n = normal range. Over the same interval, the 18°C isotherm has a slope,

$$\left(\frac{\partial \eta}{\partial n}\right)_{\text{temp}} \simeq 5.3 \times 10^{-3} .$$

Because the relation of temperature to salinity (thus of temperature to density) changes across the Stream, the slope derived from the acoustic echoes (assumed to come from isopycnal surfaces) is believed to represent a geostrophic tilt more closely than isotherms do. The corresponding speed of the baroclinic current is 150 cm/s at 100 m depth. This is in general accord with historical speeds derived from oceanographic sections across the Stream near this location.

At the Stream edge were many narrow surface slicks having some appearance of periodicity, along with short-wavelength, small-amplitude oscillations in

acoustic reflecting layers. It is not known how internal waves differ from those described above.

Satellite data were not obtained over this portion of the Stream on June 29 because of cloud cover. However, on June 30, 1974, the region to the immediate southwest of the Gulf Stream crossing was imaged by scanners on both Landsat-1 and NOAA-4 satellites. In this region the Stream meander period is of order 40 days and the daily variation in position is roughly 10 km. Therefore, the satellite data on June 30 are thought to be representative of the Gulf Stream position on June 29 to within approximately 10 km. Figure 14 illustrates the Landsat-1 imagery (Image IDs 1707-14541 and 1707-14552) and figure 15, the NOAA-4 infrared image for June 30. It is clear that the thermal boundary of the Stream as observed in the IR image is accompanied by a change in the optical reflectivity that is apparent in the Landsat-1 image. The Stream is warmer and darker than the slope water to the northwest. In the Landsat-1 image there were also narrow, highly reflective filaments oriented parallel to the boundary that could be the surface slicks observed from the ship, but this is only conjecture.

D. Measurements of Oceanic Internal Waves, June 30, 1974

The data presented in this section were gathered on June 30, 1974, as the Westward proceeded shoreward on a course of 332° starting at 39°49'N, 71°21.5'W at 1251 UT (fig. 1). This area is immediately northeast of Hudson Canyon. The data may be conveniently divided into three regions:

Region I, in deep water, seaward of the continental shelf;

Region II, on the shelf rise;

Region III, on the continental shelf.

Region I. In this region the thermistor was towed at a depth varying between 30 and 35 m; the ship's speed was approximately 2.3 m/s; the sea-surface

temperature was 21°C. The temperature at the thermistor (33 m) was approximately 17°C (fig. 16). A definite strong scattering layer is present between 20-25 m depth. At 1315 UT the echo-sounder showed a deepening of the reflecting layer, and at 1320 UT the thermistor recorded an abrupt 2°C increase in temperature at 33 m depth. The crossing of an oceanic front was also marked at 1320 UT. The ship exited from this region at about 1340 UT. For reasons to be elucidated below, this region is denoted as "packet A" and will be treated in a discussion on interpacket separation (Section III.D.3). It is believed that the formation of internal-wave packets begins with the formation of fronts in Regions I and II.

At 1358 UT, a dramatic deepening of an acoustic reflection located at a depth of 35 m occurred (fig. 17). By 1416 UT this layer had descended to a depth of 65 m. The rate of change of depth of the reflecting layer with horizontal range (i.e., dh/dr, where h = reflecting layer depth and r = horizontal distance) was 0.01. An XBT was taken at 1400 UT. This XBT is shown in figure 18 (a surface bucket temperature reading at 1400 UT yielded 21.0°C). There are three features of interest shown in this XBT trace: (1) a relatively well-mixed layer exists to a depth of 20 m; (2) a layer of cold water exists near a depth of 50 m (the temperature at a depth of 48 m is 14.4°C); and (3) a temperature inversion exists at a depth of 60 m (the temperature at 60 m is 17.1°C).

Region II. This region was observed between 1400 UT and 1500 UT (fig. 17). An increase in acoustic reflected energy was observed between 1400 UT and 1500 UT. This was particularly clear in the upper 50 m of the water column; in fact, the entire water column was filled with material capable of causing acoustic reflections. It is not possible to say at this time what the material is; it could, for example, be biological or particulate. Speculation on the nature of the material leads to the suggestion that particulate material is

being stirred (perhaps from the bottom) and placed into the water column; some of this material makes its way up into the upper 50 m of the water column and enhances acoustic reflections at certain scattering layers. There is some question as to how much of the material makes its way into the shallow (i.e., upper 20 m of the water column) mixed layer; there are experimental and theoretical reasons to expect this amount to be relatively small compared to that in the 20-50 m depth range. Admittedly, this interpretation is speculative and requires further experimentation for confirmation; nevertheless, it is consistent with all experimental observations made during NYBERSEX. Note finally the presence of many acoustic reflecting layers throughout the water columns (perhaps made visible by the presence of bottom material). The steepest part of bottom has a slope of .045.

The corresponding temperature record (fig. 17) shows a general decrease in temperature at the depth of the thermistor (30 m). There were several encounters with low temperature ranges, e.g., at 1445 UT and at 1457 UT. An XBT was taken at 1500 UT and is shown in figure 18. Note the dramatic decrease in temperature at 48 m depth (10°C) from the temperature at 1400 UT (14.4°C).

Region III. In this region well-defined internal-wave packets propagating up the shelf were encountered. At 1530 UT, temperature fluctuations with high wave number were registered by the thermistor. The wavelengths of these fluctuations were, very roughly, 150 m and less. At 1535 UT, at a depth of approximately 22 m in the acoustic record of figure 19, a horizontal patch of high acoustic return was observed. There were, as well, rapid oscillations in this patch; patch dimensions are 2250 m in the horizontal and 6 m in the vertical, giving a height-to-width ratio of $6/2250 \simeq .0026$. An XBT was taken at 1630 UT and is shown in figure 18. The two warm temperature spikes shown

between 1520 UT and 1525 UT in figure 19 are thought to be part of a developing internal-wave packet (Sections II.D.3 and IV.A). The large increase in temperature at 1640 UT is mirrored in the acoustic record by a downward dip in the acoustic reflecting layer (fig. 20).

At this point the vessel came upon a well-defined internal wave, denoted by wavepacket B-1, which was proceeding shoreward in the direction of progress of the Westward. A well-defined series of surface slicks was observed, alined roughly along bathymetric contours. The Westward was proceeding very closely parallel to the wave propagation direction. From 1700 UT to 1728 UT, a remarkable temperature and acoustic record of the internal-wave packet was made. As the ship progressed through the packet, larger and larger internal-wave amplitudes were recorded. Also, longer and longer wavelengths were encountered as the ship proceeded through the packet. (From data of July 1, 1974, it will be shown that lower and lower frequencies were encountered as well.)

Peak-to-peak temperature excursions of 7° were registered by the thermistor at the depth of the V-fin (30 m). Peak-to-peak amplitudes of 10 m were registered by the acoustic recorder. By coupling information from the thermistor and from XBT's, it is possible to make an amplitude estimate from temperature information alone. This has been done (Apel et al., 1975a) for part of the present data and will be discussed presently. XBT's taken at 1715 UT and 1728 UT are presented in figure 18.

The cross-correlation function of the acoustic and temperature records for wavepacket B-1 (1700-1728 UT), as transformed to distance, has been computed and is shown in figure 21. Note that the peak correlation of 0.4 is observed near zero lag. There are several factors which prevent the correlation from being higher; two of these factors are as follows: (1) the acoustic reflecting layer and the thermistor were not always at the same depth (This effect will be more evident in data to be presented.); (2) the

acoustic record does not contain the high wave-number detail of the temperature record. (Note: Presently this appears to be a limit imposed by the relatively crude acoustic apparatus and recording devices used and is not an inherent limitation of the acoustic technique.)

The acoustic-temperature cross-spectrum is shown in figure 22. Note the prominent spectral peak at wavelengths of 450 m and 300 m. A peak is also present at very low wave numbers; the significance of this peak is discussed in subsequent paragraphs. However, it is clear that, due to the shortness of the record, such long wavelengths, amounting to one-fourth and one-half the length of the data stretch, are only approximately estimated by spectral analysis. Indeed, none of the spectra presented in this document have more than two degrees of freedom, so that no statistical reliability is realized. These "spectra" are simply Fourier transforms of the data. The wave number periodogram computed from the acoustic record is shown in figure 23. (The record length used runs from 1630 UT to 1728 UT.). The wave number periodogram computed from the corresponding temperature record is shown in figure 24. From the cross-correlation function, one is led to expect corresponding spectral peaks at a wave number of 2.2 cycles/km or a wavelength of roughly 450 km. Such a peak is present in both the temperature and acoustic records. Additional corresponding peaks are present at roughly 300-320 m and at 600-610 m. Less agreement is obtained at smaller wave numbers. As indicated in the previous paragraph, this disparity is believed to be due (at least partially) to the difference in depth between the thermistor and the acoustic reflecting layers.

The ship and wavepacket were traveling in essentially the same direction. The internal waves thus appear to have a longer wavelength than they actually possess. In other words, the Fourier transforms in figures 23 and 24 are

"encounter" spectra which have been Doppler downshifted. To verify this interpretation the ship reversed course, this time proceeding antiparallel to the direction of propagation of the packet, which is now termed wavepacket B-2. This run took place between 1731 and 1805 UT (fig. 25). As can be seen by comparing figures 20 and 25, the corresponding acoustic and temperature traces have many features in common.

Figure 26 shows an excellent correlation of 0.85 near zero lag. The acoustic temperature cross-spectrum for this record is shown in figure 27. Note the appearance of the spectral peak at a wave number of 2.9 cycles/km (i.e., λ = 350 m). The individual temperature and acoustic spectra are shown in figure 28. Here again, these records are "encounter" spectra, being Doppler upshifted. Several spectral peaks are indicated in figure 28; for example, peaks occur at wavelengths of 311-318 m, 435 m, and 710 m.

It is possible to obtain an estimate of the true dominant wavelength of the internal-wave packet under consideration. By "true wavelength" is meant the non-Doppler-shifted wavelength. It is easy to show (assuming no mean currents) that

$$\lambda_T = 2 \frac{\lambda_+ \lambda_-}{\lambda_+ + \lambda_-} ,$$

where λ_T = the non-Doppler-shifted wavelength,

λ_+ = the up-Doppler-shifted wavelength,

λ_- = the down-Doppler-shifted wavelength.

λ_+ and λ_- are taken from the peak of the respective acoustic temperature cross-Fourier transform. From figure 22, λ_+ = 450 m and from figure 27, λ_- = 350 m; hence, $\lambda_T \simeq$ 400 m.

Commencing at 1800 UT (fig. 29) the ship began a turn which placed its direction of travel parallel to the propagation direction of the packet. The ship had completed its turn by 1810 UT. From 1810 UT to 1845 UT, the ship

once again passed through the packet, now termed wavepacket B-3. The acoustic temperature cross-correlation function for this pass is shown in figure 30. Note that a peak correlation greater than 0.5 is obtained near zero lag. The cross-spectrum for this pass is shown in figure 22 together with the cross-spectrum for the first pass. Transforms for the acoustic and temperature data for this packet are shown in figures 31a and 31b, respectively.

From 1840 UT to 1950 UT the RV Westward held station and executed two STD casts. The data from these casts are discussed in the following paragraphs.

Two additional segments of simultaneous acoustic and temperature data are shown in figures 32 and 33. An internal-wave packet (from 2155 UT to 2207 UT) is shown in figure 33. In addition, two large zones of warm water, 2215 UT to 2235 UT and 2245 UT to 2300 UT, are shown. Data-taking ceased at 2300 UT.

1. Expendable Bathythermograph and STD Records

The XBT records gathered on June 30, 1974, are shown in figure 18. One of the most noticeable features in this sequence of XBT's is the sharp decrease in temperature at 50 m depth, occurring at the edge of the continental shelf. On the continental shelf there is a temperature minimum (at about 50 m) with a warming as the bottom is approached.

Figure 34 portrays a typical density profile (which has been smoothed) observed on the continental shelf during NYBERSEX. Also portrayed in figure 34 is the corresponding Brunt Väisälä profile. The corresponding mode structure is shown in figure 35. The dispersion curves for the first five modes are shown in figure 36. Finally, the phase and group speeds for the first five modes are shown in figure 37.

2. Interpacket Separations (Data of June 30, 1974)

From the data shown in figures 16 through 33 for June 30, 1974, it is possible to construct a table of interpacket separations. The leading edge of the first packet for that day, packet A, appears at 1345 UT. This packet is not well-formed. In the analysis section it will be argued that the packet shown in figure 16 is in the first stage of development. The second packet (B-1, B-2, and B-3), makes its appearance with its leading edge encountered at about 1730 UT. This packet is well-formed and will be discussed at some length in the analysis section. The next possible packet occurs at about 2020 UT. This packet (if indeed it is a packet) is weakly developed as an oscillatory structure and is not considered to be an internal-wave group. The next well-formed packet occurs at about 2213 UT and is denoted by packet C.

From these three packets table 1 may be constructed. The column entitled "Corrected Interpacket Separation" is computed using the following rationale. The corrected interpacket separations are the distances between packets A, B, and C from figure 3 as corrected for propagation during the ship transit. A wavepacket propagation speed of 0.5 m/s was assumed in order to derive the corrected separations (cf. fig. 37). Corrected separations between A-B and B-C are 25.8 and 25.5 km, respectively, and are to be compared with an expected separation of 22.4 km, assuming semidiurnal generation. An assumed propagation speed of 0.56 m/s would further bring these numbers into excellent coincidence: 25.0 and 24.5 km compared with a semidiurnal separation of 25.0 km. Thus the assumed propagation speed need only be in error by 10% in order to reconcile the results--an amount that nonlinear effects can easily introduce. Therefore it is clear that the internal-wave packets appear on a semidiurnal and not a diurnal basis.

Table 1. Interpacket separations constructed from data of June 30, 1974.

Packet No.	Time of Encounter (UT)	Time Difference (min)	Apparent Interpacket Separation (km)	Corrected Interpacket Separation (assumed group speed 0.5 m/s)
A	1340			
		220	32.4	25.8
B	1725			
		290	34.2	25.5
C	2210			

Predicted interpacket separation, assuming semidiurnal generation and group speed of 0.5 m/s: 22.4 km.

E. Measurements of Oceanic Internal Waves on July 1, 1974

There are three prime events registered in the data gathered on July 1, 1974. These are the following:

1. The triangle maneuver;
2. The on-station maneuver;
3. The slick-acoustic measurement.

The triangle maneuver is shown in figure 4. The northwest corner of the triangle is located at 39°51'N, 72°38'W. This maneuver is defined to commence at 1525 UT, with a course heading of 115°T.

Data were gathered, however, prior to the commencement of the triangle. Two important sections of the pre-triangle data are shown in figures 38 and 39. In section 1 of the data (fig. 38), temperature fluctuations can be observed. The possible existence of a poorly formed internal-wave packet is shown between 1320 UT and 1350 UT in that figure. Section 2 (fig. 39) contains data obtained between 1430 UT and 1520 UT. This section of data was obtained while running a course antiparallel to the course run during Leg 1 of the triangle. Two clear temperature spikes are observed in these data; one at 1448 UT and one at 1457 UT. These spikes may be part of a poorly developed internal-wave packet. In the discussion of the data gathered during Leg 1 of the triangle, it will be pointed out that these same features may possibly have been observed again later.

1. The Triangle Maneuver

The data gathered in the triangle maneuver established the following facts:

(a) The direction of alinement of the crests and troughs of the underlying internal wave is the same as the alinement of surface slicks.

(b) The underlying high-frequency internal-wave field is clearly anisotropic, with dominant wave energy propagating in a direction normal to the crests and troughs as indicated from surface slicks.

(c) Characteristic features of the underlying internal wavepacket (e.g., a down-going sharp onset and wave amplitude) are approximately preserved over the horizontal (i.e., along a slick) direction. This observation carries the implication that high horizontal (i.e., along slicks) coherencies may be expected.

(d) The large-amplitude features, generally (but not always) found predominantly toward the leading edge of an internal wavepacket appear to retain their general characteristics as a function of horizontal separation "better" than smaller amplitude, high-frequency oscillations toward the rear of the packet.

Leg 1

Leg 1 of the triangle maneuver is shown in figure 4 and was defined to run from 1525 UT to 1602 UT. The data from Leg 1 (labeled section 3) is shown in figure 40. Note the large temperature spike beginning at 1538 UT with maximum at 1539 UT. Several spikes follow in the temperature record, and there is a gradual warming trend at the thermistor depth. The time 1539 UT was interpreted by the authors as being the time of onset of an internal wavepacket propagating up the continental shelf. A surface slick was in evidence at or near this time. This particular wavepacket does not appear to be well-developed, as can be seen by comparing this packet with the packet data obtained on June 30, 1974.

It is possible that the wavepacket observed in Leg 1 (commencing at 1539 UT) is the same wavepacket (fig. 38) observed before the triangle maneuvers and discussed in the preceding paragraphs. In particular, the temperature spike at 1539 UT in Leg 1 corresponds to the temperature spike occurring at

1457 UT. In Leg 1 the ship was proceeding against the general direction of propagation of the packet; in the pretriangle maneuver, the ship was proceeding in the general direction of propagation of the packet. There appears to be substantially more "oscillatory" structure to the packet in the second (parallel) pass through.

Periodograms and acoustic temperature cross-correlation functions have been computed for Leg 1. These are shown in figure 41. These plots indicate a dominant wavelength of about 350 m. A peak correlation of about 0.7 is observed near zero lag.

Leg 2

Leg 2 of the triangle is shown in figure 42 and is defined to run from 1602 UT to 1629 UT. The course heading was 25°T, i.e., generally up the continental shelf. A clearly defined wavepacket is evident in the data, and the packet extends from the beginning of Leg 2 to 1620 UT. Additional oscillations are visible commencing at 1627 UT; however, the authors do not believe that these oscillations are part of the first wavepacket which terminated at 1620 UT. The packet in this leg was very similar in form to those observed on June 30, 1974. It is believed that the wavepackets observed in the pretriangle maneuvers of Leg 1 and in Leg 2 are probably one and the same. In Leg 2, the packet was overtaken by the ship. The spatial extent and orientation of the wavepacket as deduced from these observations are shown in figure 43. Periodograms and the acoustic temperature cross-correlation for these data have been calculated and are shown in figure 44.

As was pointed out in the preceding paragraph, the wavepacket seen in Leg 2 is relatively "well-formed," using the data of June 30 as a yardstick. The question may now be asked: Why is the wavepacket in Leg 2 so "well-formed"

compared to the pre-triangle packet and the packet in Leg 1? (By "well-formed" is meant the persistence of several clearly defined oscillations beyond the first one or two temperature spikes.)

There are some theoretical arguments that bear upon this question; they will be discussed in the analysis section. It can logically be argued that since the data in Leg 1 and the pre-triangle packet data are separated by a minimum of 41 minutes (1538 UT-1457 UT), the packet in Leg 1 represents the time-evolved form of the pre-triangle packet. However, it is difficult for this argument to account for the difference in packet form from Leg 1 to Leg 2. The difference in packet form would surely imply a rapid change. This is particularly true for the form of the latter half of the packet, since the ship did not get "out" of the packet in going from Leg 1 to Leg 2.

There is an alternative explanation, however, for the difference in packet form observed between Leg 1 and Leg 2. It may be hypothesized that the ship's track in Leg 1 (as shown in fig. 1) just barely encountered an "edge" of the wavepacket. That is, it may be that the lateral extent (i.e., at right angles to the wavepacket's direction of propagation) of the latter part of the wavepacket is not as large as the lateral extent of the leading portion of the packet. This is, of course, consistent with satellite observations. In Leg 2, the ship passed more nearly in the "center" of the wavepacket. As is discussed in the analysis section, there are theoretical reasons to expect the oscillations in the latter portion of the wavepacket to be weak (or small) compared to those in the leading edge. There are also reasons to expect that the spatial coherency of these oscillations would be small compared to the lead portion of the wavepacket. Such a lack of spatial coherency would lead to dissimilar waveforms (apparently, at least, for the distances involved in Leg 1 and Leg 2).

Leg 3

Leg 3 is defined as extending from 1630 UT to 1715 UT. The ship's course while executing Leg 3 was 250°T. The temperature and acoustic records for this leg are shown in figure 45. Groups of fluctuations (which may be wavepackets) occur from about 1627 UT to 1640 UT and from about 1647 UT to 1710 UT. The fluctuations occurring from 1647 UT to 1710 UT are possibly associated with the wavepacket observed on the earlier legs.

If one assumes that the signal occurring at 1647 UT is the leading edge of the wavepacket observed on Leg 2 and shown in figure 42, then one can estimate the wavepacket propagation speed. On the basis of the information gathered in Legs 1 and 2, one can determine the orientation of the wavepacket propagation sector to within $\pm$ 11°. By adding the data from Leg 3, assuming that the signal occurring at 1647 UT does indeed originate with the leading edge of the wavepacket, one can estimate the wavepacket's direction of propagation even more closely. This leads to a northerly direction of propagation (shown in fig. 43) and a wavepacket travel speed of about 0.6 m/s. This speed of travel, if assumed to be a speed of propagation (in still water), is higher than expected from the computations of phase and group velocity shown in figure 37. However, a very slight current of roughly 0.05 m/s in the general direction of wavepacket propagation may be present (see the on-station discussion), and such a current could reduce the required propagation speed to a compatible value of about 0.55 m/s. A sequence of photos was made of the ocean's surface from shipboard. Figure 46 shows slicks associated with the wavepacket of the triangle maneuver. Visual and photographic observations showed the surface slicks to be propagating in a northerly direction, in confirmation of results of analysis of acoustic and temperature data.

2. The On-Station Measurement

The on-station measurement is defined to occur from 1733 UT to 2030 UT (figs. 45-48). The Westward's location at the start of the on-station experiment was 39°49.8'N, 72°29.0'W. Some interesting features appear in the acoustic and temperature records prior to 1733 UT, however. Note from figure 45 that a white band of little or no acoustic return begins at 1714 UT. Just prior to 1733 UT, large excursions in both the acoustic and temperature records can be observed, particularly the excursion at 1731 UT. These excursions are believed to be associated with the onset of a wavepacket whose time history is shown in figures 47 and 48.

This wavepacket made its way past the Westward and occupied essentially all the on-station acoustic record. The V-fin, having dropped to a depth of 45 m upon the ship's taking station, was readjusted to be at a depth of approximately 28 m. This caused the thermistor data to portray only an incomplete record of the temperature oscillations. Figure 45 shows a second large downward excursion of the acoustic record occurring at about 1735 UT. Note the flattened crests and sharp troughs. In this leading portion of a wavepacket the width of the trough was at most 3 minutes, while the crest width was roughly 7 minutes. The amplitude of the second downgoing oscillation was 20 m, fully one-third of the total depth. This is clearly a highly nonlinear condition. As time passed, wave amplitude diminished. The change of frequency with time (the observance of which was one of the prime goals of NYBERSEX) is demonstrated nicely by the spectra in figures 49 and 50. Note particularly the acoustic periodogram (fig. 49, upper left) for the earlier time interval. The peak at 3 cycles/hr is twice the size of the peak at 4.5 cycles/hr. In the equivalent periodogram for the later data interval, the peak at higher frequency (5 cycles/hr) is about twice as high as the peak

at 3 cycles/hr. Energy clearly shifts from lower to higher frequencies from front to rear in the wavepacket. This substantiates satellite observations that show wavelength increasing with progression inward from the front of a wavepacket. The overall spectral energy is less in the later than in the earlier interval, indicating diminishing wave amplitudes with time.

The presence of a steady current does not affect the conclusion reached above, i.e., the frequency of the waves in the wavepacket increases with distance from the front edge of the packet. The relative amount of energy at the two frequencies will remain the same in the presence of a steady current. What can change, however, is the absolute value of the frequency measured. This is a well-recognized problem in the measurement of internal-wave spectra (Garrett and Munk, 1972). Indeed, another facet of this basic problem is the distinction of internal waves from relatively stable structures being advected by the current field. In order to rule out the effects of currents, one must know what currents are present; i.e., some current measurements are required. In NYBERSEX, no current measurements were made because of financial and logistical problems.

Some information on currents may be obtained, however, from a study of the ship's drift during the on-station maneuver. The times of several fixes obtained on-station are given in figure 4. The error in any given fix is about 0.8 km. From one fix to the next, position changes at a rate that is nearly constant both in magnitude and direction. A straight line fit to the positions leads to a drift speed of 0.11 m/s in a direction 60° west of north (300°T).

3. Correlation Between Surface Slicks and Internal Waves

We now turn our attention to the question of the location on an internal-wave cycle of a surface slick. Indeed, one of the central questions in our

investigations is how to define the process or processes by which an internal-wave field manifests itself on the ocean's surface. The answer to this question proved to be very difficult to obtain in the field. Slick regions devoid of short capillary waves were indeed observed, but when viewed from a ship at close range became very difficult to identify.

From the data gathered on July 17, 1974, presented in the following section of this article, it is clear that a ruffled region may also simultaneously be associated with internal waves. This possibility is discussed in the following section. From shipboard, no definite evidence on ruffled regions was obtained, even visually. However, cat's-paw-like structures were seen on occasion and did appear to be affected by the presence of internal waves.

One attempt to correlate visual sightings of slick regions with acoustic and temperature recordings of internal waves was made on July 1, from 2050 UT to 2125 UT. The acoustic and temperature data from this period are shown in figure 51. Also visible in this figure are light vertical lines in the acoustic record. These lines denote positions at which slicks were encountered by the ship. Start slick and end slick positions are marked by these lines. (Additional lines marking times are also present.)

A table has been constructed relating acoustic and temperature internal-wave records with visual shipboard slick observations for the data gathered between 2050 UT and 2125 UT. A slick width interval (as determined by the time spread between the start slick and end slick positions) was observed to encompass a trough or a crest. The results of these observations are presented in table 2.

As can be seen from table 2, the observed surface slicks are associated with troughs rather than crests. To be more precise, the observed slicks appear to be more closely associated with that portion of an internal-wave

which is rising from a trough. In other words, the surface slicks appear to be "surfing" on the internal waves. However, it must be borne in mind that this result is extremely tentative and is based on a very small data base. More fieldwork is clearly needed.

Table 2. Visual slicks and acoustic and thermal waves.

Slick No.	No. of Crests	No. of Troughs
1	1	2
2	0	1
3	0	1
4	0	1

F. Oceanic Internal-Wave Observations, July 17, 1974

July 17, 1974, provided one of the few clear days for satellite imagery during NYBERSEX. A portion of the data has already been published (Apel et al., 1975b). We begin our discussion with figure 52 which is a standard Landsat-1 image (134 km × 184 km) which has been photographically enhanced. Figure 53 is a line drawing presenting several features of interest in this image. Notice the large internal-wave field marked A in figure 53. These waves are judged to be shoreward propagating waves according to two simple tests: (1) the wave-front curvature, and (2) the arrangement of the internal-wave wavelengths within the packet (i.e., the longest waves are at the front of the packet).

This group of internal waves (marked A in fig. 53) clearly illustrates the presence of successive zones of intense reflectivity-low reflectivity-background reflectivity associated with the internal waves. This phenomenon was mentioned briefly earlier in this report. Figure 52 is a positive print

so that the order of intensities is indeed background-high-low-background. Such a sequence is apparently associated with each wavelength within packet A. The zone of intense reflectivity suggests "ruffled" water while the zone of low reflectivity suggests "calm" water. To be more precise, the zone of intense reflectivity suggests the existence of diffuse reflection occurring from short wavelength (e.g., capillary range) surface waves. The zone of low reflectivity indicates the absence of such waves. Zones of low reflectivity are expected to correspond to the "slick" lines previously discussed in this article.

Now notice the group of internal waves marked B in figure 53. Using the two simple criteria mentioned earlier in this section (i.e., curvature and wavelength arrangement), this group of waves is judged to be propagating away from the shore. Whether these waves are generated by reflection of incoming wave groups, by topographical interaction of outgoing tides, or by other means is not presently known. A striking feature of internal-wave group B is that the strong intensity variation background-high-low-background apparent in wave group A is lacking. Such an arrangement of reflectivities may be present, but if so it is far less discernible, particularly the high reflectivity portion.

This particular Landsat-1 scene (fig. 52) contained such interesting features that the scenes were reprocessed using the Image Analysis Laboratory facilities developed at Atlantic Oceanographic and Meteorological Laboratories (AOML), partially under ARPA sponsorship. This process (basically contrast stretching) resulted in the series of excellent images portrayed in figure 54. Note the clarity with which wave groups A and B (figs 52 and 53) are illustrated. Note the appearance of additional outgoing and ingoing wave groups north of these groups. Figure 54, in fact, contains outgoing and ingoing

wave groups that are passing through each other. The fact that the ingoing and outgoing wave groups appear at essentially the same position suggests that the different reflectivity effect noted earlier does not arise because of sun angle illumination effects.

It is interesting to note that the integrity of the internal-wave surface signature is preserved through the internal-wave interaction. Such an integrity-preserving interaction (i.e., elastic scattering) may even be expected if the leading internal waves are solitons. Such expectations are not readily obvious for the corresponding surface signatures, however (even though such expectations may nevertheless be fulfilled).

Other features of interest are sand waves, visible in the Nantucket Shoal area, and a pattern of extremely long wavelength (~ 2 km) surface waves, visible on the original computer-enhanced images.

IV. ANALYSIS OF INTERNAL-WAVE CHARACTERISTICS

A. Packet Characteristics

1. Amplitude and Wavelength Variations

An internal-wave packet on the New York continental shelf is a dynamic entity. This may be clearly noted by comparing figures 20 and 29, which portray the same internal-wave packet. All wave packets observed from the RV Westward during NYBERSEX have begun with a sharp down-going oscillation. In addition, a general deepening of isopycnals and isotherms occurs with the onset of a wavepacket.

Prior to the undertaking of NYBERSEX, Landsat-1 (formerly ERTS) data indicated (Apel et al., 1975a) that the longest wavelengths within a given internal-wave packet were at the front of the packet. The wavelength gradually decreased with increasing distance from the front of the wavepacket. It was not clear from the satellite imagery whether it was also true that the largest wave amplitudes were at the front of a wavepacket. It was, however, anticipated that the wavelength arrangement could be understood by a combination of nonlinear and dispersive effects.

First, a clarification of the word "wavelength" is required. The authors of this report believe that nonlinear effects are present, at least in the leading portion of a wavepacket. As is discussed in the following section, it is possible that the first few leading isotherm or isopycnal down-going excursions may be associated with solitary waves or solitons. In such a case, the term "inter-slick distance" is perhaps better than wavelength. In the linear case, inter-slick distance and wavelength coincide. Some degree of judgment must be exercised in determining both the onset of a wavepacket and wavepacket amplitudes. Consider the first wavepacket to be discussed--the wavepacket in figure 20. The leading perturbation occurring at 1725 UT is

somewhat separated in space (by about 1 km) from the rest of the packet. However, this leading perturbation has been included as being part of a wavepacket. The wavepacket, in addition to being made up of short-wavelength (or short-period) internal waves is characterized by a sudden deepening of isotherms or isopycnals. This depression gradually decreases as the packet passes. The authors have measured all amplitudes from the peak of a disturbance to an estimated minimum lying at the depth of overall depression. In figure 55 are plotted the experimental data of inter-slick separation versus time (measured from the leading oscillation in the wavepacket). Note the general tendency toward shorter wavelengths (i.e., shorter encounter periods or wavelengths) as one proceeds farther into any given packet. This confirms the satellite observations mentioned earlier. The decrease is by no means monotonic, but a general decreasing trend is present.

A second set of data is presented in figure 56. This figure presents a graph of wave amplitude versus distance (or time) into the wavepacket. As in figure 55, the initial oscillation is taken as the time origin. No estimate of this amplitude distribution was made from satellite data prior to NYBERSEX. As a general rule, larger amplitudes occur near the leading edge. Note that the largest-amplitude perturbation does not lead in any of the three cases shown in figure 56.

2. A Model of Amplitude Variations

The authors of this article have used various acoustic and satellite observations to generate a model for an internal-wave packet. A schematic diagram that summarizes the salient characteristics is shown in figure 57. This figure defines several quantities used in an empirical mathematical model for the amplitude of the packet, equation (1):

$$N(r) = N_o(R_c(x,y))\ W(z)\ \frac{x}{\ell_1}\ e^{-x/\ell_2}\ . \qquad (1)$$

$$\{\sin\ [K_o(1 + \frac{x}{\ell_3})\ x - \frac{\pi}{2}]\}$$

Here, $N_o(R_c(x,y))$ describes the peak amplitude and the curvature, R_c, of the front of the packet; $W(z)$ is the solution to the linear eigenvalue problem for the density profile existing.

Three scale lengths are defined: ℓ_1 is the rise-length of the first perturbation of a wavepacket; ℓ_2 is the overall length of a packet; and ℓ_3 is the distance over which the wavelength shortens by a factor of 2. Typical values for these lengths from NYBERSEX (on the New York continental shelf) are: for ℓ_1, 100 m; for ℓ_2, 3-5 km; and, for ℓ_3, 2-3 km.

It is possible to consider the definition of an additional scale length, ℓ_4, which is the crest-length (as measured along the crest). This additional possible length is made possible because of the large surface area coverage of a satellite image. However, such a length depends heavily on the distance of the crest from the point of origin (roughly circular spreading) and other factors, such as water-mass boundaries, topography, etc. From satellite data, it is clear that crest-length dimensions can be tens of kilometers.

B. Front or Surge Interpretation

The tidal origin of internal-wave packets is shown by data acquired and displayed within this article, in particular, the acoustic-temperature data of June 30, 1974, and the satellite data of July 17, 1974. The question now is: Through what mechanism does the tide convert a portion of its energy to internal waves? Unfortunately, no current data were gathered during NYBERSEX due to financial and equipment constraints. This lack of data prohibits the authors from stating whether the gradient Richardson number Ri, is greater than or less than 1/4. As is well known (Woods, 1968; Lee and Beardsley, 1974),

when Ri approaches 1/4 it is possible to obtain internal waves through a type of shear instability.

Several authors (Barnes, 1973; Long, 1955; Prinsenberg and Rattray, 1975) have discussed processes by which tidal energy may be partially converted into internal waves at the continental slope. Lee and Beardsley (1974) have recently shown that tides can form an internal front and generate internal waves through topographic interaction even when Ri is larger than 1/4. These authors propose that internal-wave groups are formed in a three-stage process: (1) the formation of an initial (warm) front by partial blocking of the stratified flow by a topographic obstacle; (2) the nonlinear steepening of this internal front; (3) the formation of internal waves due to the interplay of dispersion and nonlinearity.

The data from NYBERSEX, in particular the data from June 30, display features similar to those proposed in the Lee and Beardsley theory. The first stage of the L-B process is the formation of a front. Such a front is depicted in figure 16. The location of this front is correct for semidiurnal generation sequence (see Section III.D.2). The bottom depth at 1300 UT is greater than 300 m. The front passes a 2°C temperature rise at 1500 m. The next appearance of a wave group occurs at 1525 UT. Two wave peaks appear to be present. A well-developed wave group occurs at 1725 UT (fig. 20). This is stage three in the L-B process. Consider the wavepacket shown in figure 20: if it is assumed that the leading wave is a solitary wave, then it is possible to estimate the range to the formation point of the internal-wave packet.

A solitary wave moving on a density interface at depth h_2 above the bottom is expected to travel at speed c where

$$c = g'(h_2 + a))^{\frac{1}{2}} , \qquad (2)$$

where a is the wave amplitude and g' is the reduced gravity. In a two-layer model,

$$g' = \frac{\rho_2 - \rho_1}{\rho_2} \cdot g \ , \tag{3}$$

where ρ_2, ρ_1 = the density of the lower and upper layers, respectively. The values a = 13 and $h_2 = 50 \times 10^2$ cm gives

$$c \cong 0.8 \text{ m/s} \ . \tag{4}$$

The long-wavelength, linear approximation for internal-wave speed is

$$c' = g' h_1 \ . \tag{5}$$

In our case the thickness of the upper layer is 25-30 m, and

$$c' \cong 0.50 \text{ m/s} \ . \tag{6}$$

The wavepacket shown in figure 20 will thus have traveled a distance, d, where

$$d = \frac{L}{c - c'} \cdot c' \ , \tag{7}$$

and L is the spatial extent of the packet.

For the packet shown in figure 20, L = 4.5 km. Thus,

$$d = \frac{4.5 \times 10^3}{0.30} \times 0.8 \approx 12 \text{ km} \ . \tag{8}$$

The distance, 12 km, should be roughly the distance from the point of observation of the wave group (shown in fig. 20) to the "point" of origin of the wave group. The use of the word origin in the previous sentence requires amplification. In that sentence, the word "origin point" refers to that point where both the nonlinear solitary waves and the linear waves evolved. The origin of the front from which the waves are thought to have evolved is farther east (on the continental slope). The distance from the point of observation of the wave group to the point of the front shown in figure 16 is roughly 31 km. This is consistent with the view that the observed wave group did evolve from a front generated at the continental slope. The calculated distance, ~12 km, also agrees very roughly (within 100%) with the distance between packets A and B on table 1. This suggests that this figure portrays the area in which a front evolves into a train of internal waves.

A major experimental observation made during NYBERSEX was that every internal-wave group observed began with a depression of isopycnals, isotherms, and acoustic reflectors. It should also be mentioned that the open-ocean internal-wave group shown in figure 11b also began with a depression. This observation is in accord with shallow-water internal-wave theory as it is now understood.

The most elementary equation governing the propagation of finite-amplitude long-wavelength internal waves in shallow water is that of Korteweg and de Vries (1895). Using the work of Berezin and Karpman (1967), Hunkins and Fliegel (1973) pointed out that, for a wide variety of conditions, solitary waves may be expected to evolve from an initial perturbation if

$$\ell^2 c >> 2h_1^2 c' ,$$

where ℓ is a characteristic length of the initial perturbation, and c is the speed of the initial disturbance.

In NYBERSEX, estimates of ℓ, h_1, and c' were obtained. A direct measure of c was not obtained. The amplitude of the initial front was measured, however. Hunkins and Fliegel assume that c and c' are roughly the same. This is probably also true of the NYBERSEX data. One argument for this is as follows: The internal-wave groups are separated by distances appropriate for semidiurnal tidal generation assuming a wavepacket propagation speed of c = 0.5 m/s. This includes the location of the front. In order for all the wave energy "contained" within the front to advance to the next semidiurnal position (which has been identified as the "origin" of the linear and solitary waves), the front must have moved with a speed of roughly 0.5 m/s. It is therefore assumed that c and c' are on the same order of magnitude. It is then only necessary that

$$\ell^2 >> h_1^2 .$$

At the most, $h_1 \approx 30$ m. From the acoustic data of figure 20 and a ship speed ≈ 2.3 m/s,

$$\ell \approx 2\text{-}5 \text{ km};$$

hence,

$$2 \frac{h_1^2}{\ell^2} \cong 4 \times 10^{-4} .$$

Thus the condition for the excitation of solitary waves is satisfied.

Let us now return to the question of the isopycnal depression caused by the onset of the internal-wave packet. Hunkins and Fliegel (1973) indicate that, on the basis of energy considerations, only the depression of isotherms allows loss of energy across the packet front. The elevation of isotherms corresponds to the impossible case of energy gain by the packet. From the work of Benjamin (1967) and of Lee and Beardsley (1974), it also follows that internal solitary waves must be troughs.

V. SUMMARY AND CONCLUSIONS

As stated in Section I.B, the prime purpose of the New York-to-Bermuda Remote Sensing Experiment was the verification of the internal-wave interpretation of periodic features observed in Landsat-1 imagery. Equally important was the verification of certain observational conclusions about internal waves drawn from Landsat-1.

It was hoped that it would be possible to obtain several Landsat-1 cloud-free images in which the RV Westward would be located, thereby facilitating comparison of satellite and shipboard measurements. This proved very difficult to do because of the clouds and generally poor weather conditions. The goal of having the vessel Westward in the "middle" of an internal wavepacket during a cloud-free Landsat-1 overpass was not realized. However, a situation did occur on July 17, 1974, in which the Westward was within a Landsat-1 image, though not at the time of overpass, and within an internal wave group. This situation is amply discussed by Apel et al. (1976; attached as an appendix to this report).

Let us consider next how accurately the NYBERSEX observations of internal-wave field characteristics verified the characteristics predicted from Landsat-1 data examined prior to the undertaking of NYBERSEX. The characteristics predicted in Section I.B, item (2) and items (3)(a) through (3)(f) were fully confirmed. Goal (1) (Section I.B) was partially attained, as indicated in the above paragraph.

Let us consider next the basic research goals (item (4), Section I.B). Before discussing the satisfaction of the research goals themselves, it is worth examining the state of knowledge in the general oceanographic community of the internal-wave field on the U.S. continental shelf at the time NYBERSEX was undertaken. In June 1974 it was well known that internal waves were

generated during peaks or turning points in tidal flows (Shand, 1953). By 1969 it was also certainly known that, for the Straits of Georgia at least, distinct internal-wave groups occurred with periods much shorter than tidal (e.g., 30 min) (Gargett and Hughes, 1972). In 1971, Halpern published the results of experiments he carried out in shallow water in Massachusetts Bay. These results again indicated the production by the tide of internal-wave groups made up of short-period internal waves. Halpern (1971) noticed, as had Shand (1953) and LaFond (1962) before him, that long surface slicks were associated with these groups. Halpern's data showed the rapid onset of the internal-wave groups with a sudden rise in temperature at the recording thermistor occurring within 10 min. In January of 1974, Lee and Beardsley published an analysis of finite-amplitude internal waves that compared numerical computations of waveform and its development to observations made in the laboratory and in the ocean. According to their interpretation, wavepackets form when the internal front (formed when the tidal current sweeps over a sill) steepens to the point of instability. This, then, was the state of knowledge as derived from the published literature in June 1974.

Certain questions can now be posed that were essentially unanswered in 1974. These questions include the following:

(1) Are internal-wave groups being produced at the continental shelf? The answer to this question in June 1974 was, "Probably yes."

(2) If internal-wave groups are being produced at or on the continental shelf, in what numbers are they being produced? The answer to this question in June 1974 was, "Unknown."

(3) If internal-wave groups are produced, what is the amplitude and wavelength distribution within a packet? The answer in June 1974 was, "If packets exist, they may be of the form observed by Gargett and Hughes (1972), Halpern

(1971), and Lee and Beardsley (1974); i.e., largest amplitudes and largest periods in front and nonlinear."

(4) What are the horizontal dimensions (i.e., along a crest) of a wave group likely to be? The answer to this question in 1974 was, "Not enough data at present for a complete response."

(5) How does an internal-wave group generate a surface signature and thus become detectable using satellite techniques? The answer would be, "According to LaFond (1962), surface slicks are regions where capillary waves are damped by oily film concentrated at the convergence of horizontal currents induced at the surface by internal waves. According to recent work by Gargett and Hughes (1972), the internal-wave currents interact with surface waves, alternately damping and enhancing them to produce slick and rough bands."

(6) Do internal-wave groups appear in the deep ocean and, if so, what is their structure likely to be? The answer to this question is, "Internal waves in the deep ocean have been observed for many years; however, whether these waves exist in the form of nonlinear groups is unknown.

In view of the data presented here, it is now fair to say that the occurrence of nonlinear internal-wave groups at the edge of the continental shelf and shoreward is common along the east coast of the United States. The amplitude distribution and wavelength distribution is such that the largest wavelengths and longest periods are in the leading portion of the wavepacket. This same arrangement was observed by Gargett and Hughes (1972) and by Halpern (1971). Evidence has been found (data of June 30, 1974) to support the"front-formation" theory of Lee and Beardsley (1974). The horizontal length scale of the packets is large, easily being tens of kilometers. Internal-wave packets do indeed occur in the deep ocean, as evidenced by the acoustic data in Section III.B. The data in Section III.B plus the data from GATE presented

by Ostapoff et al. (1975) and Proni et al. (in preparation), indicate a similarity of form between deep-ocean internal-wave packets and continental shelf wavepackets.

Finally, the evidence in this document supports the following conjecture: Individual internal waves within a wave group can possess two surface signatures: the first is a ruffled area, replete with capillary waves; and the second is a slick area, devoid of capillary waves. One may also surmise that both the leading nonlinear waves within a packet (solitary waves) and the trailing linear waves can generate the above-mentioned dual surface signature. If one were interested in studying the interaction of nonlinear internal solitary waves, an excellent place to do it would be about 90 km north-northeast of Cape Cod.

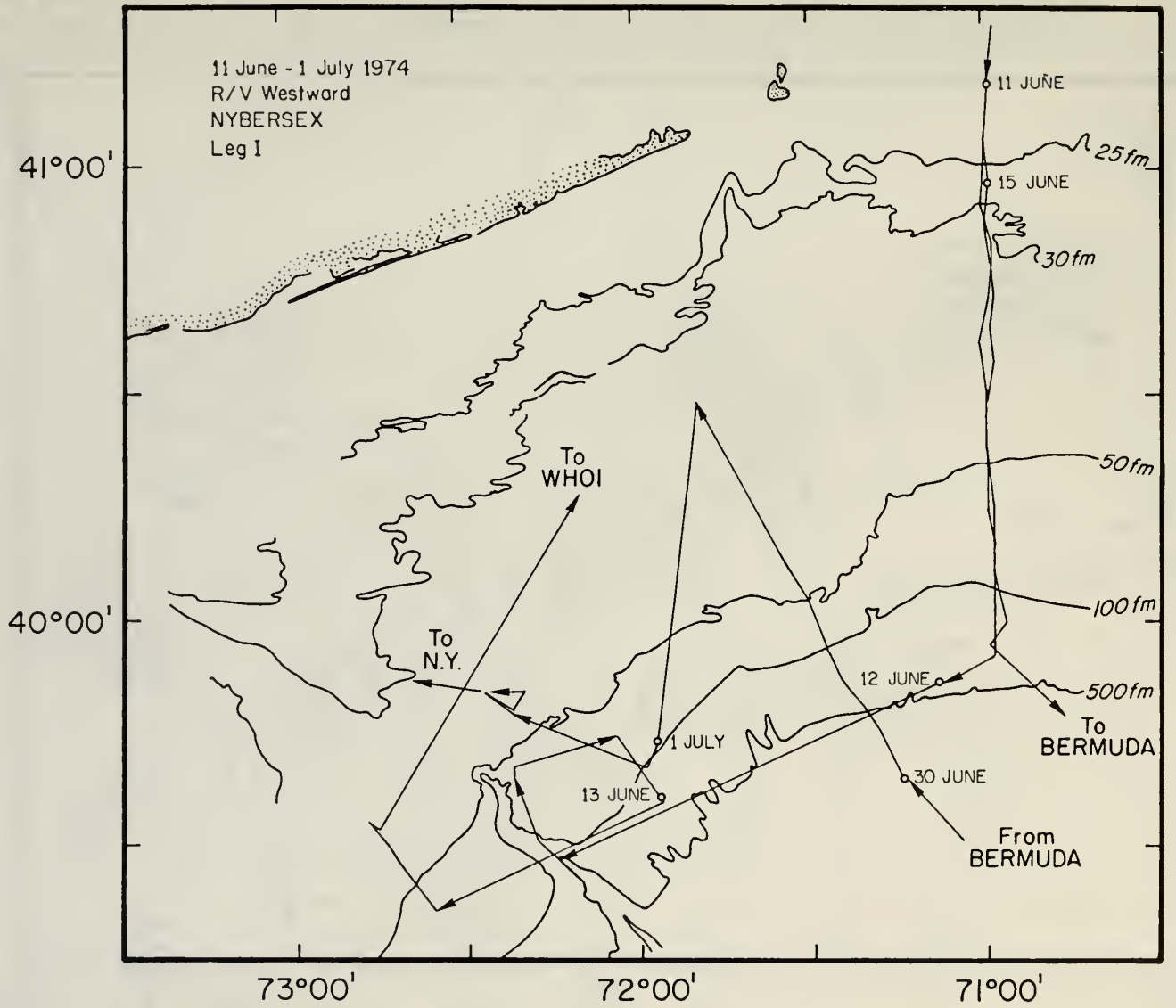

Figure 1. Course sailed by the RV Westward during Leg 1 of the New York to Bermuda Remote Sensing Experiment. The segment of the cruise from Bermuda to the U.S. continental shelf is shown in figure 2. No satellite data were taken while the ship was enroute to Bermuda.

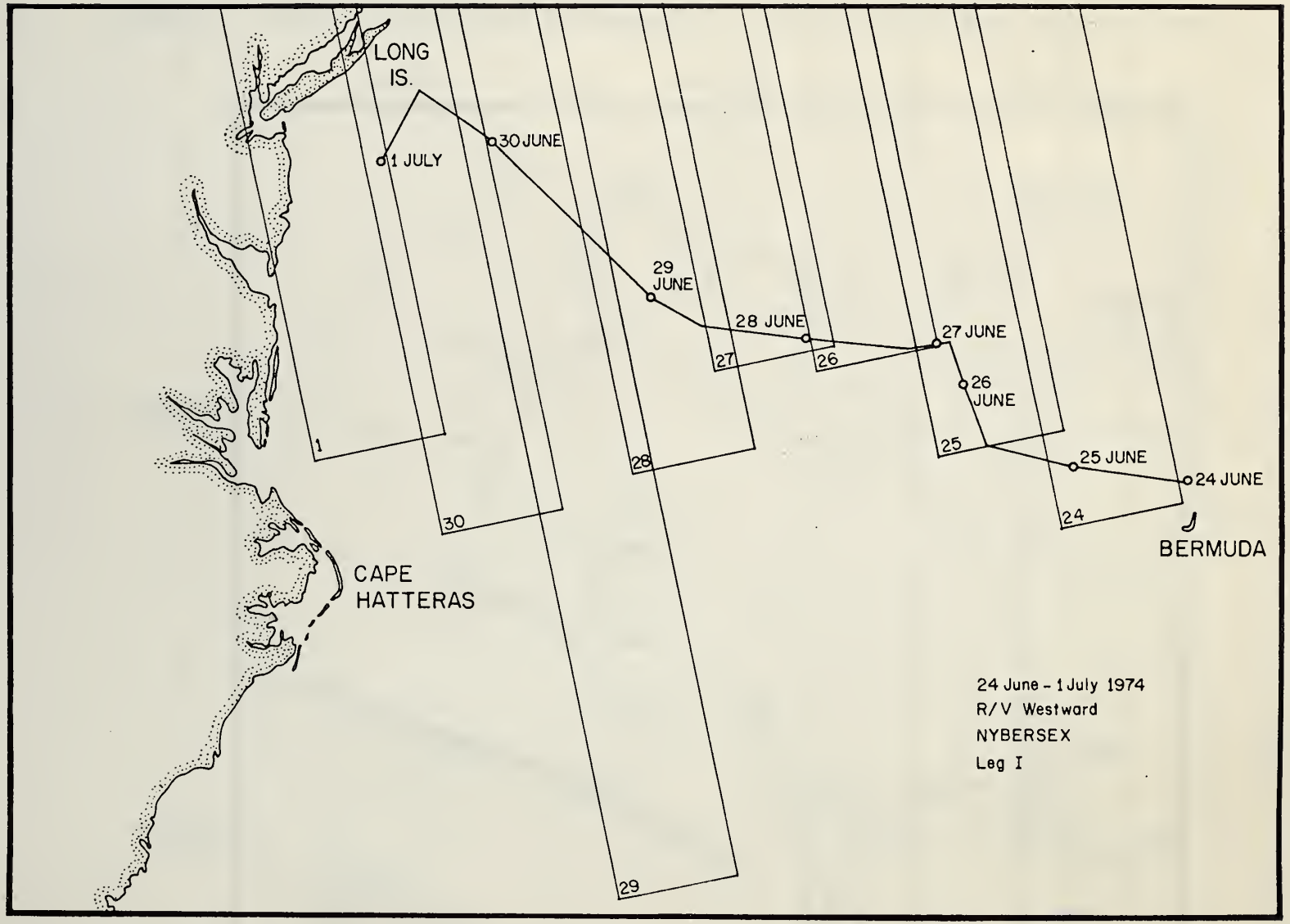

Figure 2. Course sailed by the RV Westward in going from Bermuda to New York (Leg 1). Circles indicate the location of the ship at the time of the satellite overpass for each day. The series of sloping rectangles shows the satellite viewing area on the day indicated in the lower left-hand corner of each rectangle.

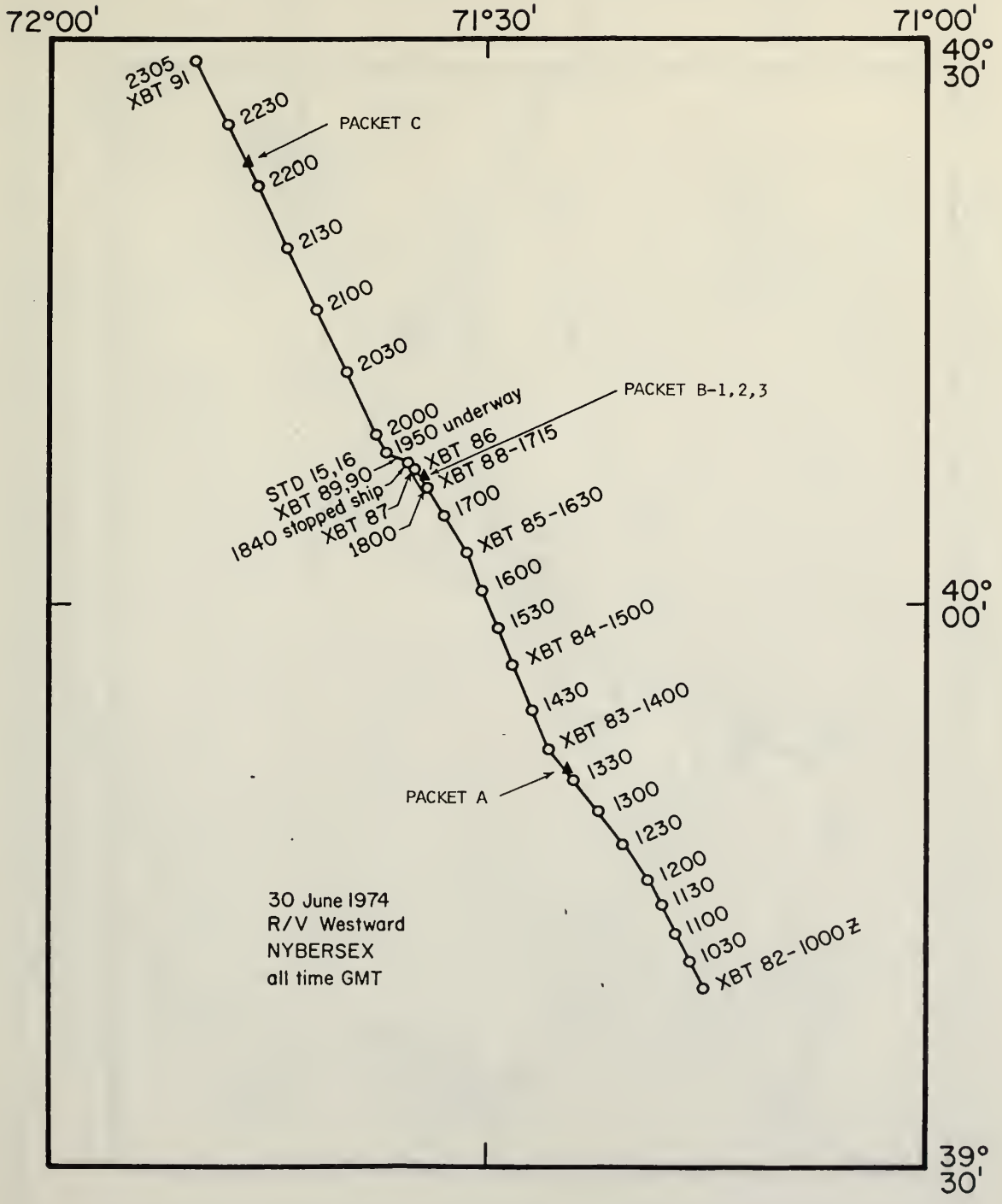

Figure 3. Course sailed by the RV Westward on June 30, 1974.

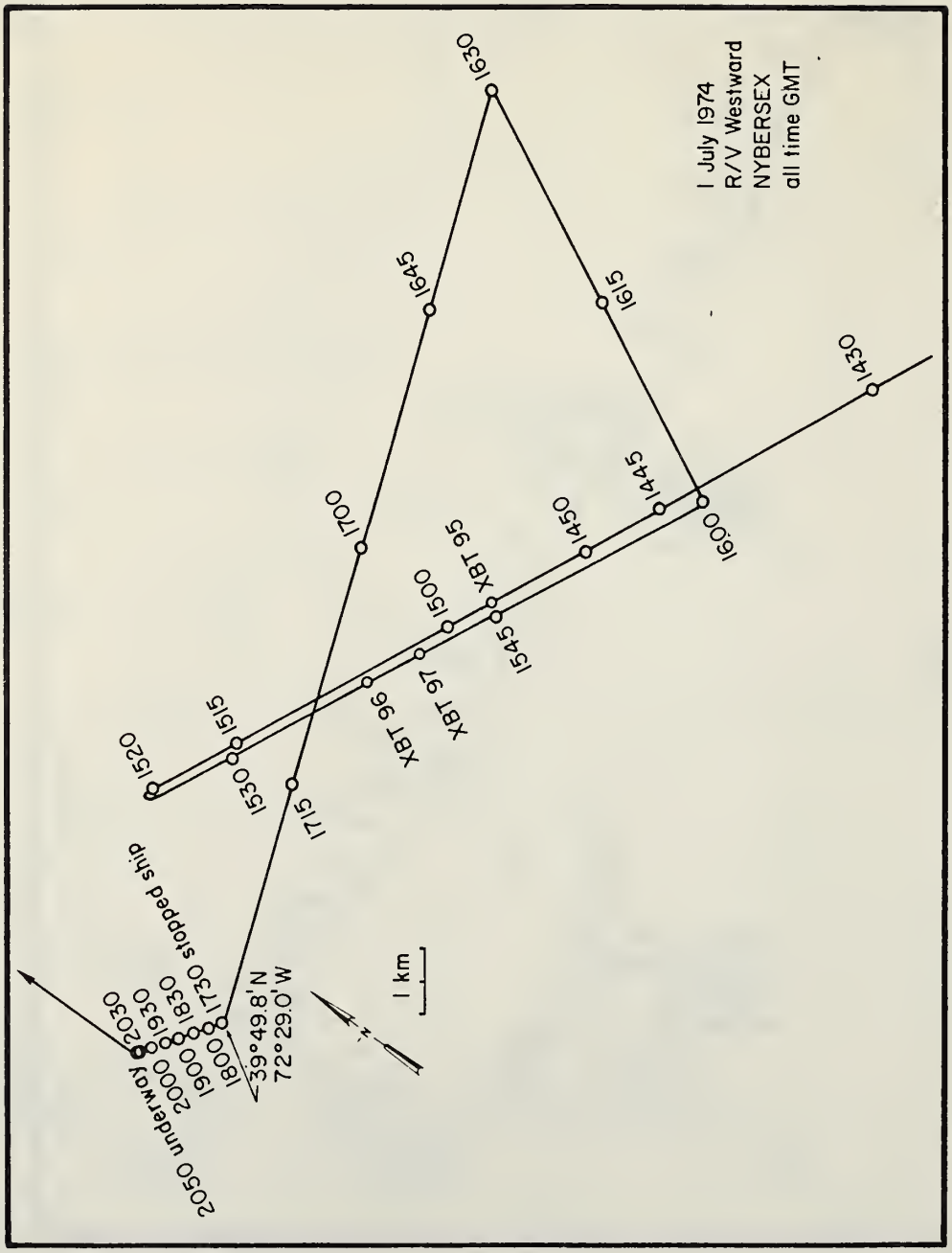

Figure 4. Course sailed by the RV Westward on July 1, 1974. The "triangle maneuver" was carried out on this date.

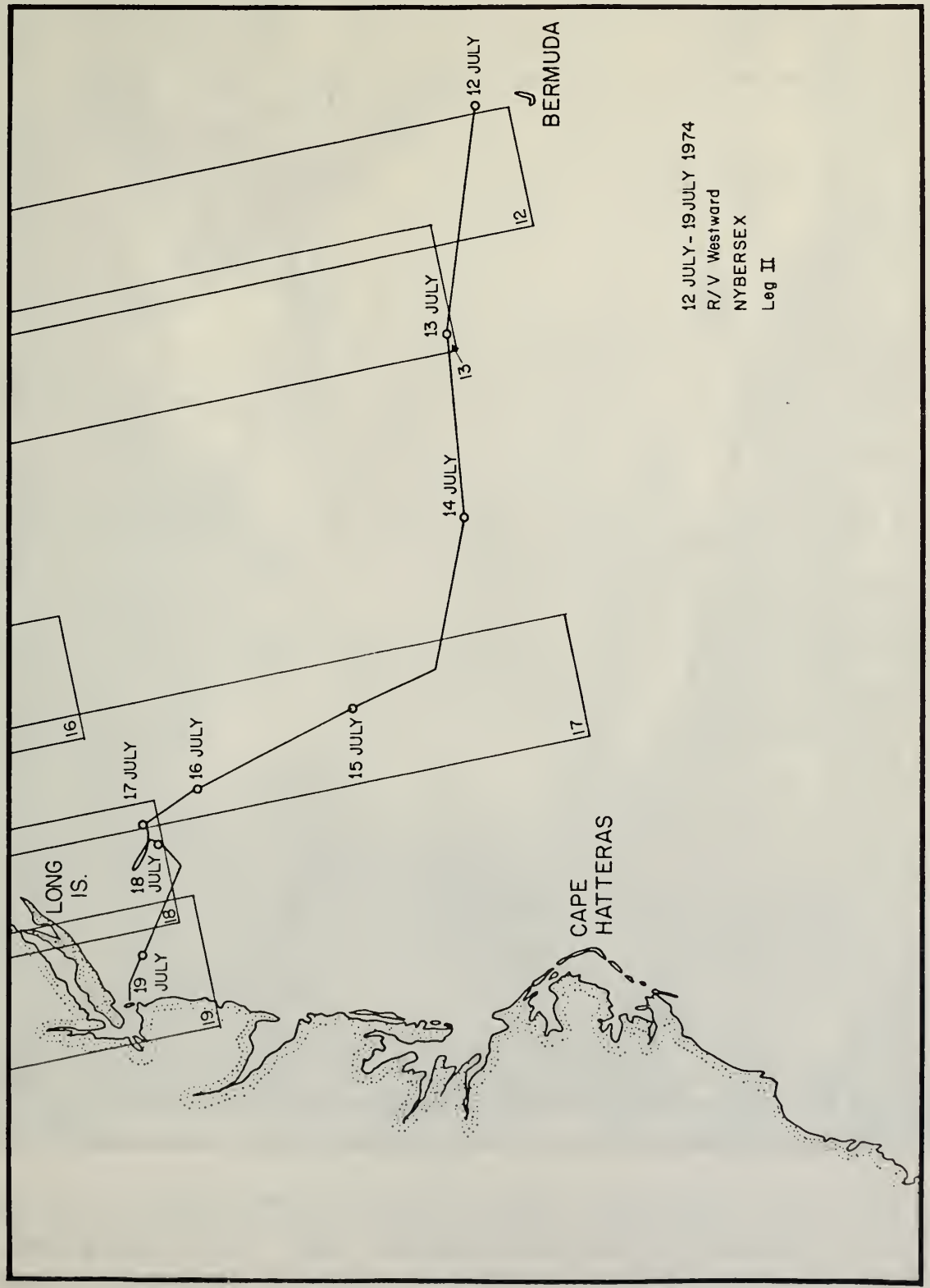

Figure 5. Course sailed by the RV Westward in going from Bermuda to New York (Leg 2).

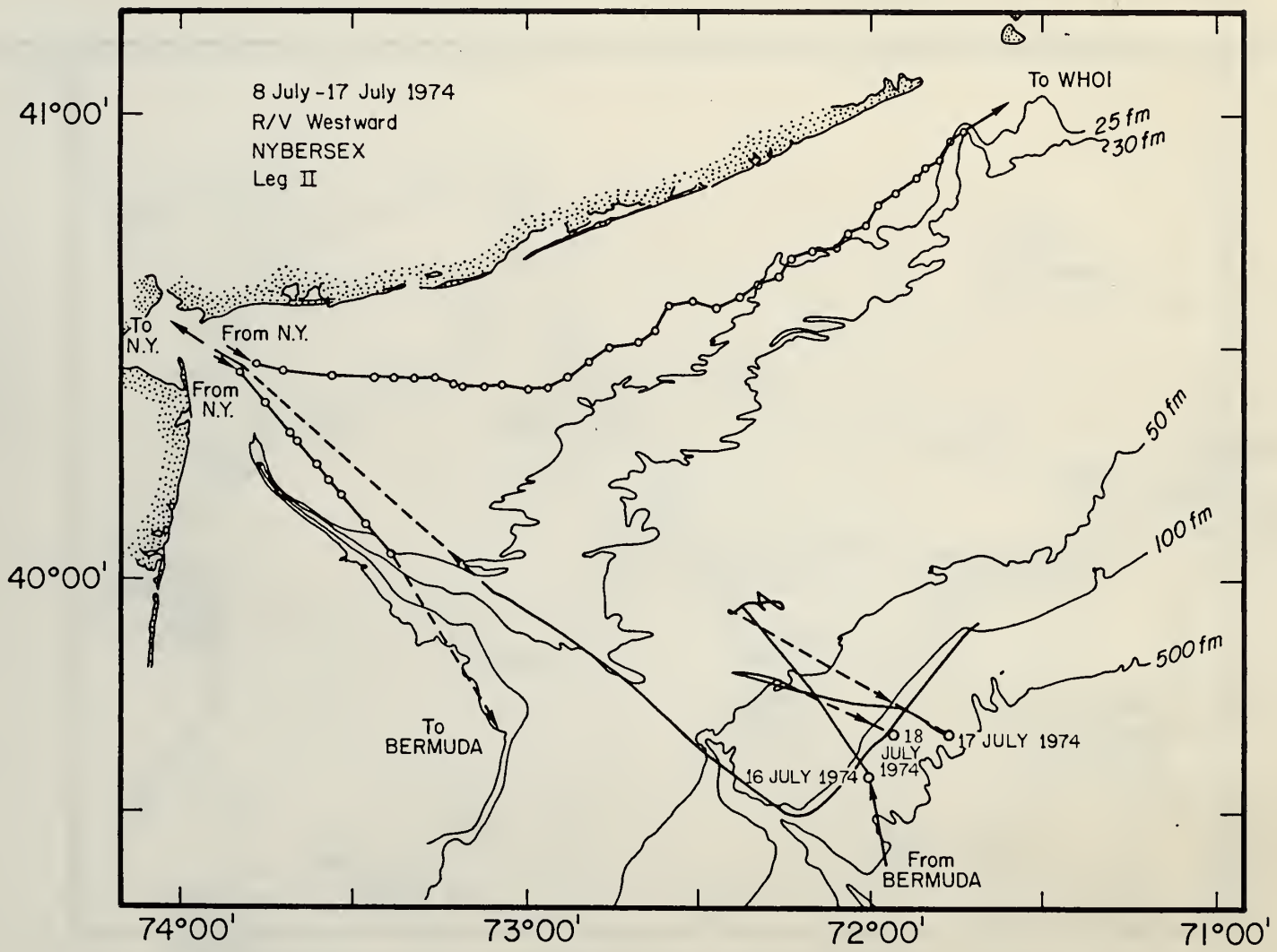

Figure 6. Course sailed by the RV Westward July 16 through July 19, 1974.

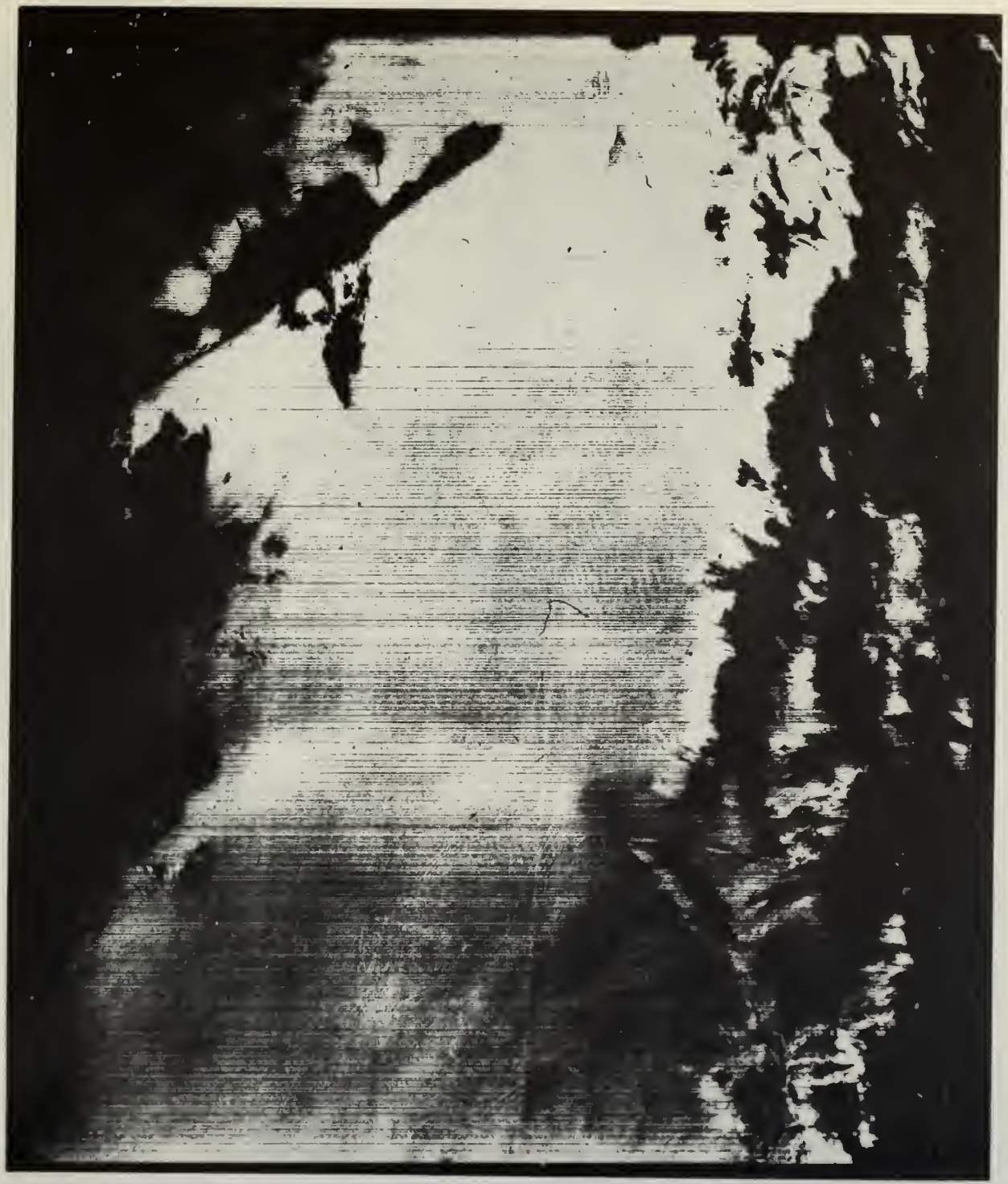

Figure 7. Landsat-1 image for June 12, 1974. The eastern tip of Long Island is visible in this image. The coordinates of the center of the image are 40°25'N and 72°15'W. Some internal-wave activity is indicated in the lower central portion of the image. The bands to the right of center, with dark and light bands of nearly equal width, are probably clouds: internal gravity waves in the atmosphere.

Figure 8. Landsat-1 image for June 12, 1974, the area immediately south of the image of figure 7.

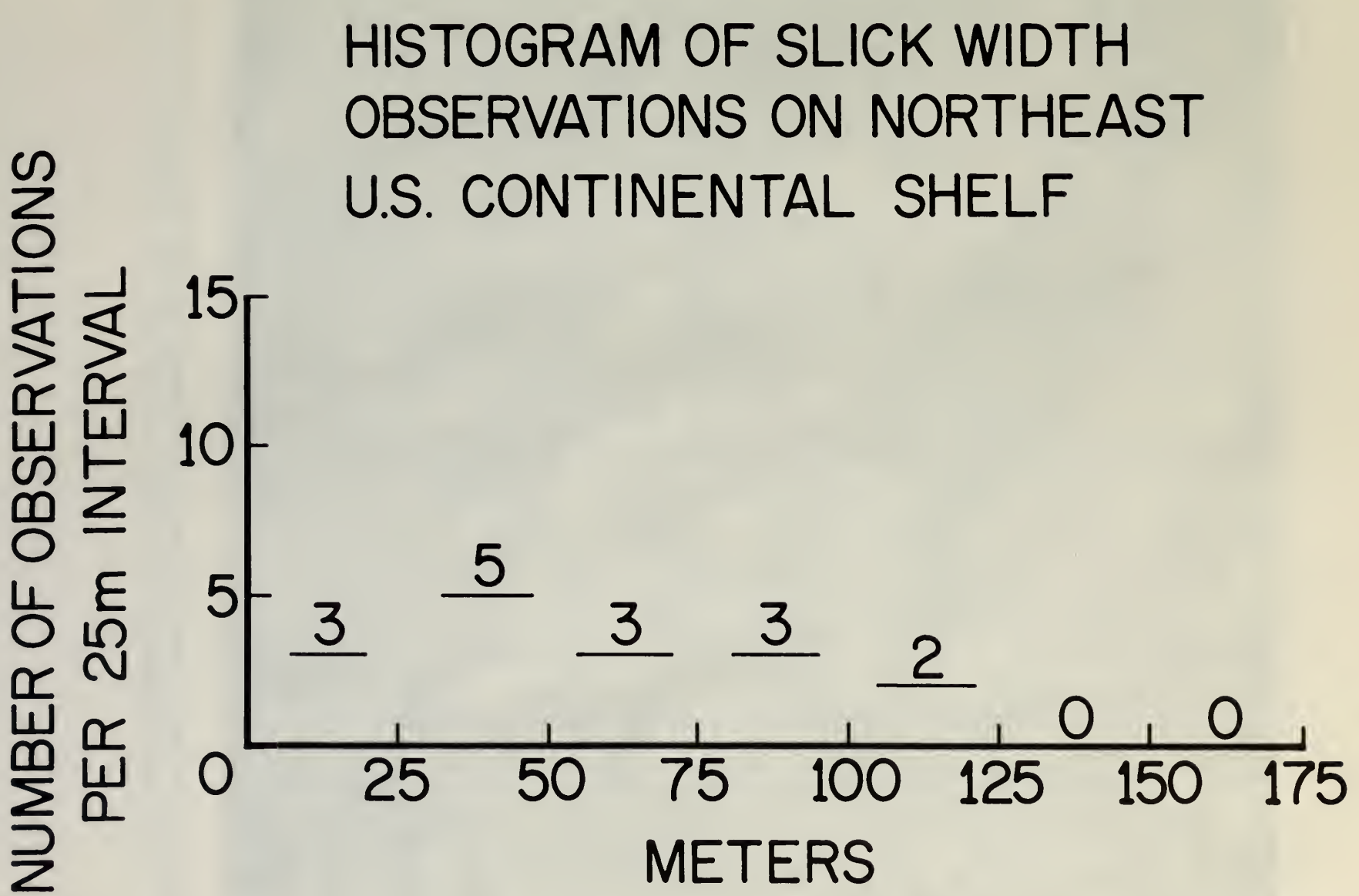

Figure 9. Histogram of slick widths observed during a passage through an internal-wave group.

Figure 10a. Landsat-1 image for June 13, 1974, showing the New York Bight area. The coordinates of the image center are 40°25'N, 73°31'W.

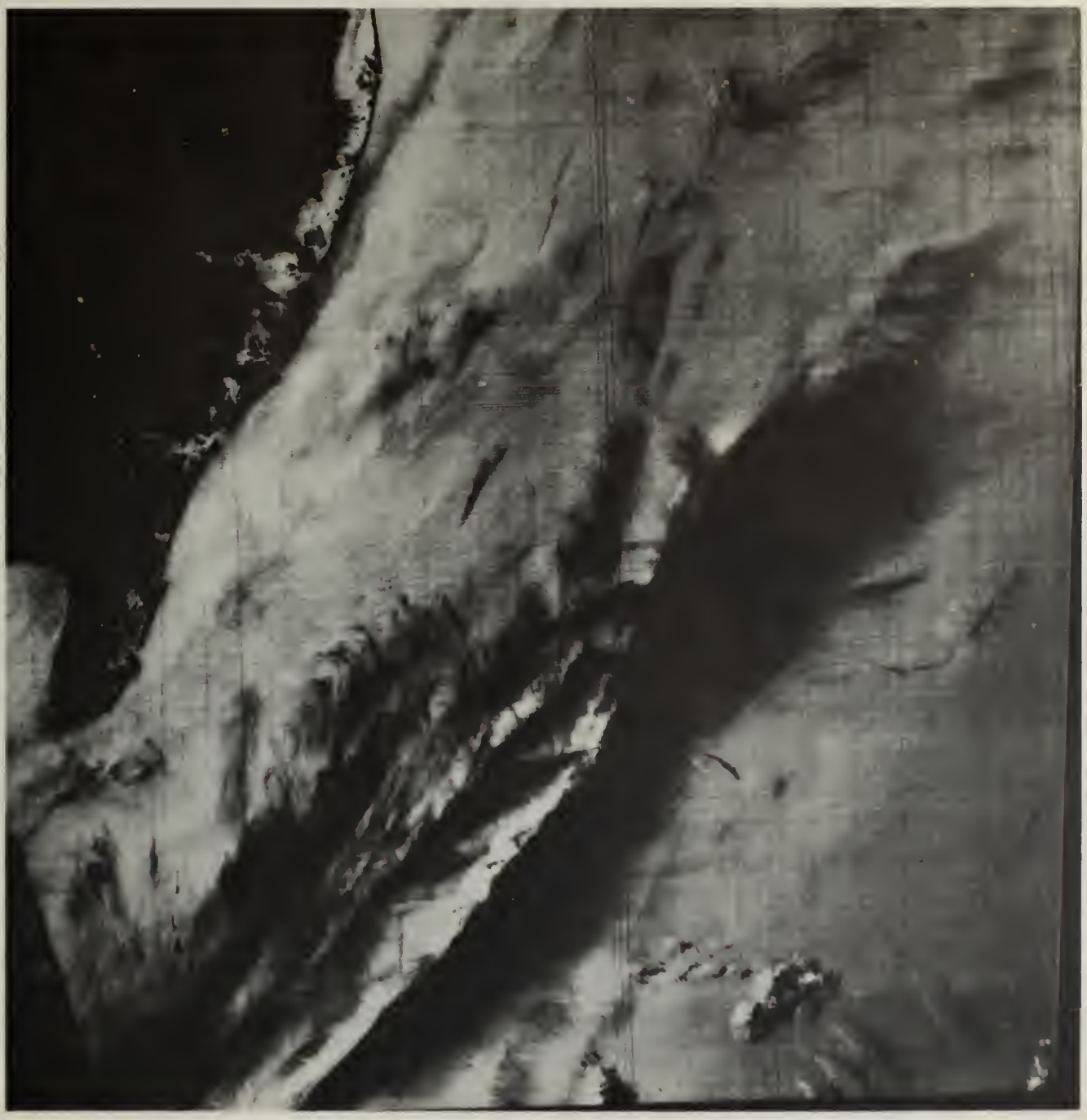

Figure 10b. Landsat-1 image for June 13, 1974, immediately south of the Landsat-1 image shown in figure 10a. The coordinates of the image center are 39°01'N, 74°06'W.

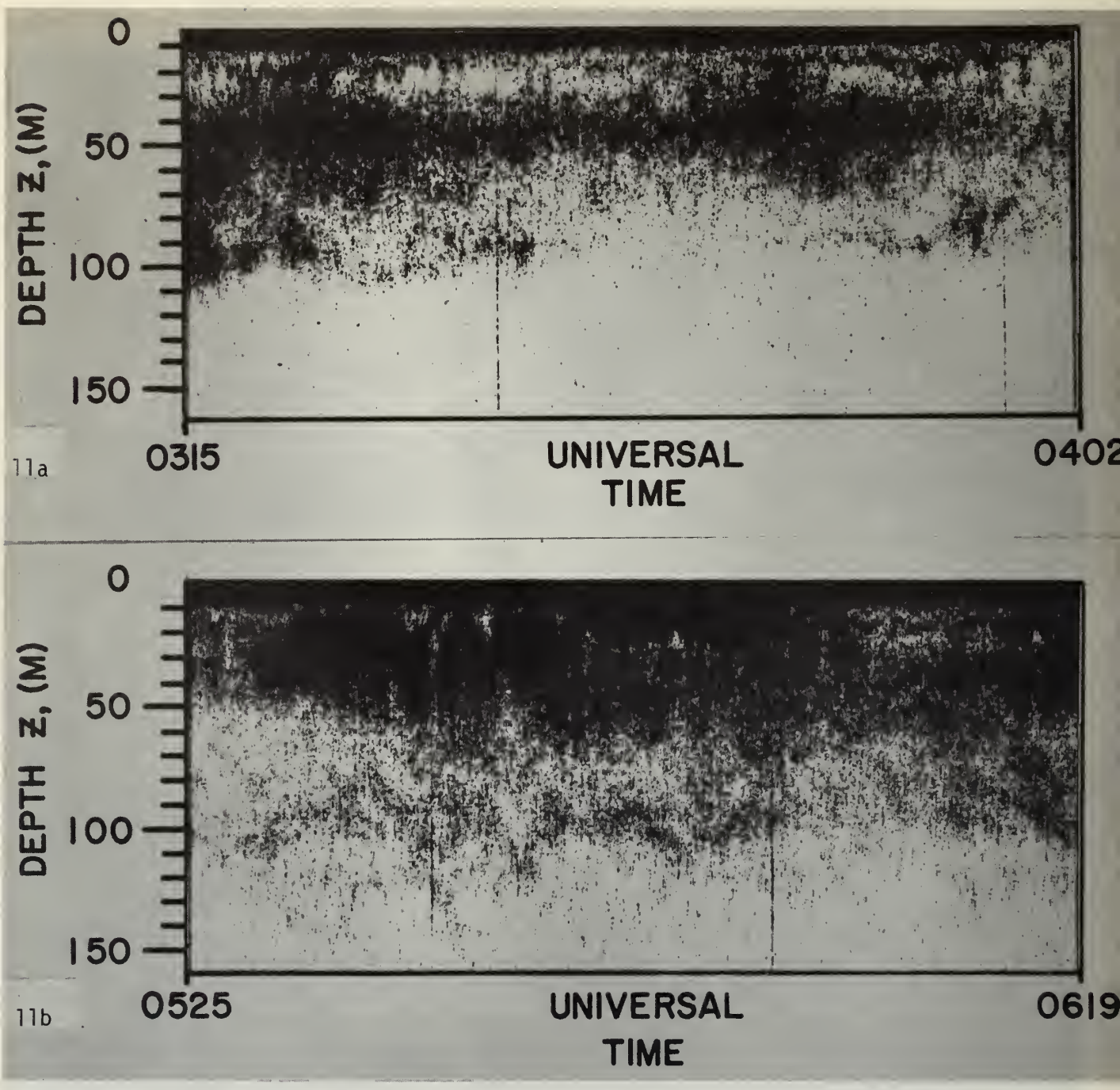

Figure 11. a. Observations of short internal waves observed on June 20, 1974. Ship's location: 33°40'N, 65°20'W. b. A localized group of large-amplitude (as large as 35 m) internal waves observed on June 20, 1974. The crests of these waves approach within 12 m of the ocean's surface. These waves are very similar to those reported by Ostapoff et al. (1975) and Proni et al. (in press).

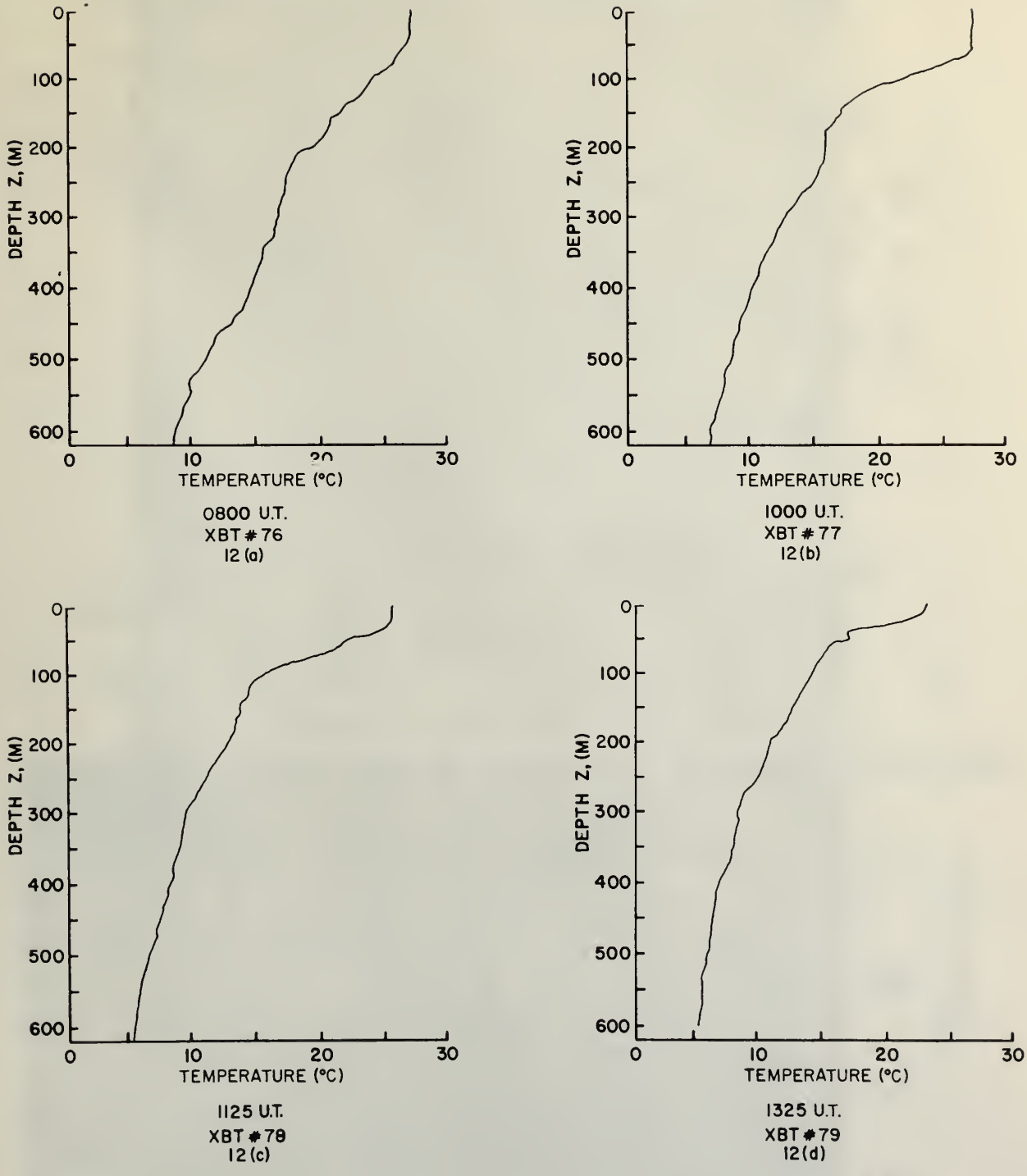

Figure 12a-d. Temperature as a function of depth according to XBT's taken along the ship track.

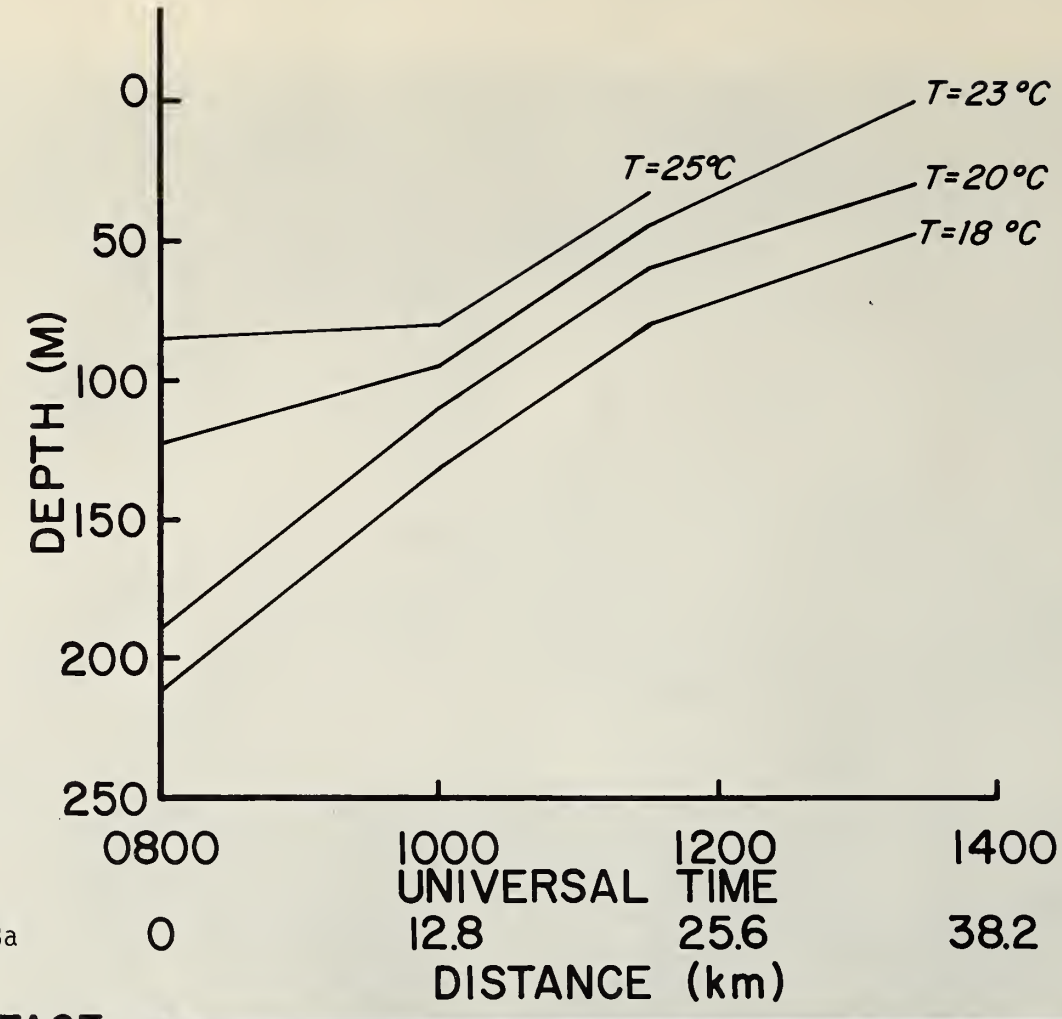

13a

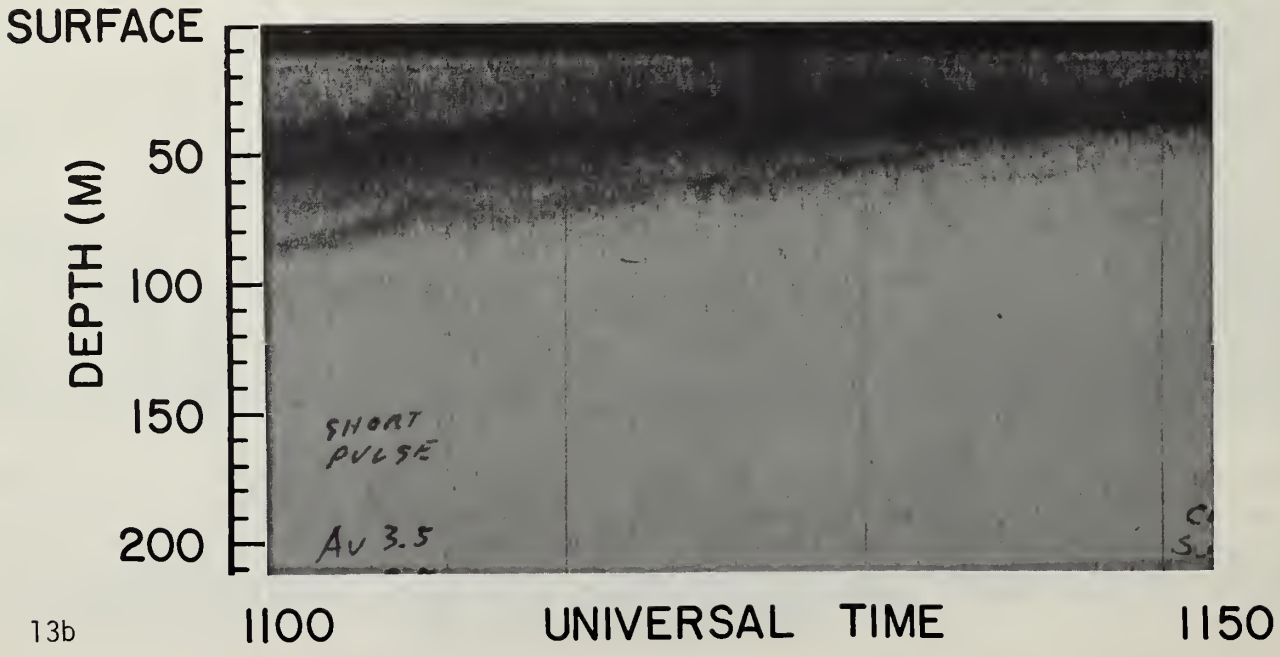

13b

Figure 13. a. Isotherms along the ship track according to the XBT data of figure 12.
b. Acoustic echo for part of the same period.

Figure 14. Landsat-1 image of Gulf Stream, June 30, 1974.

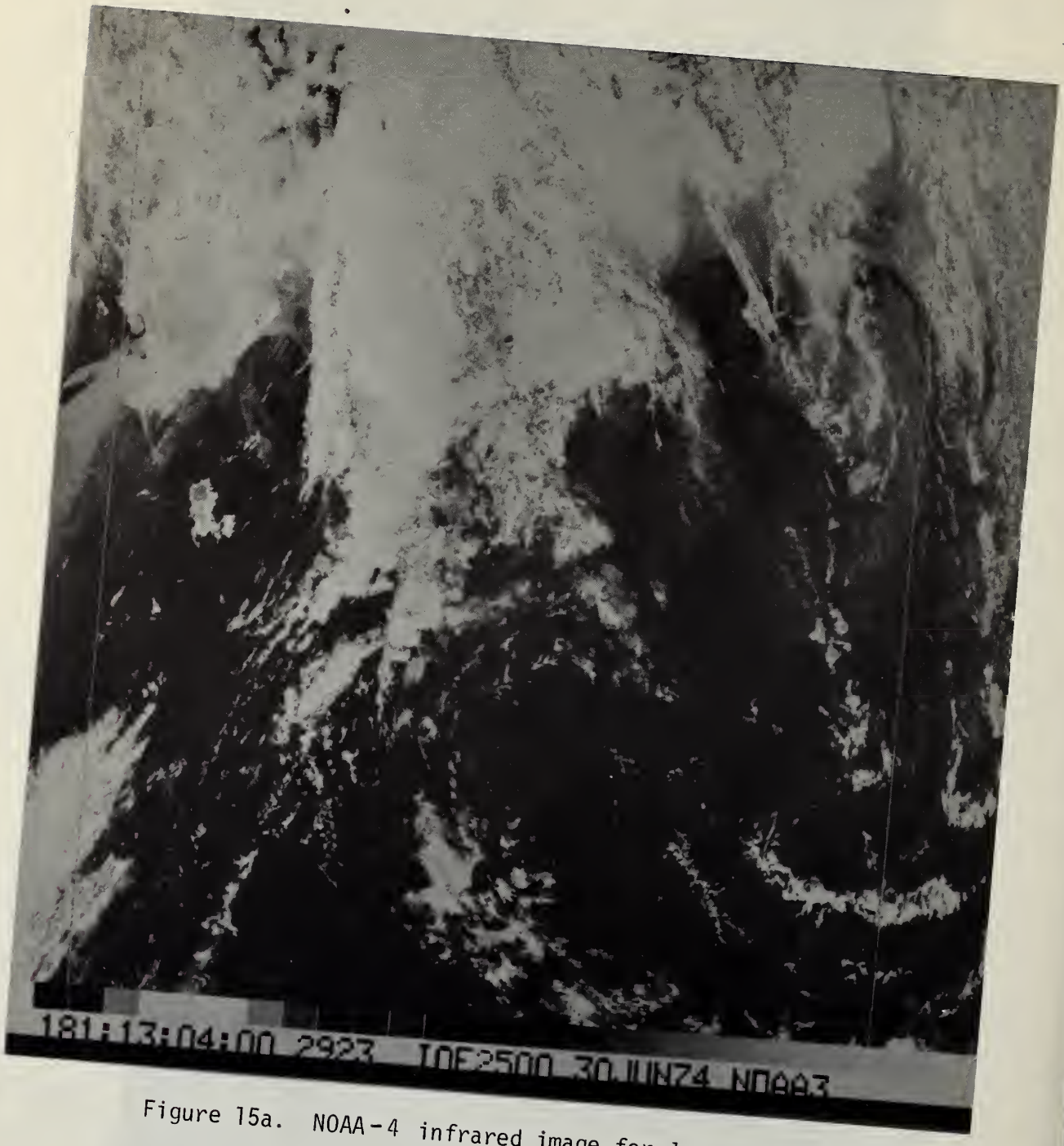

Figure 15a. NOAA-4 infrared image for June 30, 1974.

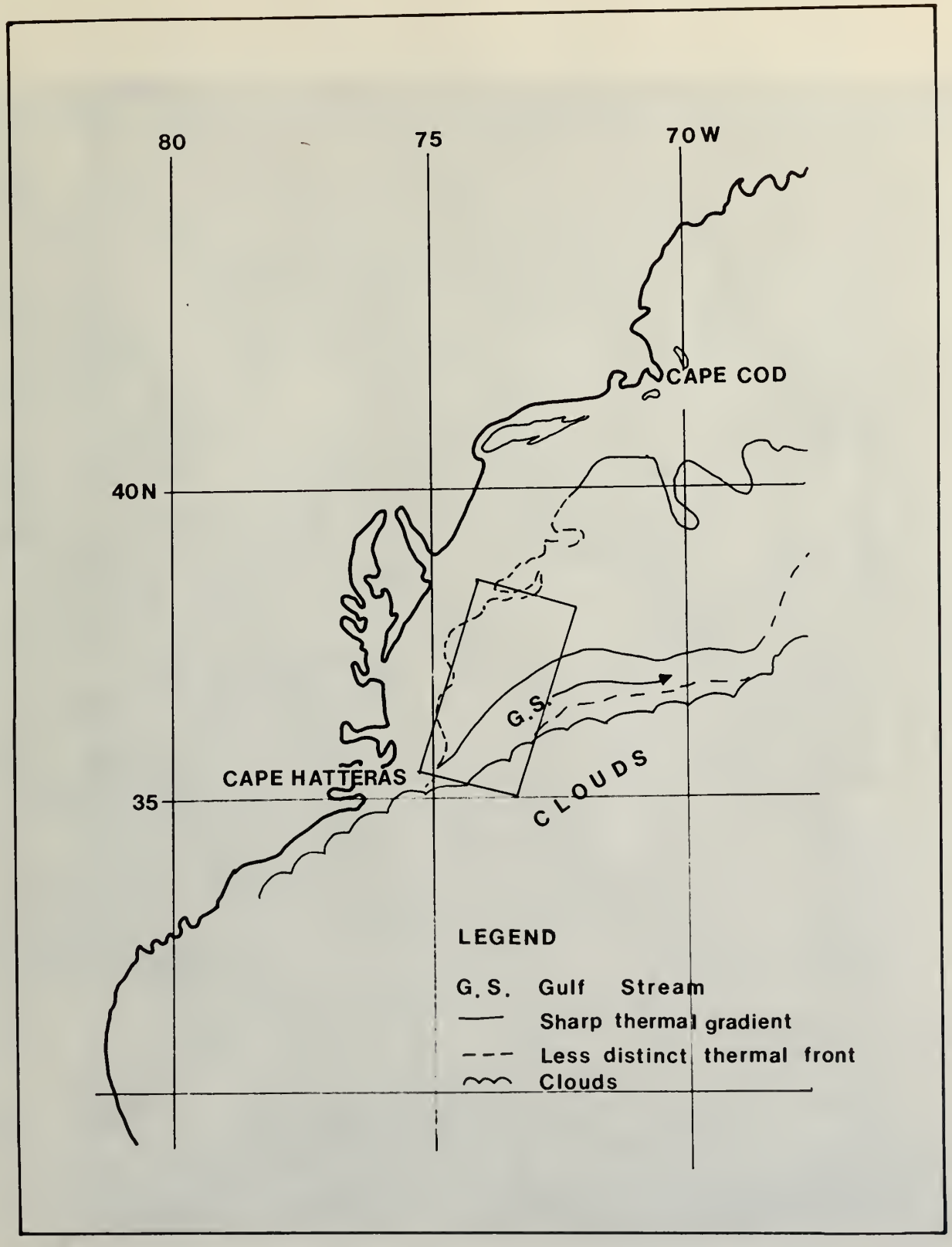

Figure 15b. Analysis based on NOAA-4 infrared images of Gulf Stream for June 28 to July 1, 1974, with position of Landsat-1 image (fig. 14) superposed.

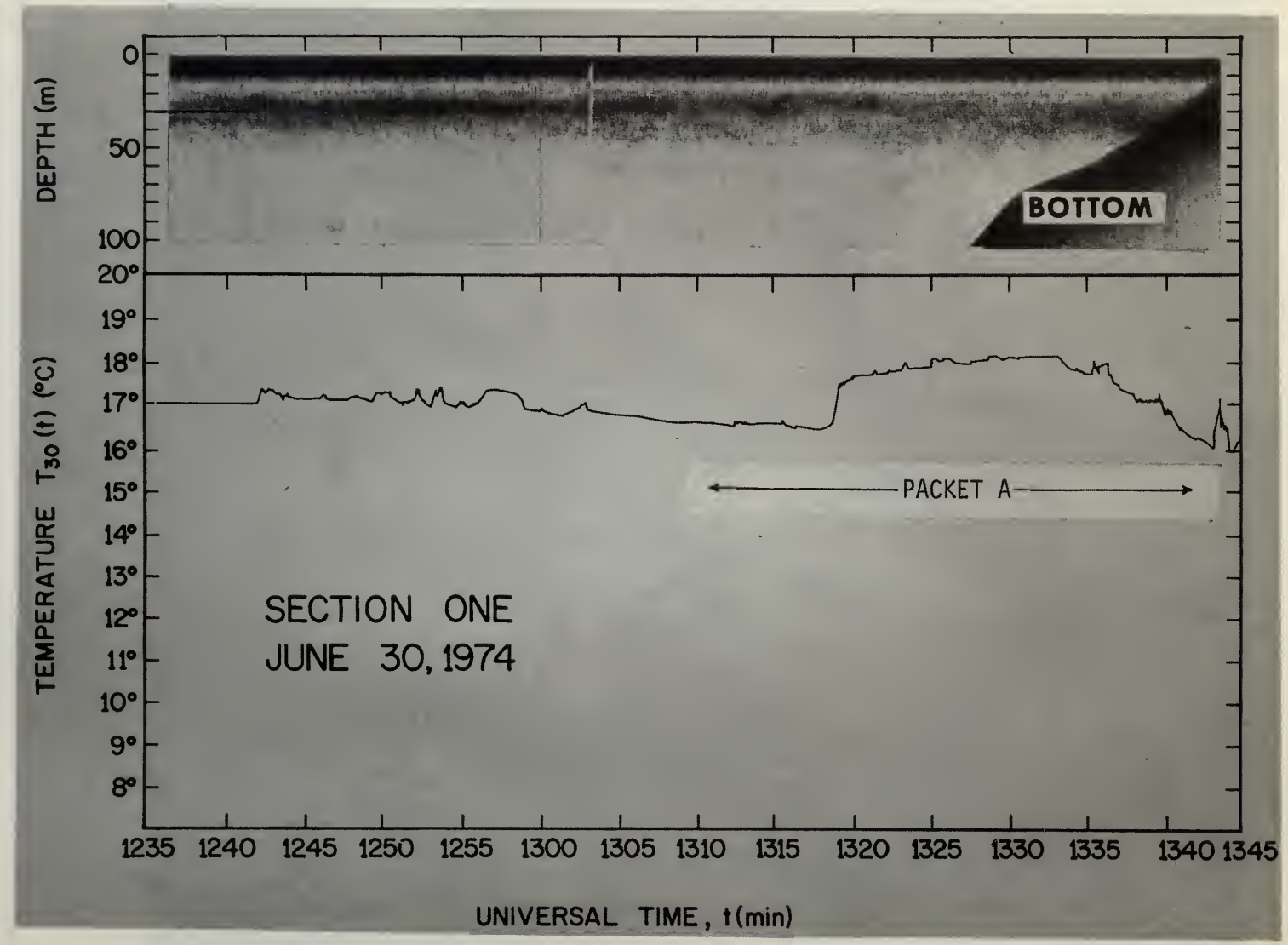

Figure 16. Region I (deep). Acoustic echo (above) and temperature from thermistor towed at 30-35 m depth as the Westward sailed shoreward at about 2.5 m/s.

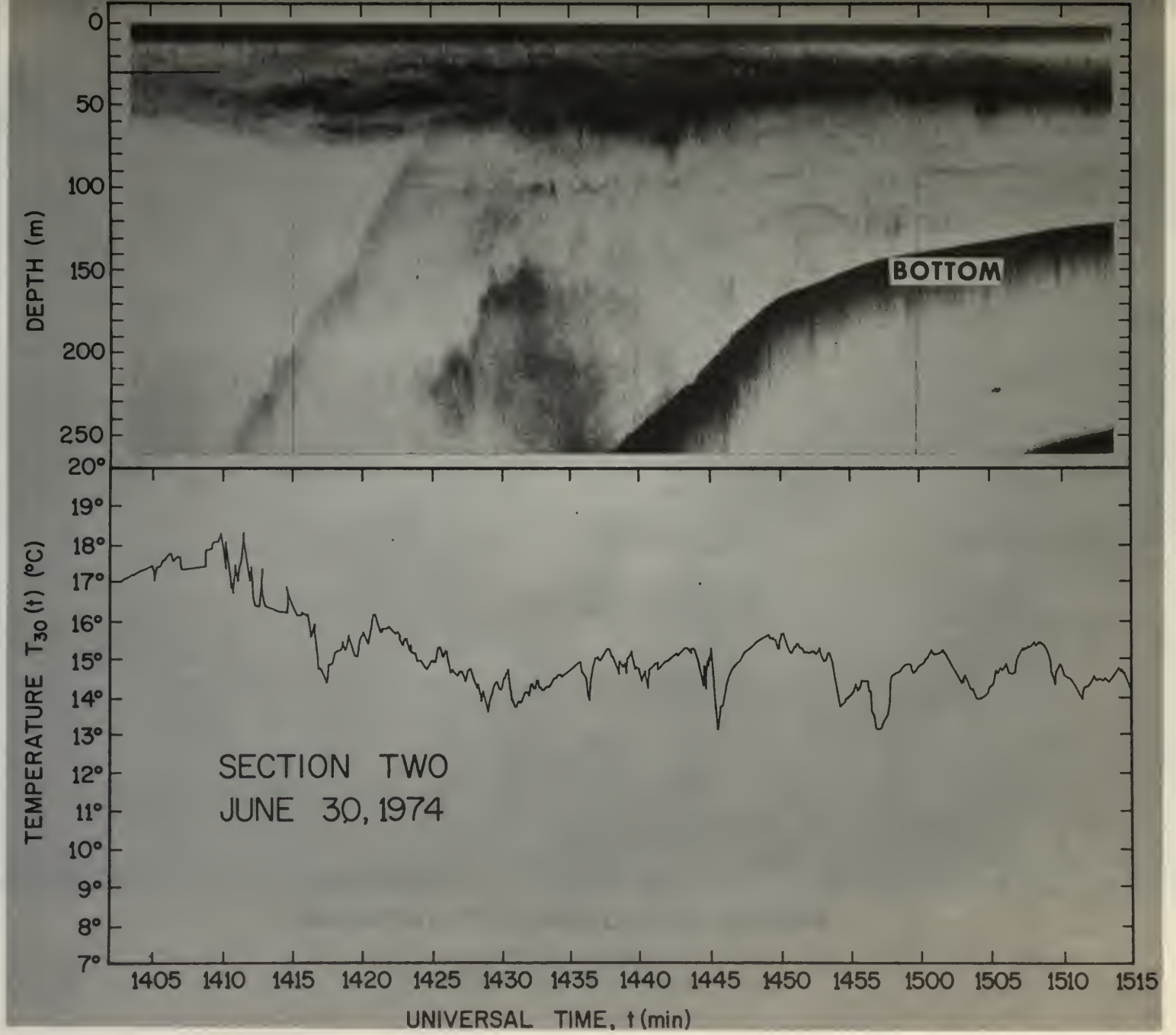

Figure 17. Region II (slope). Acoustic echo (top) and temperature from thermistor towed at 30-35 m depth. Note deepening of reflecting layer from 30 m at 1358 UT to 65 m at 1416 UT, and increase, during period, of reflected acoustic energy.

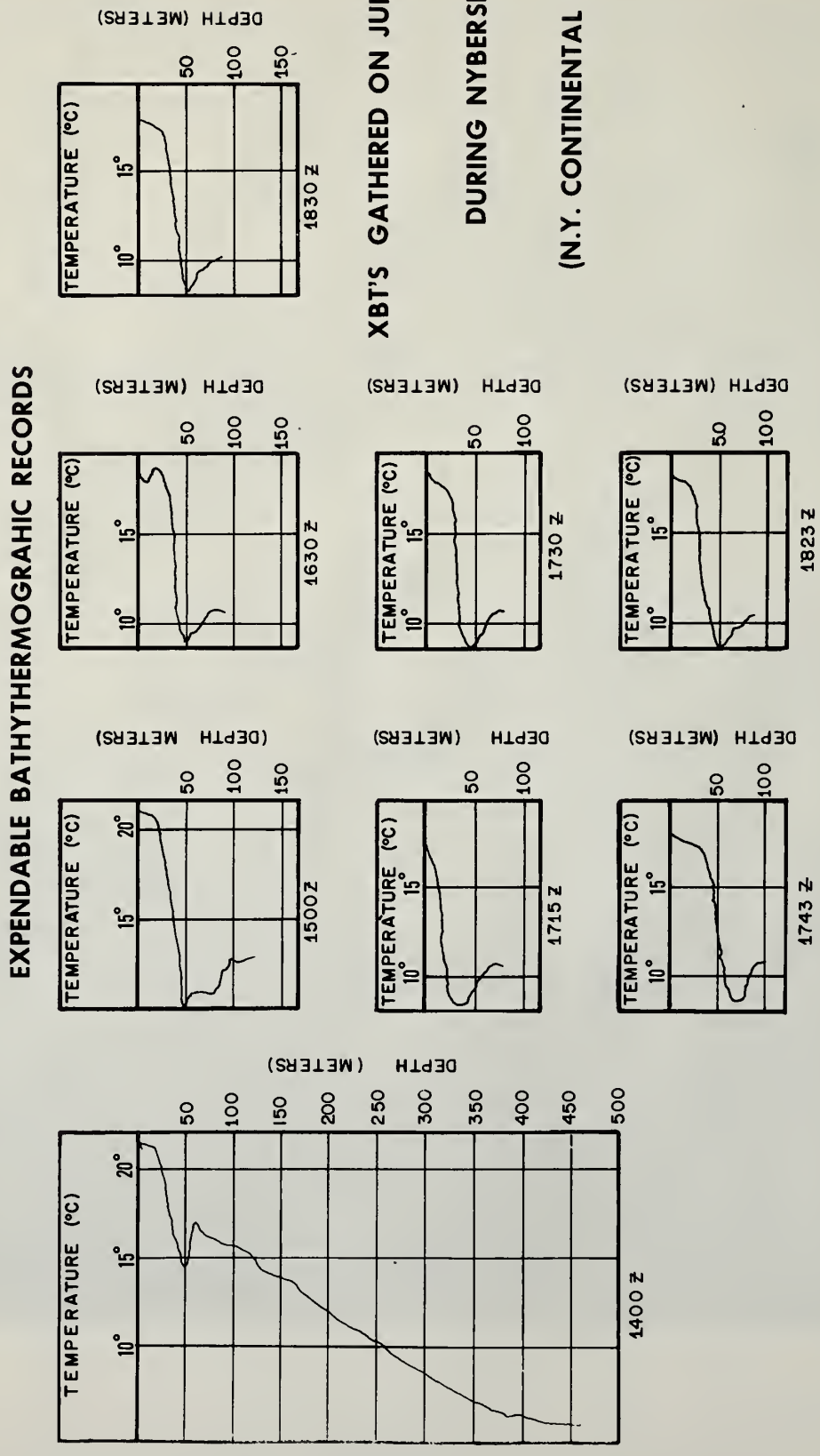

Figure 18. XBT records. Note the steep gradient in the trace for 1400 UT, and the inversion near 50-m depth. Note also the strong decrease of temperature at 50 m between 1400Z and 1500Z.

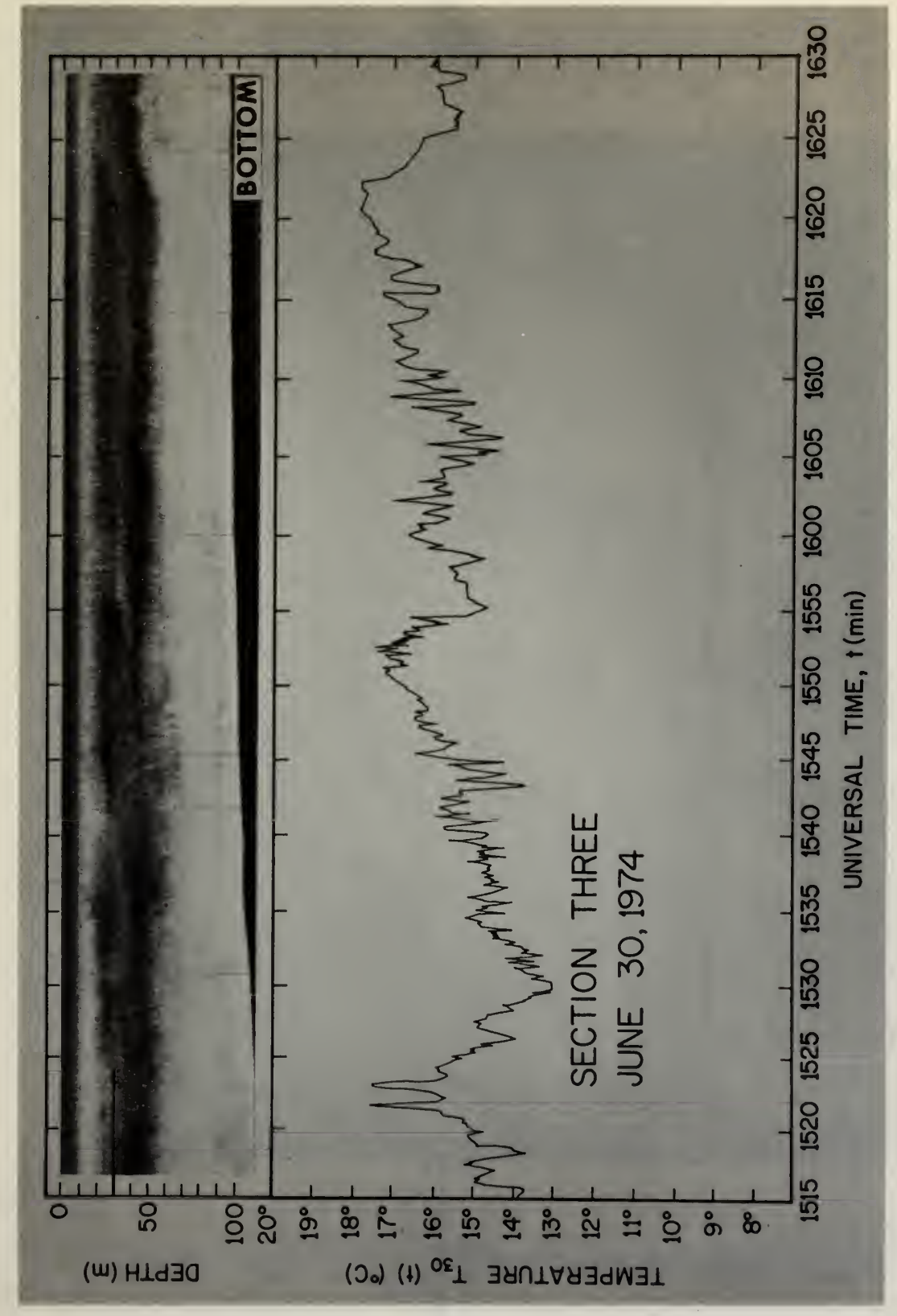

Figure 19. Region III (shelf). The warm spikes at 1520 to 1525 UT are interpreted as developing internal waves.

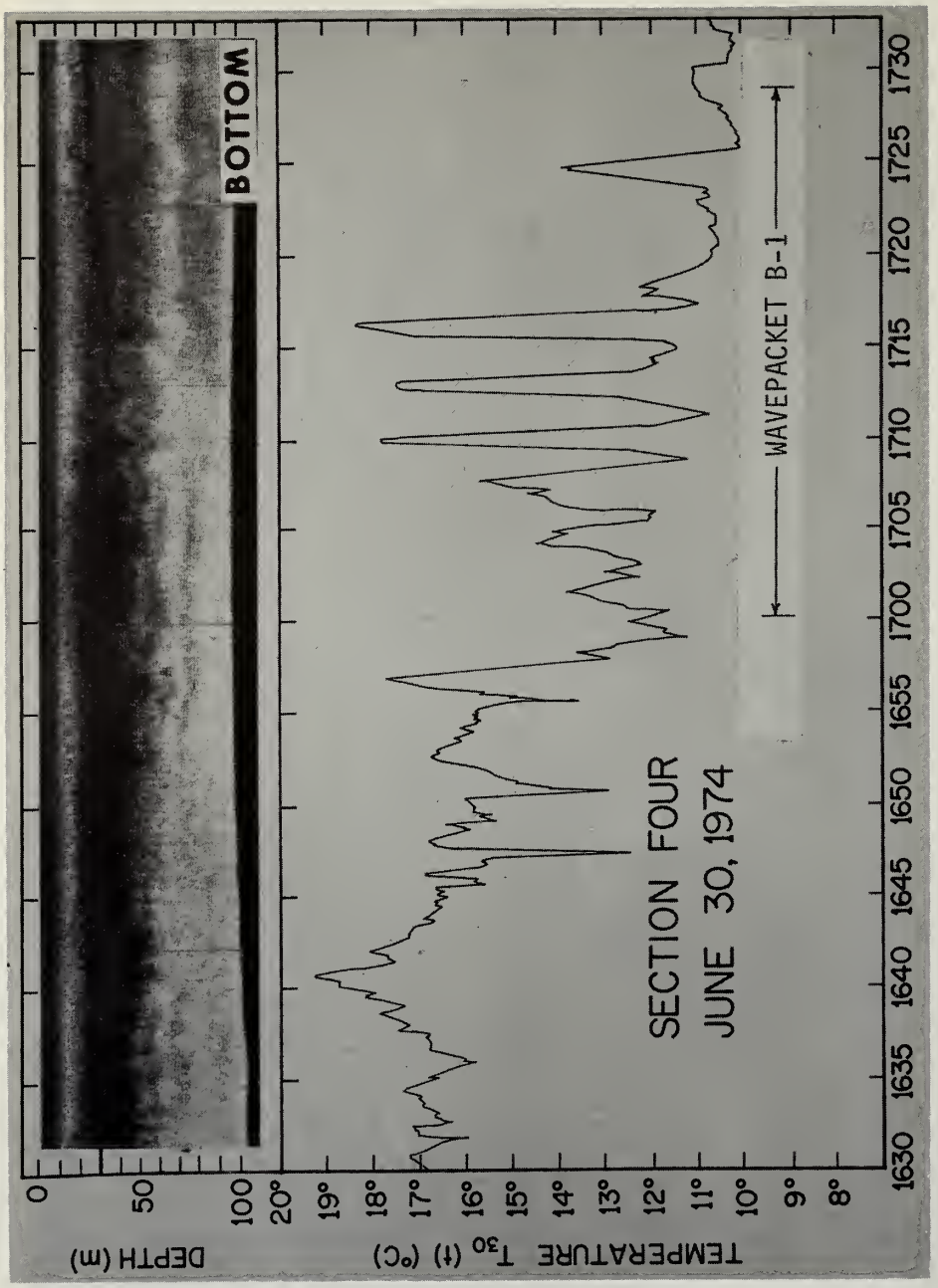

Figure 20. Region III (shelf). A continuation of figure 19. Note temperature peak at 1640 UT with dip of reflecting layer. The Westward overtook the internal-wave packet and sailed through it from 1700 to 1728 UT.

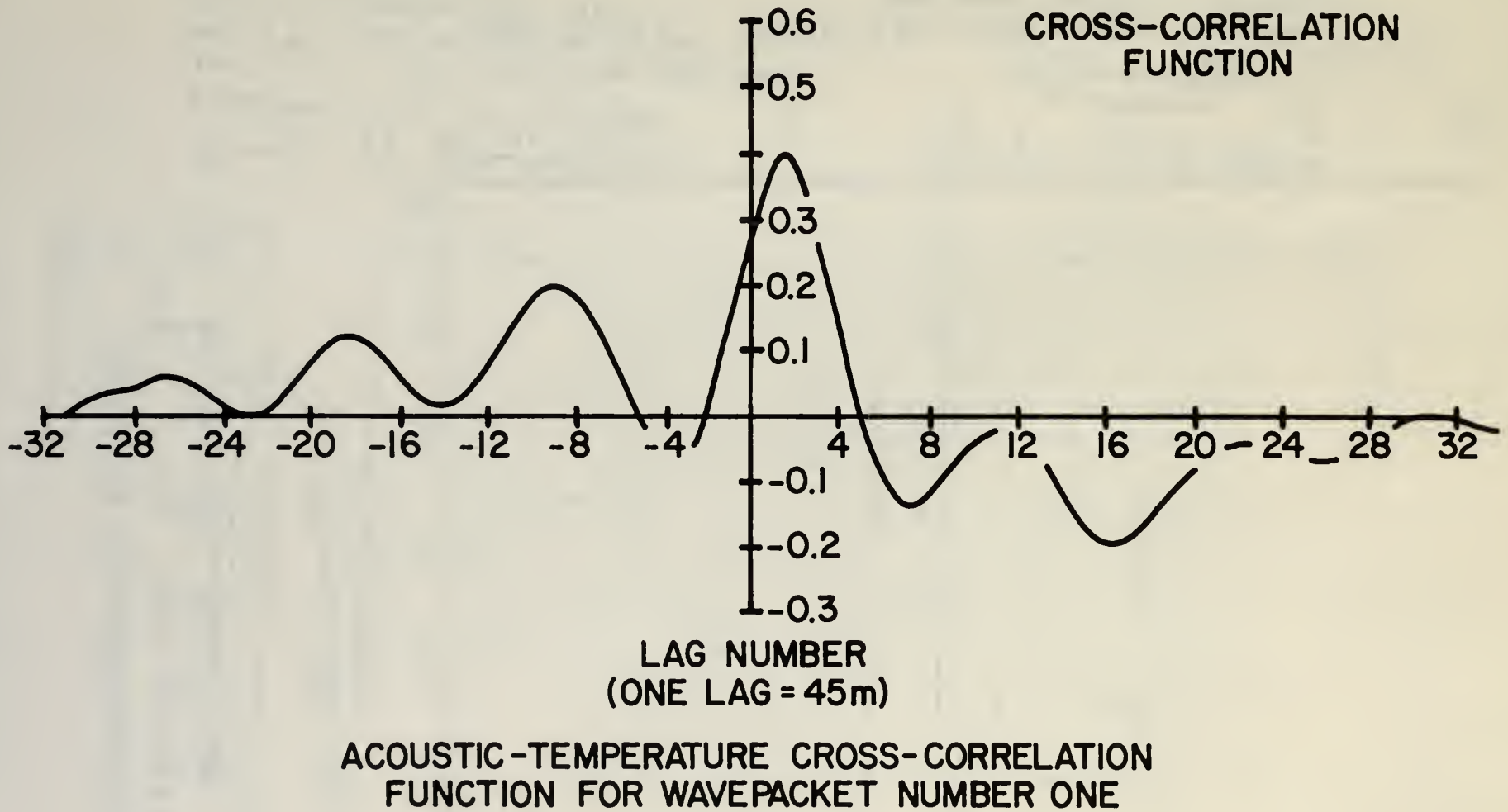

Figure 21. Cross-correlation, as a function of lag, between acoustic-echo depth and temperature recorded by thermistor towed at depth of 30 m.

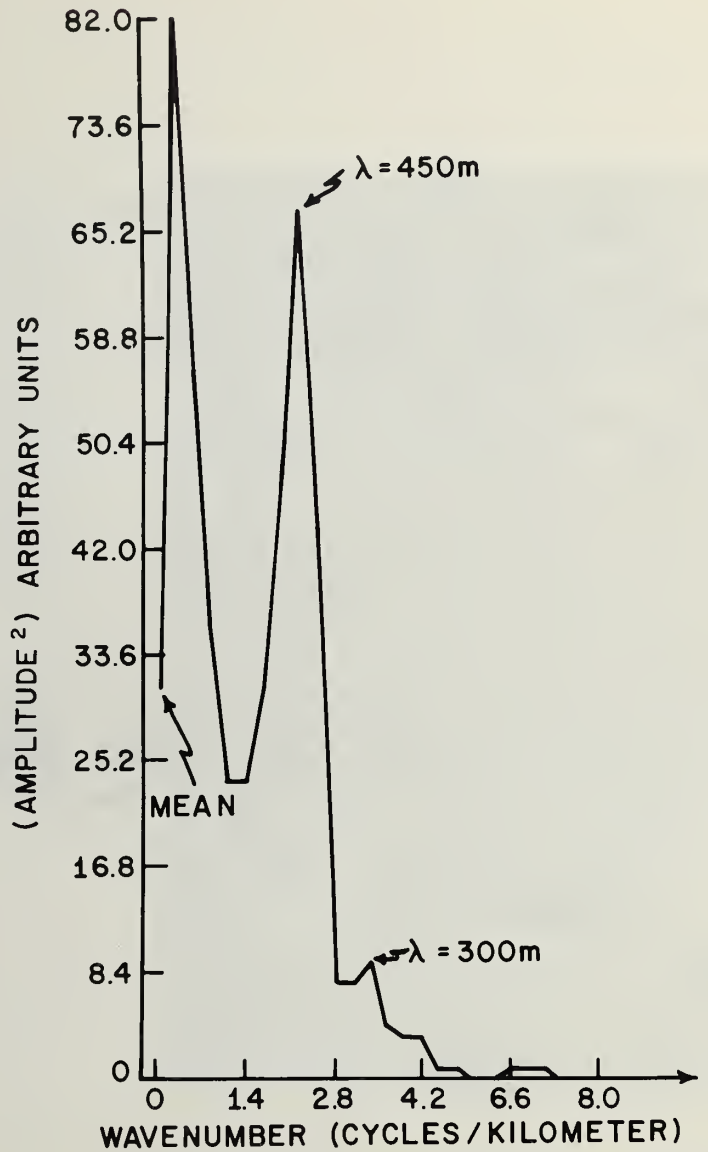

(AMPLITUDE)^2 CROSS-SPECTRUM (ARBITRARY UNITS) FOR WAVEPACKET ONE FROM ACOUSTIC--TEMPERATURE DATA.

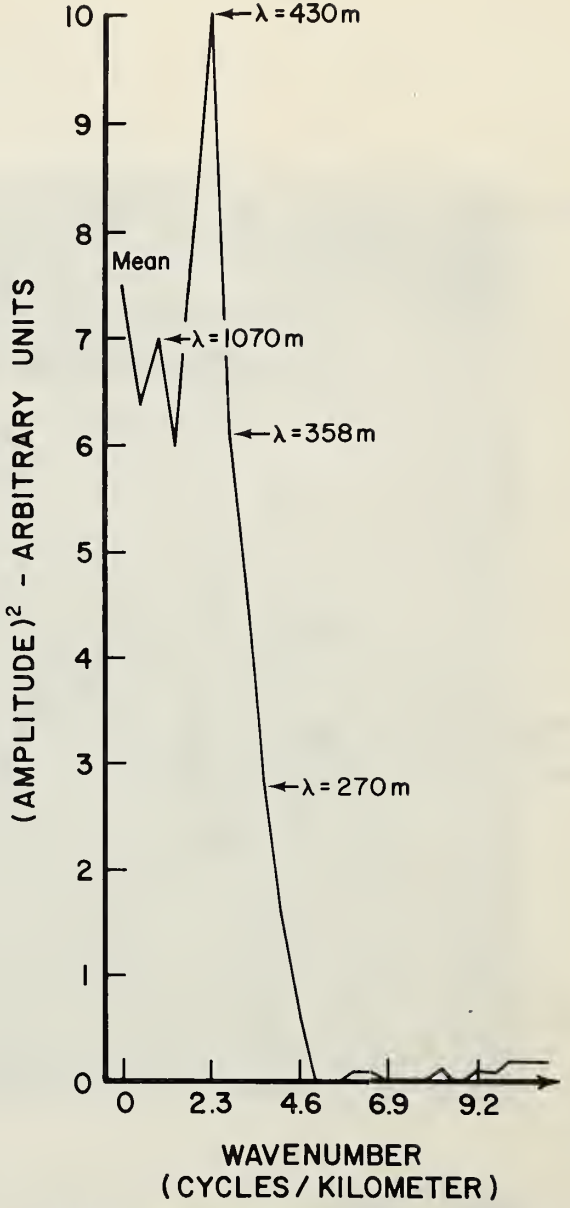

(AMPLITUDE)^2 CROSS-SPECTRUM (ARBITRARY UNITS) FOR WAVEPACKET THREE FROM ACOUSTIC - TEMPERATURE DATA

Figure 22. Power spectrum of acoustic temperature cross correlation

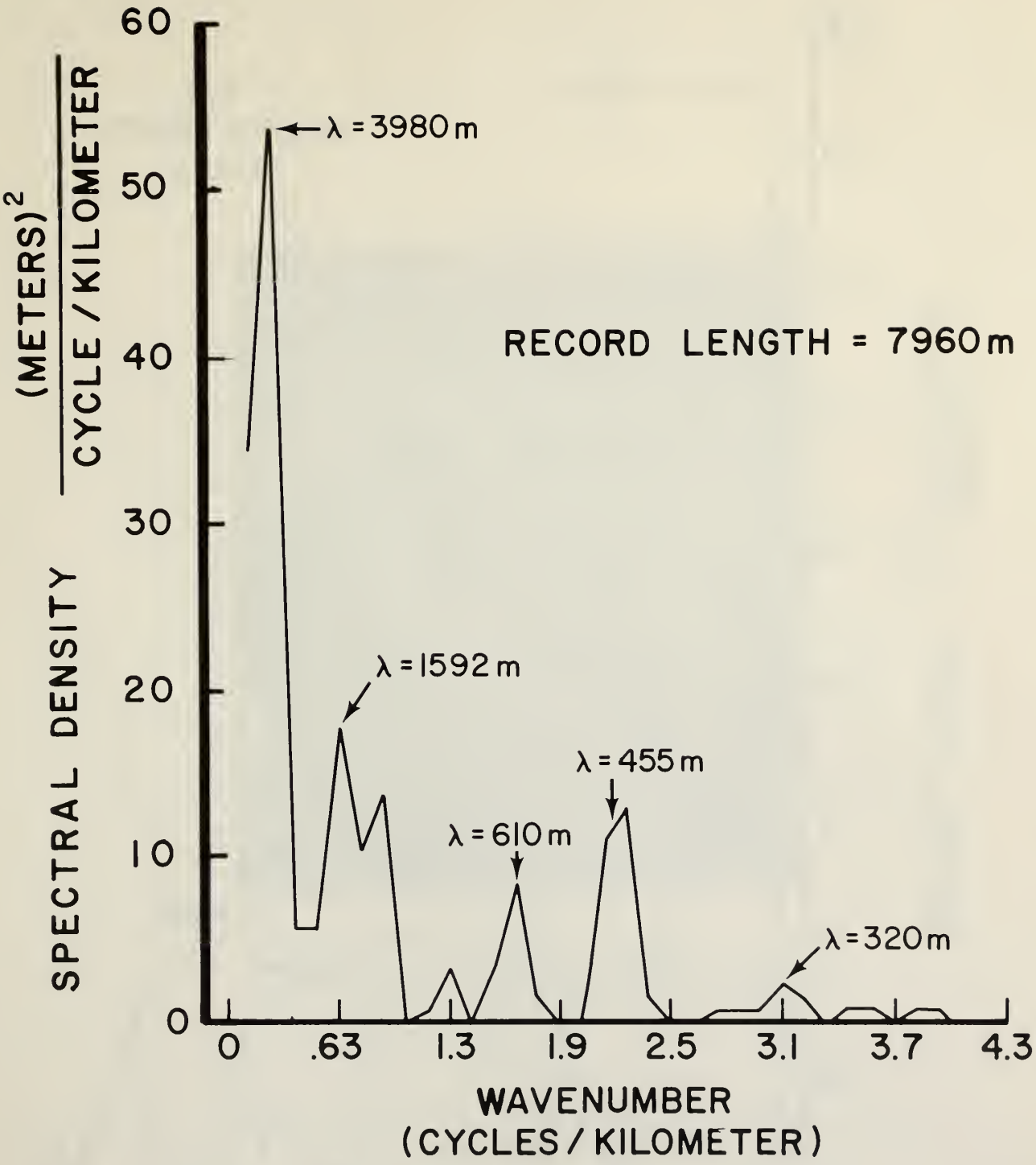

SPECTRAL DENSITY FOR WAVEPACKET ONE FROM ACOUSTIC DATA (SHIP PROCEEDING IN THE DIRECTION OF WAVEPACKET PROPAGATION)

Figure 23. Spectrum for acoustic data.

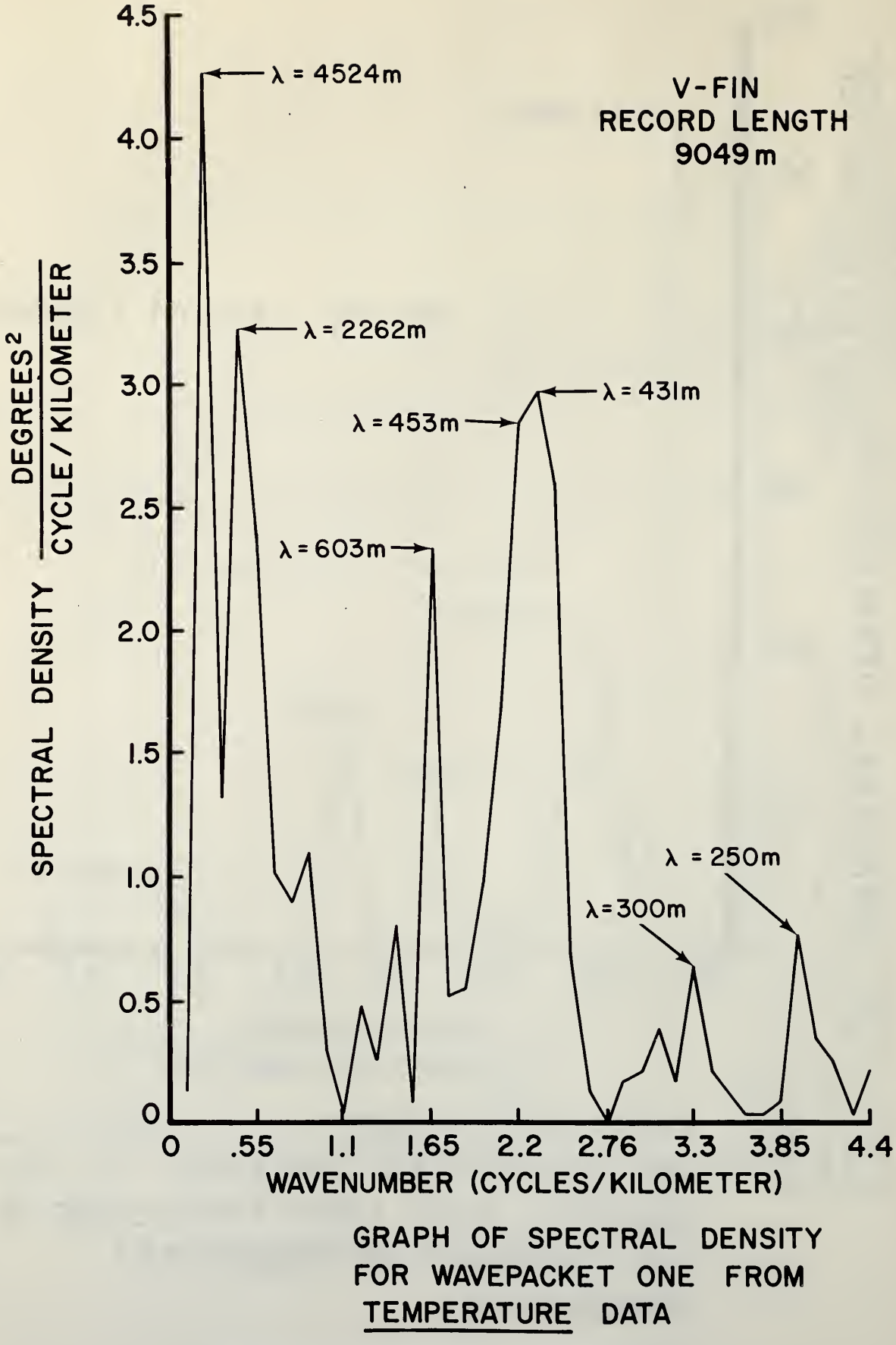

Figure 24. Spectrum for thermistor data.

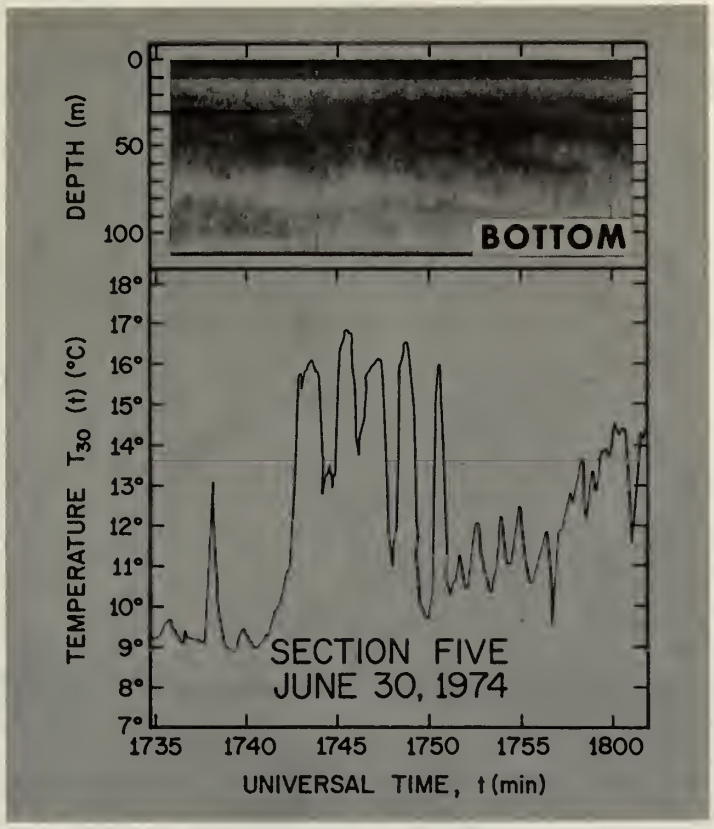

Figure 25. Acoustic and thermistor data taken as Westward met the internal-wave packet B-2 head on and sailed through it in the direction opposite to that of previous encounter (fig. 20).

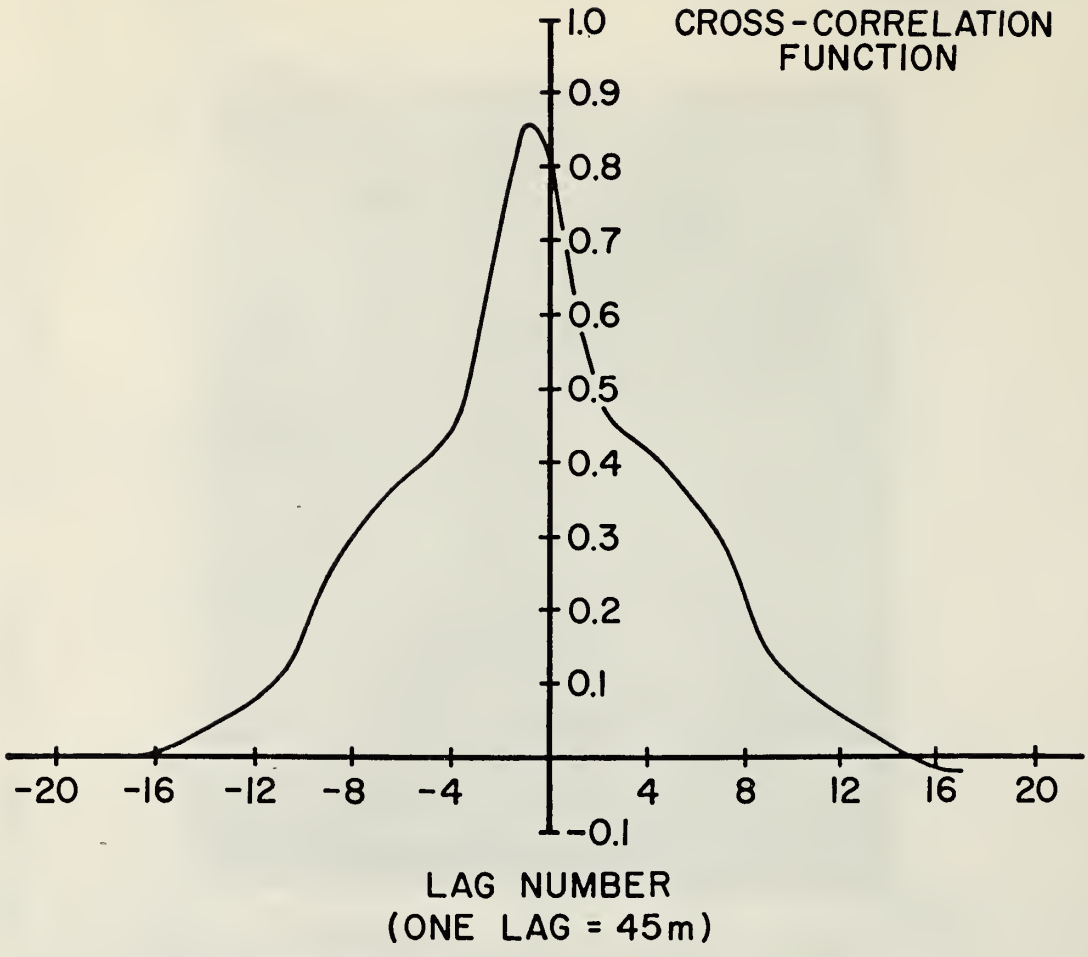

Figure 26. Cross-correlation between depth of acoustic echo and temperature at towed thermistor recorded during reverse run through the internal-wave packet.

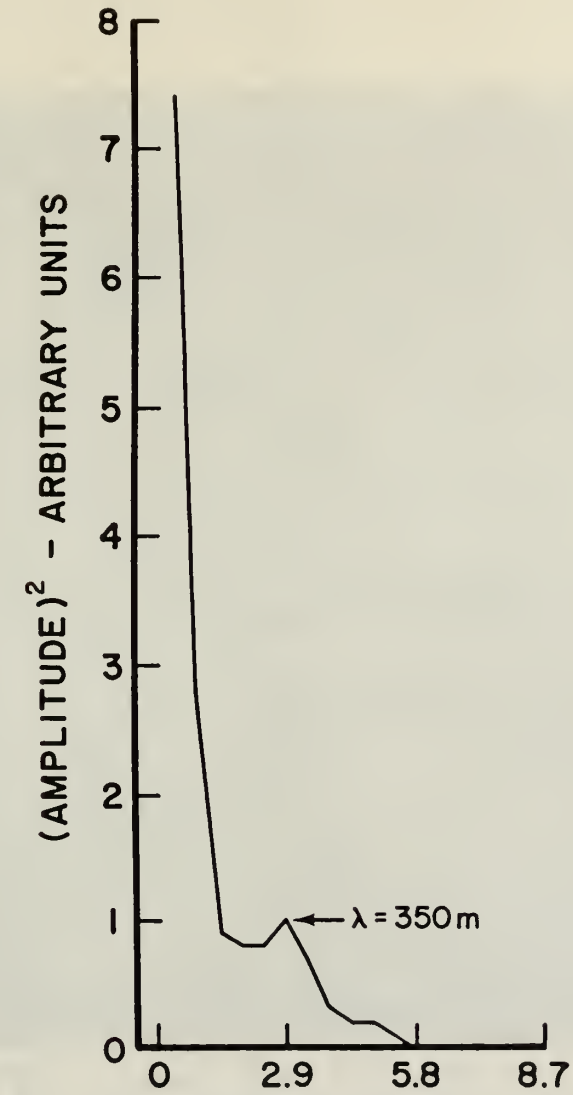

Figure 27. Power spectrum for cross-correlation function of figure 26.

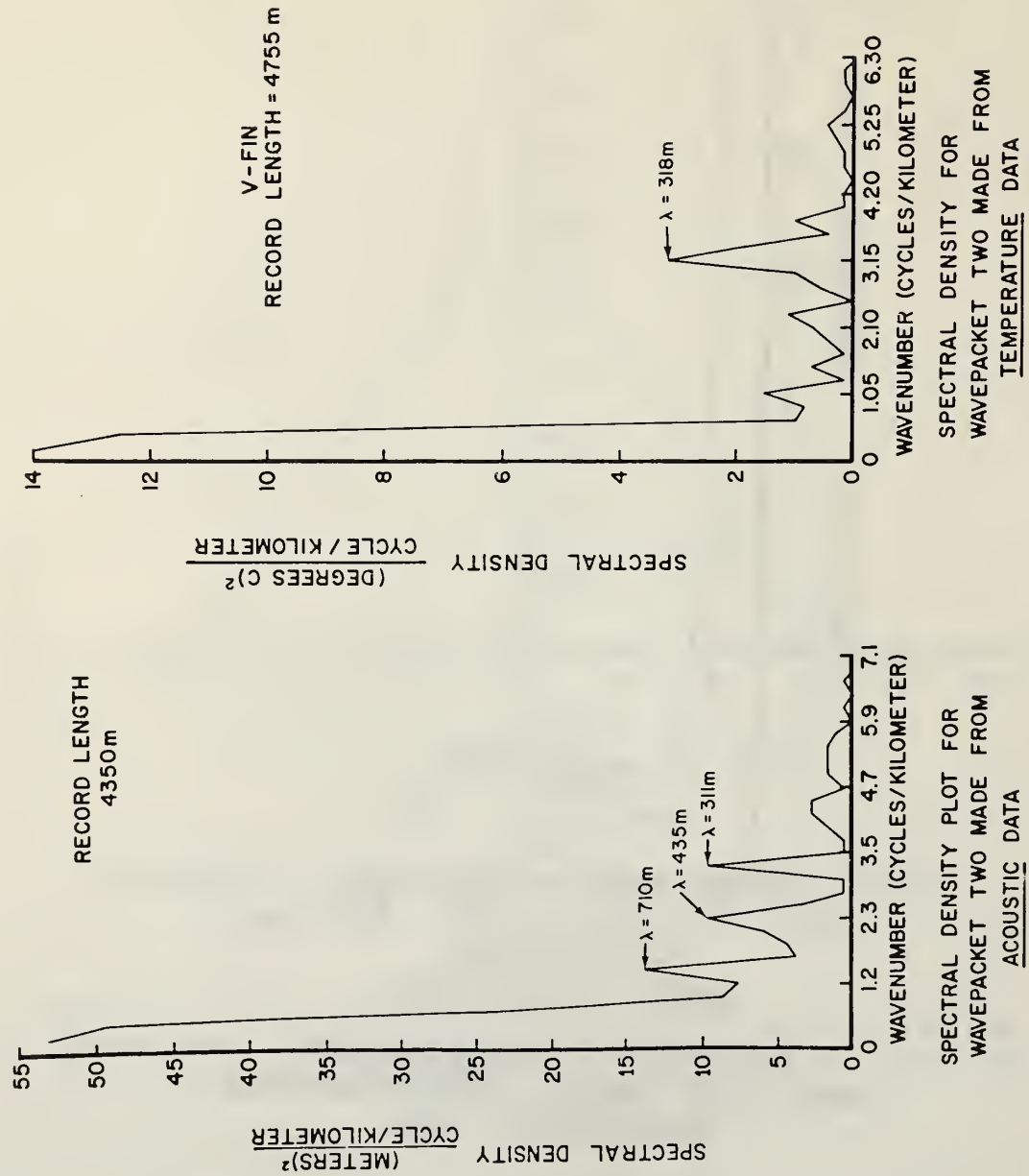

Figure 28. Spectra for acoustic data and temperature data taken during reverse run through wavepacket.

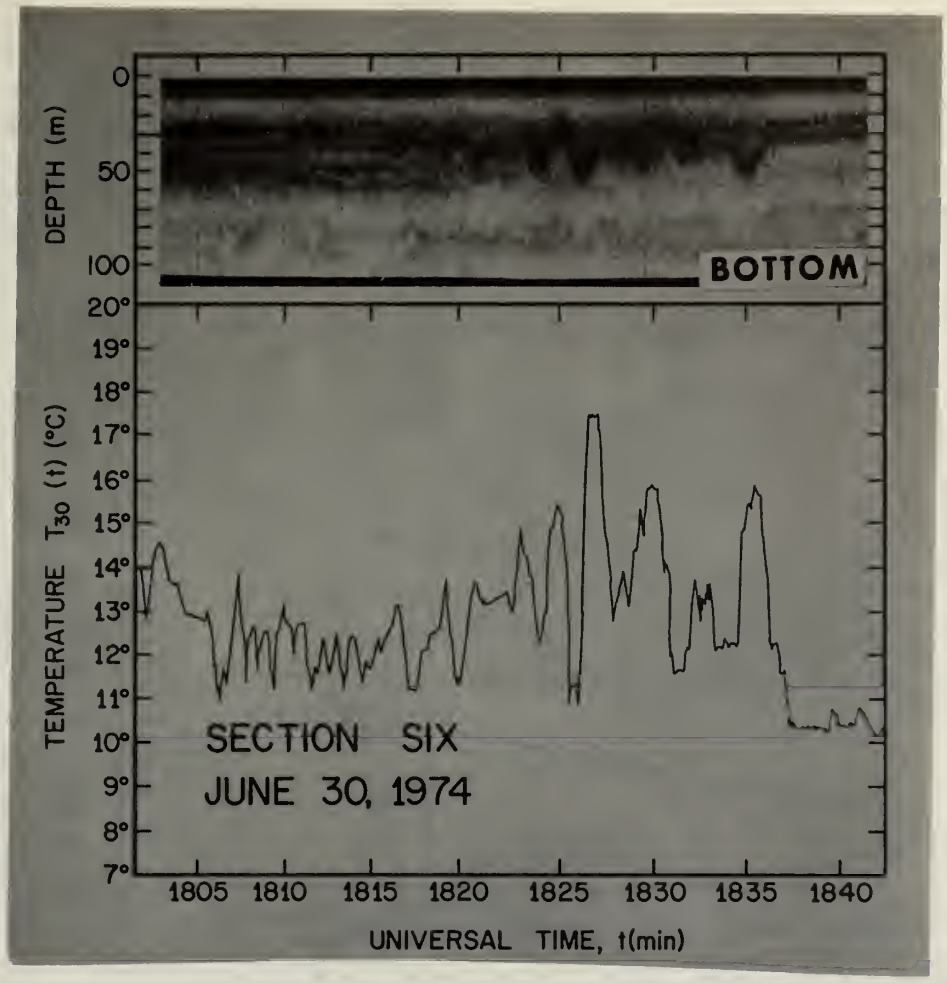

Figure 29. Acoustic echo and temperature recorded by towed thermistor on third pass through internal-wave packet B-3 in the forward direction.

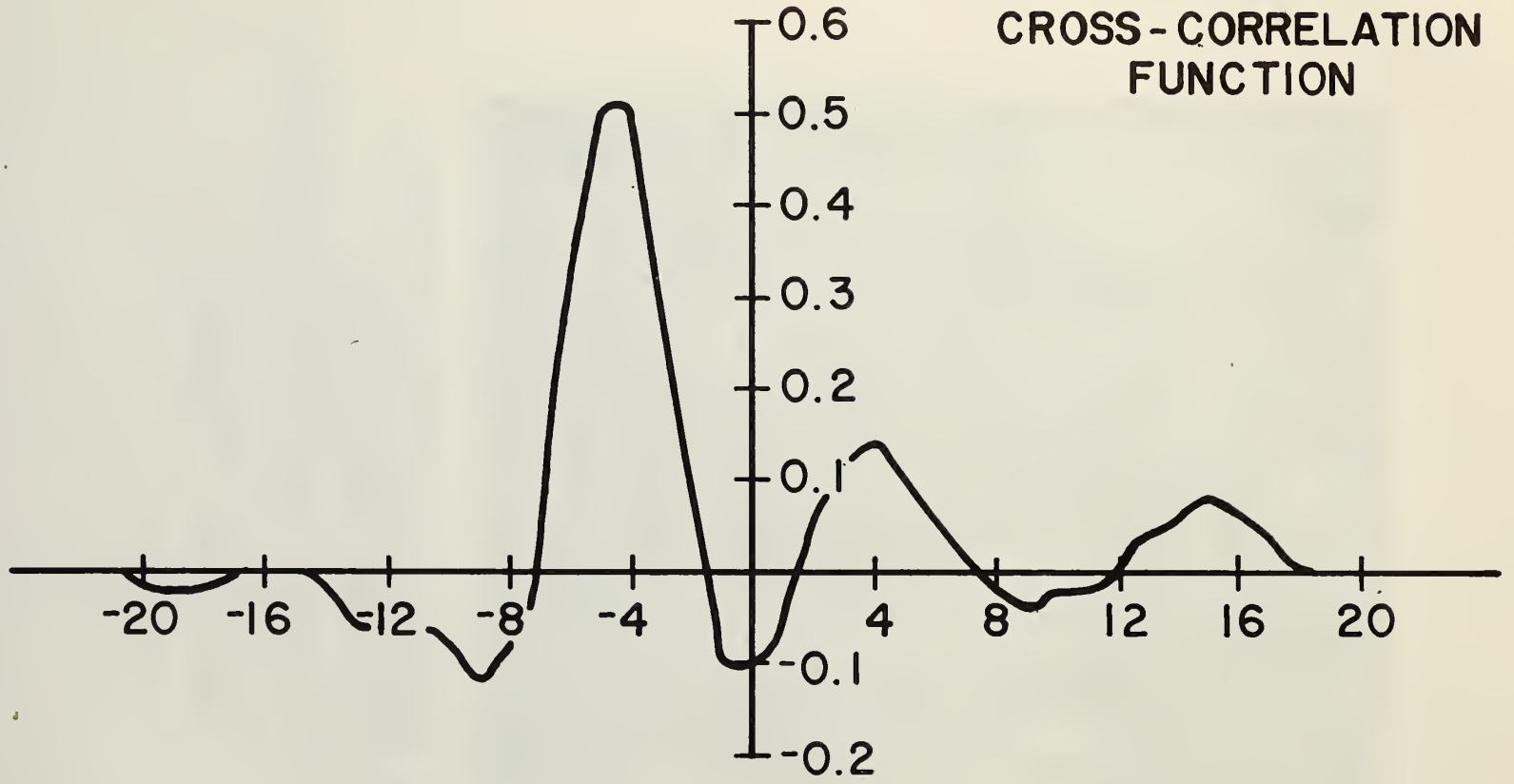

Figure 30. Cross-correlation between acoustic and thermistor data taken during third pass.

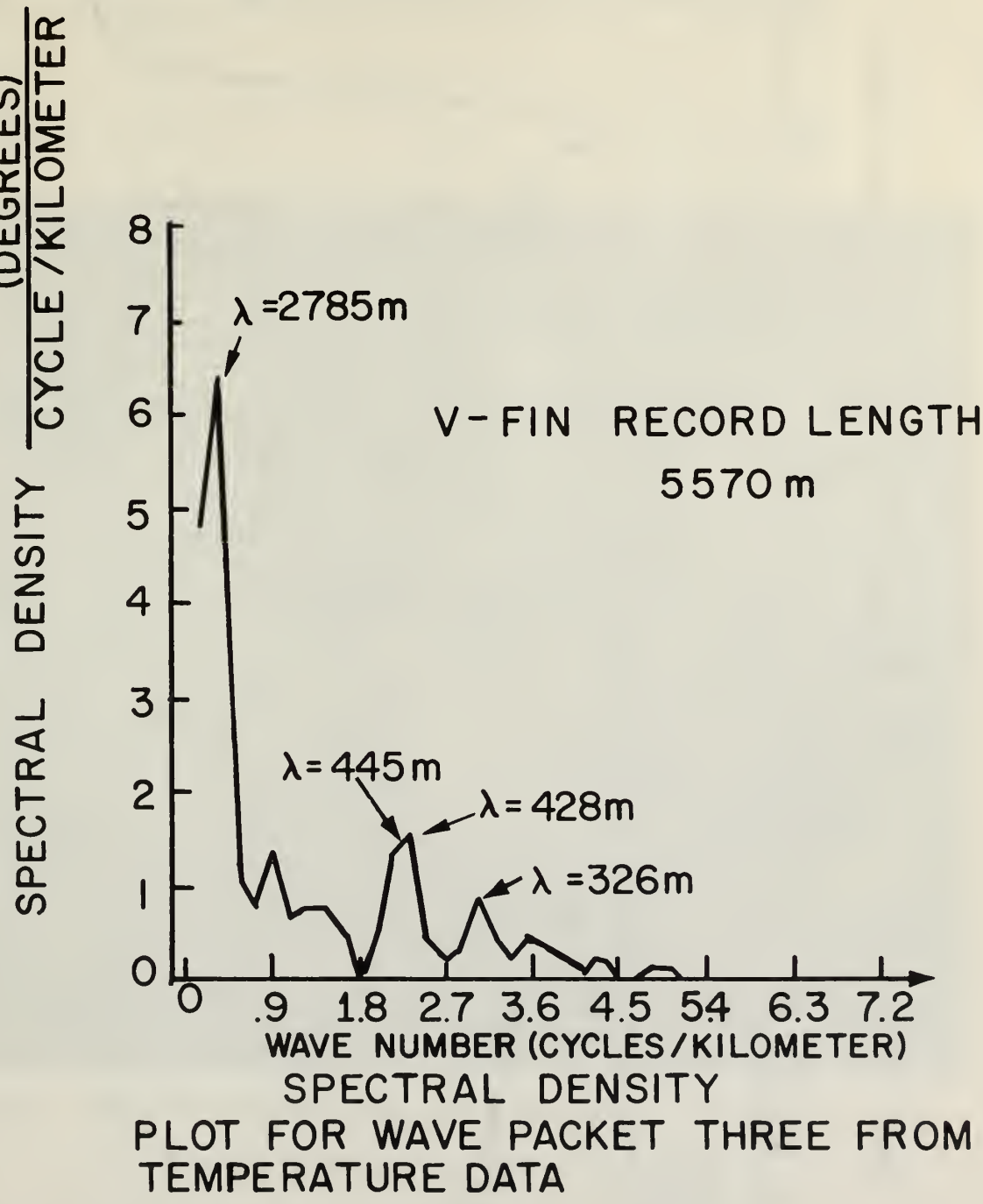

Figure 31a. Power spectrum for temperature data, third pass through wavepacket.

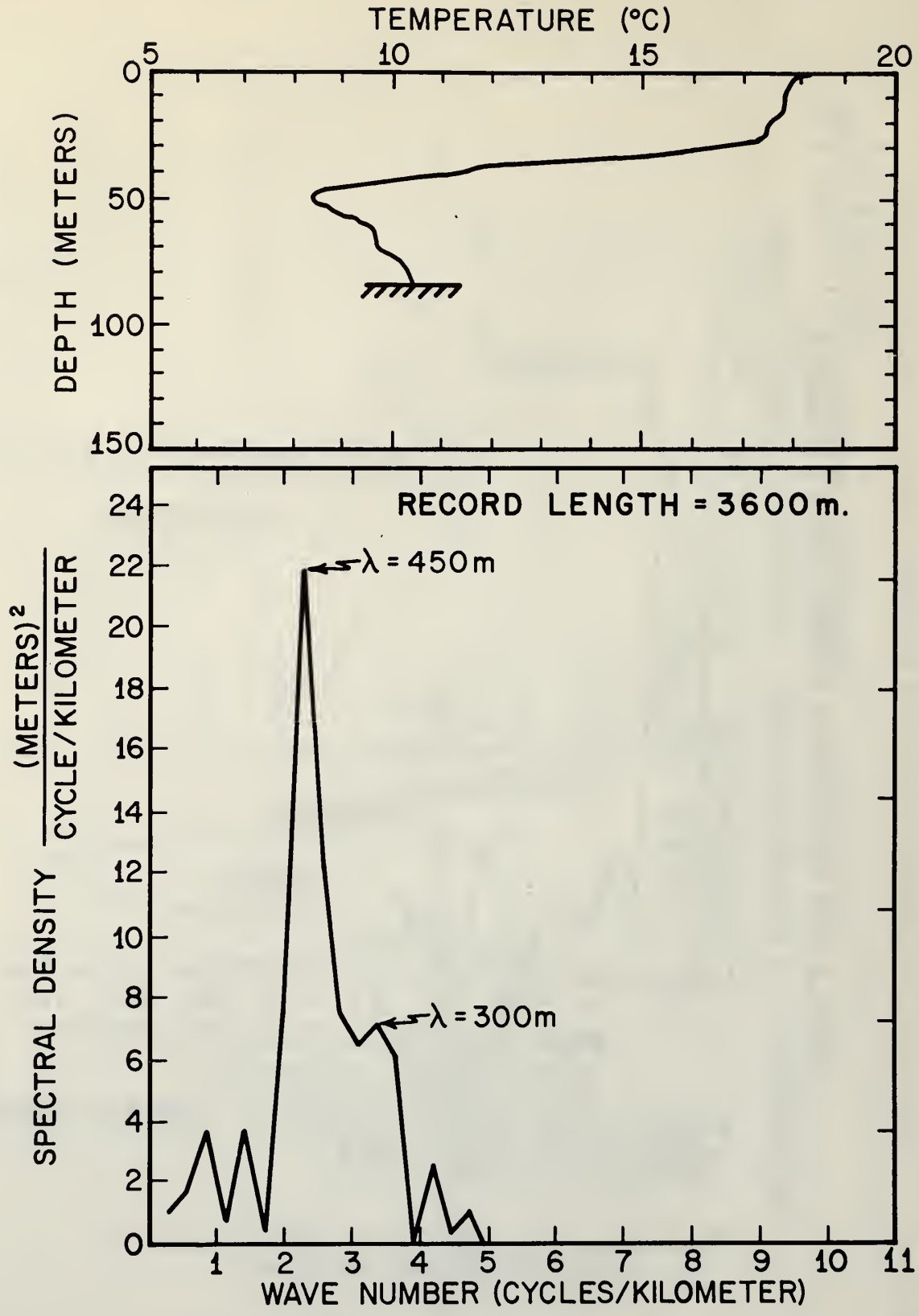

SPECTRAL DENSITY PLOT FOR WAVE PACKET THREE FROM ACOUSTIC DATA.

Figure 31b. Power spectrum for acoustic data, third pass through wavepacket.

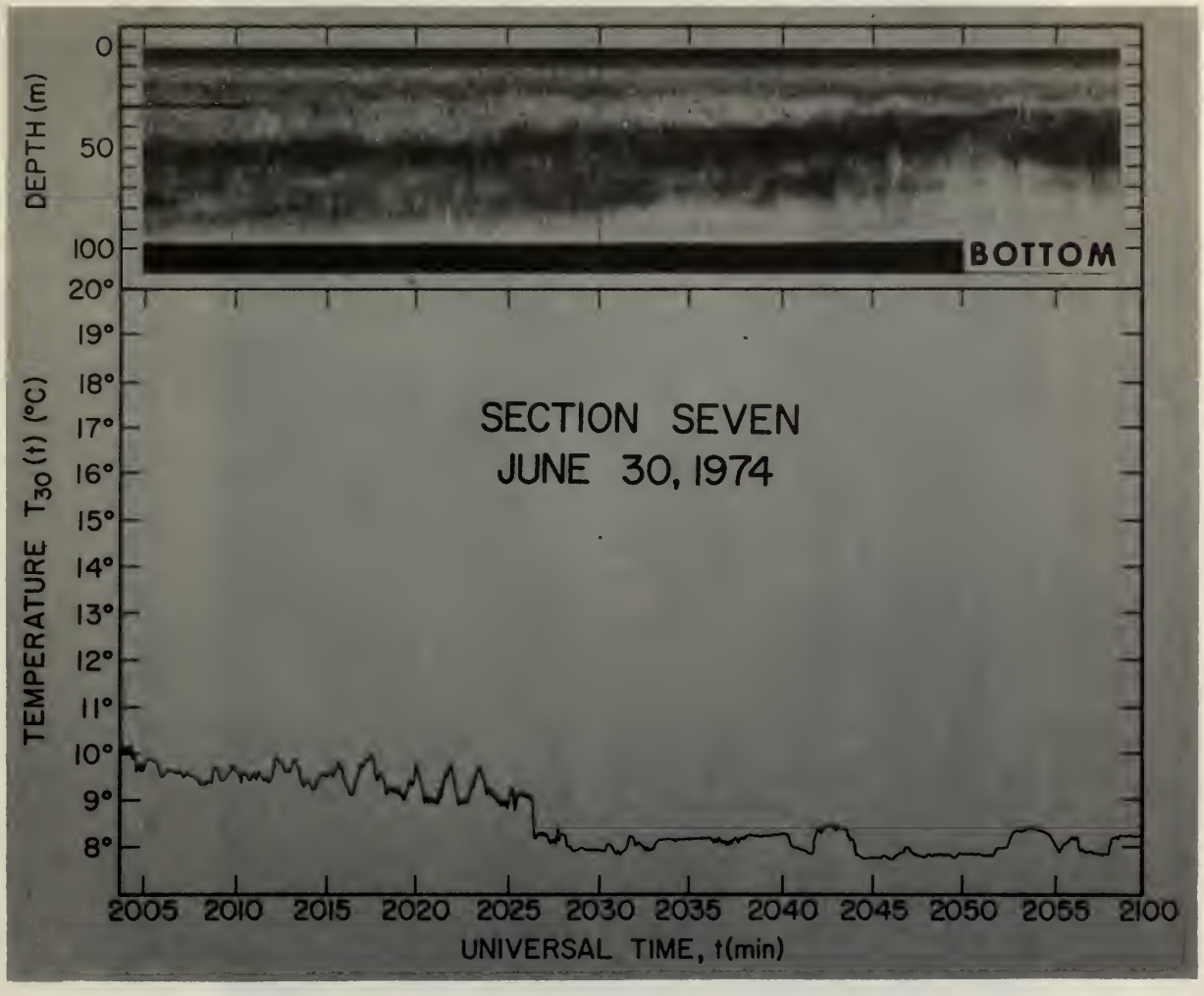

Figure 32. Acoustic and thermistor data taken on the continental shelf.

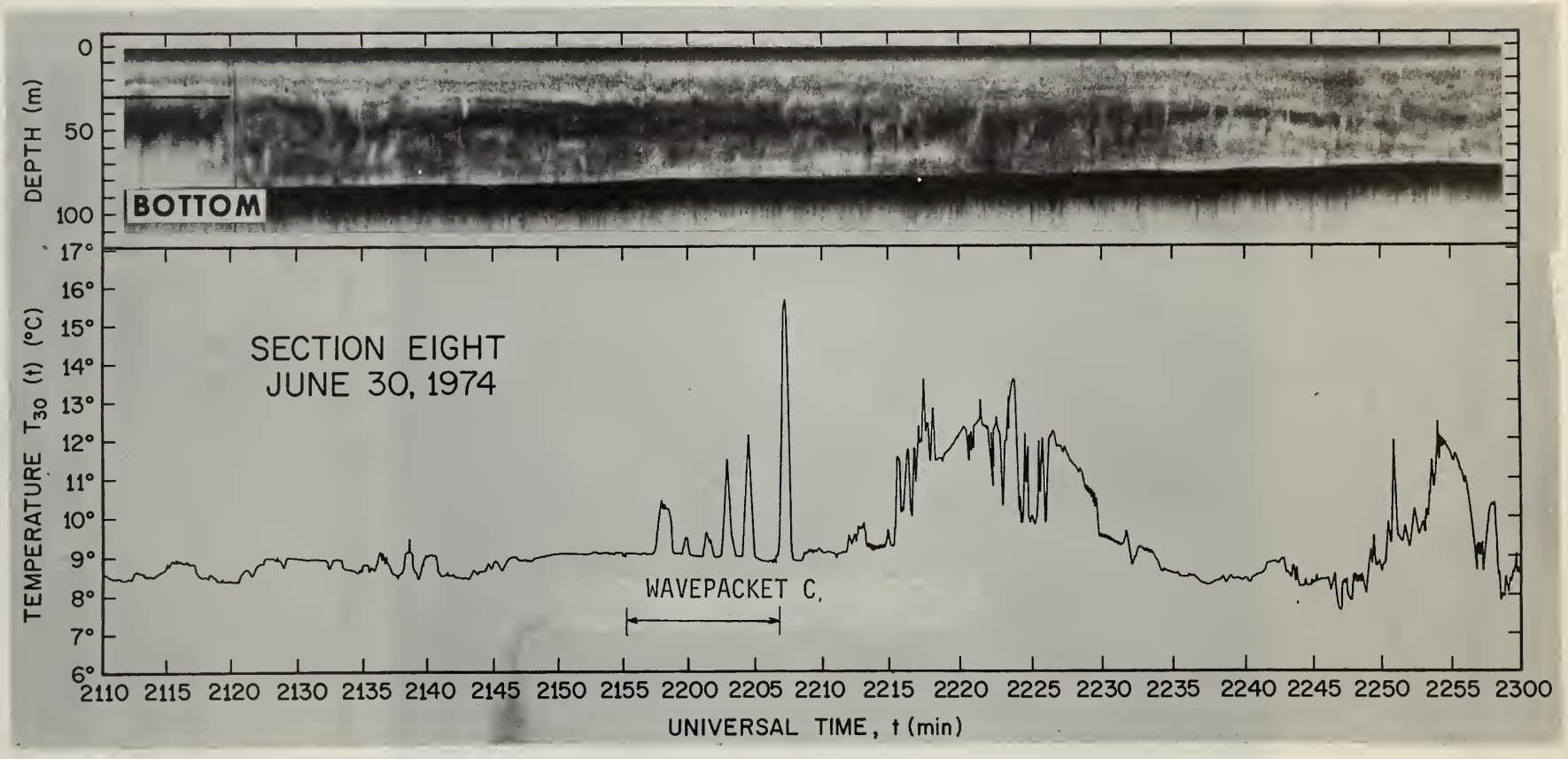

Figure 33. Acoustic and thermistor data taken on the continental shelf showing an overtaken internal-wave packet (2155 to 2207 UT) and zones of warm water (2215 to 2235 UT and 2245 to 2300 UT).

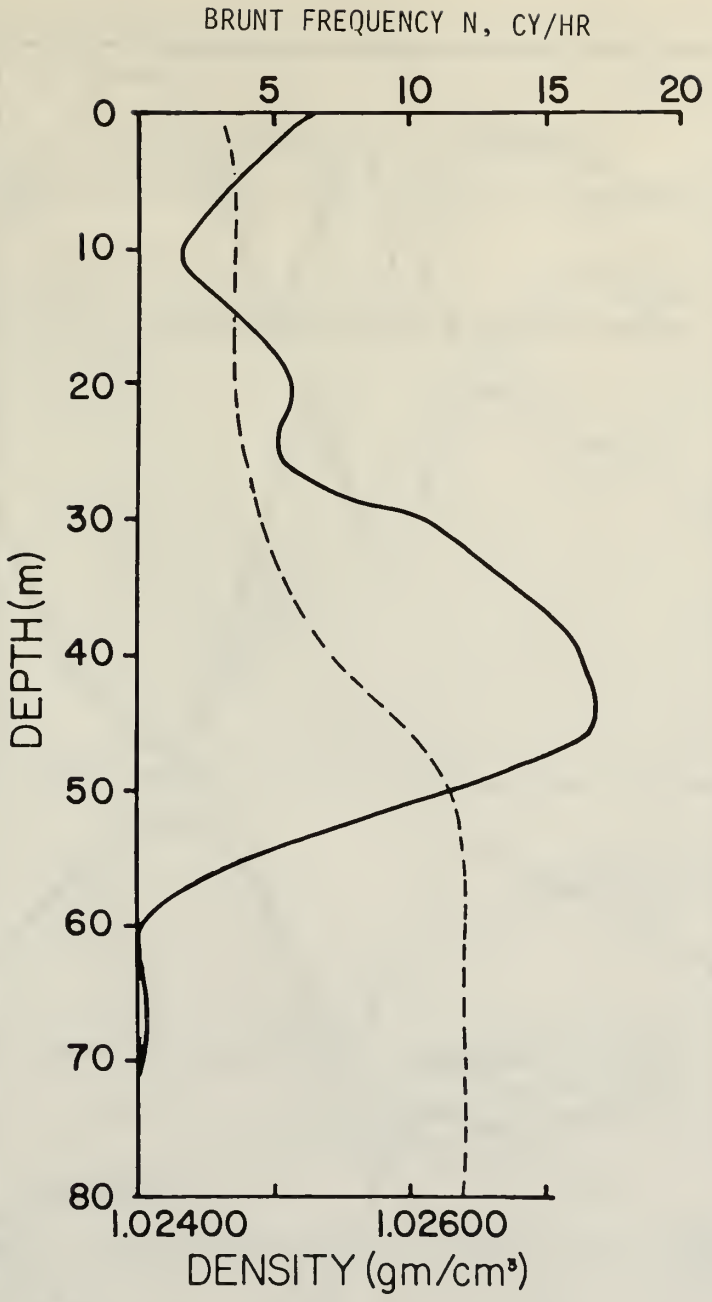

Figure 34. Vertical profiles of density (dashed) and Brunt-Väisälä frequency (solid) on the continental shelf during NYBERSEX.

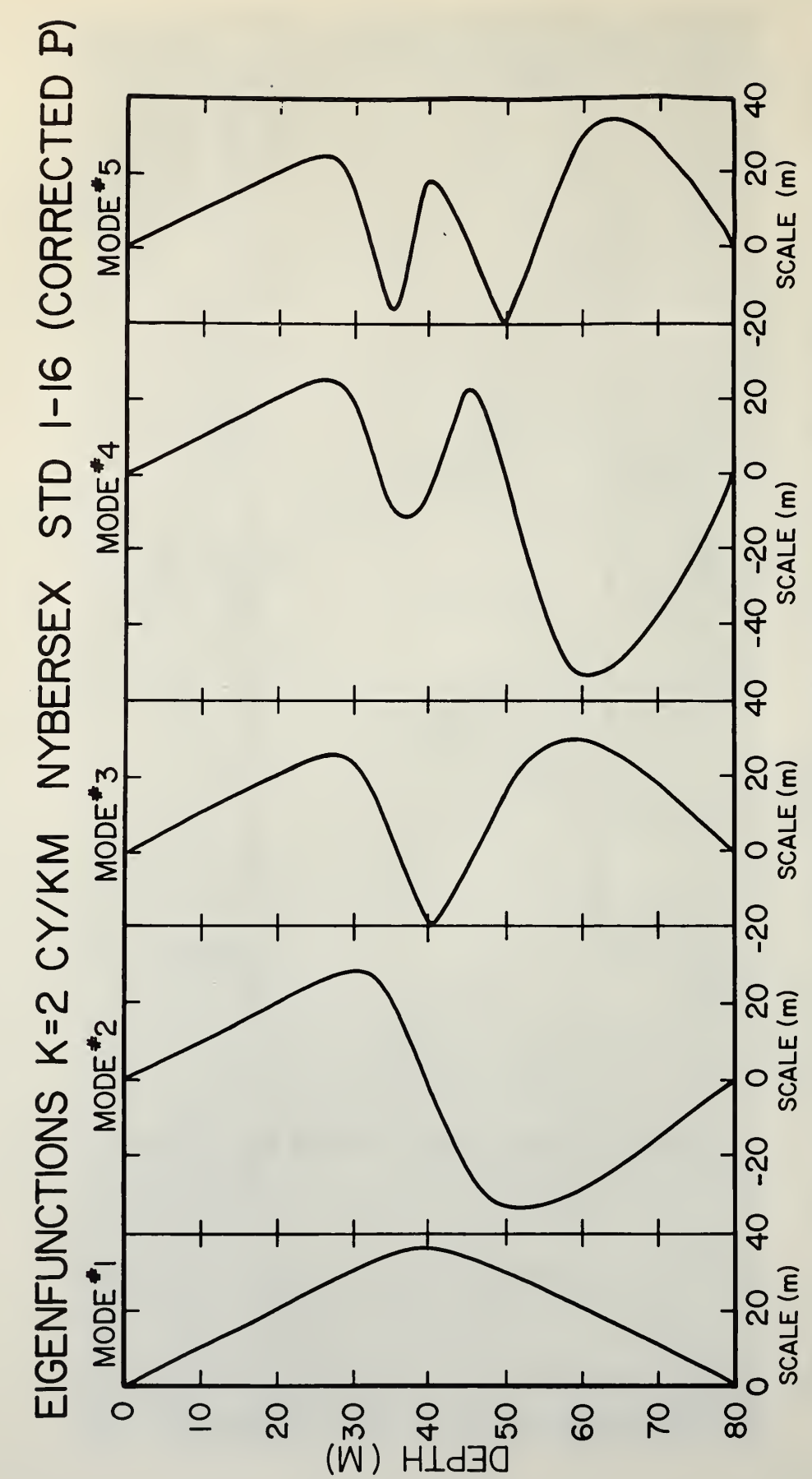

Figure 35. Eigenfunctions for the first five modes calculated from the density profile of figure 34.

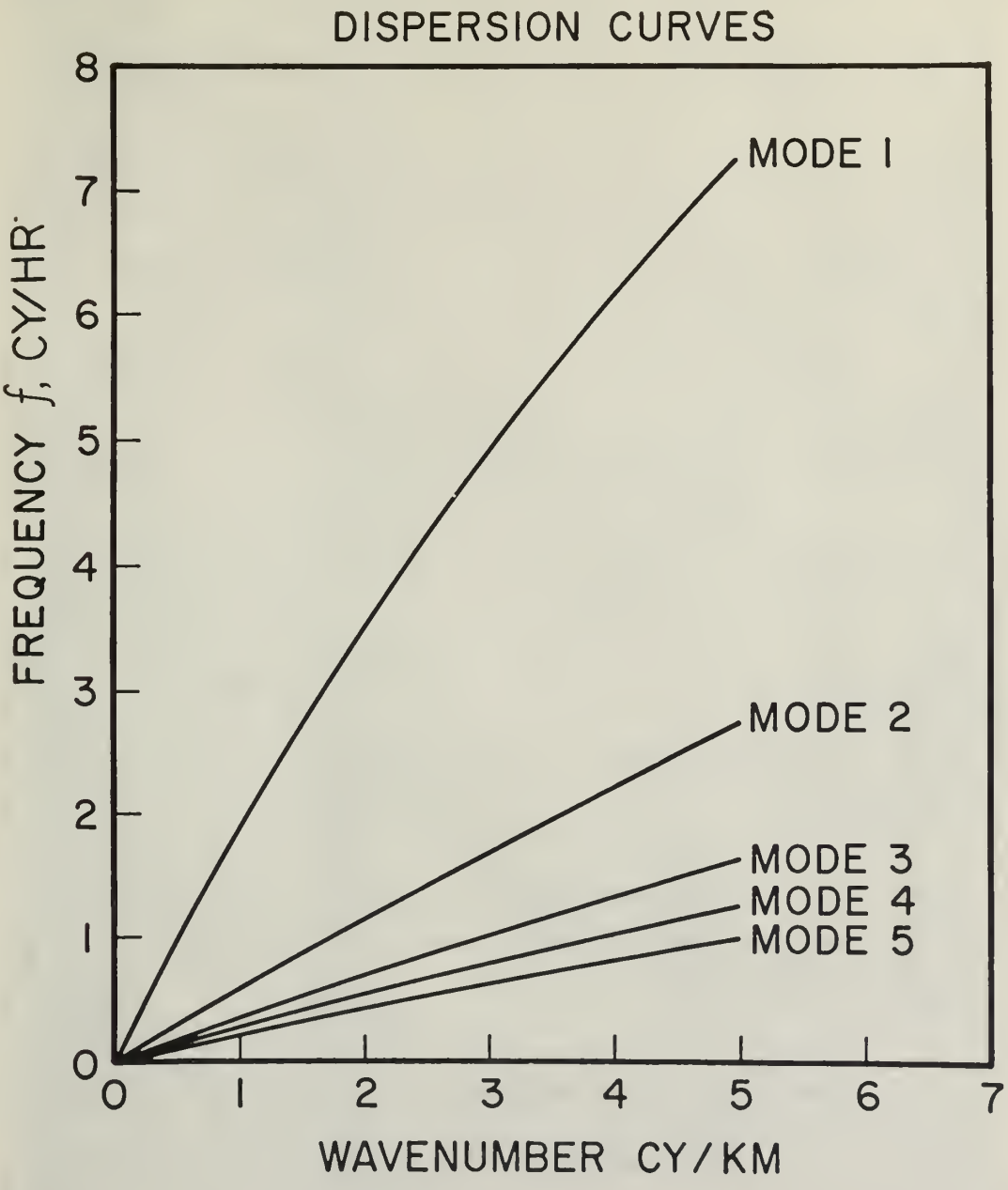

Figure 36. Dispersion curves relating frequency to wave number for the first five modes with the density profile of figure 34.

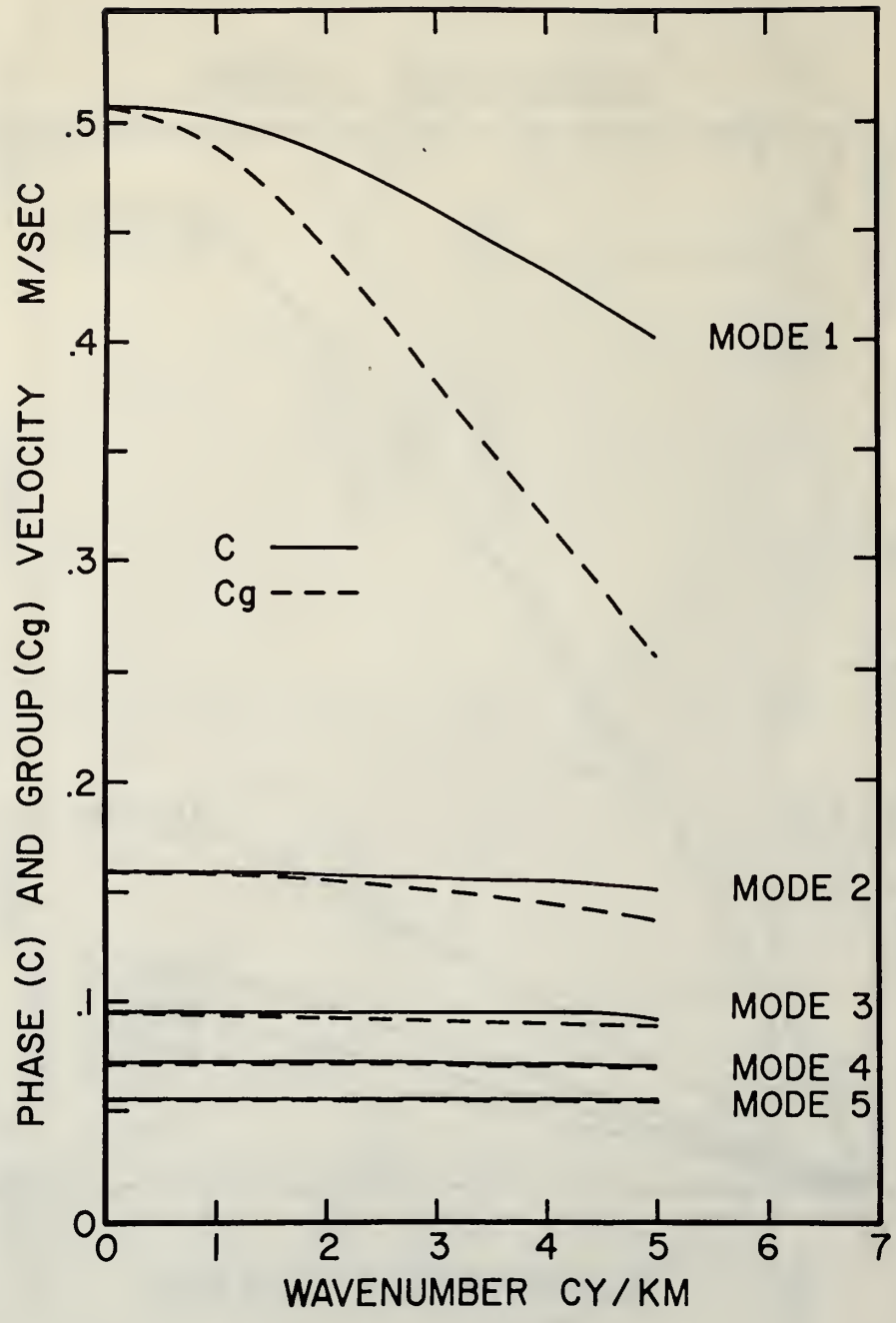

Figure 37. Phase speed (solid) and group speed (dashed) for the first five modes with the density profile of figure 34.

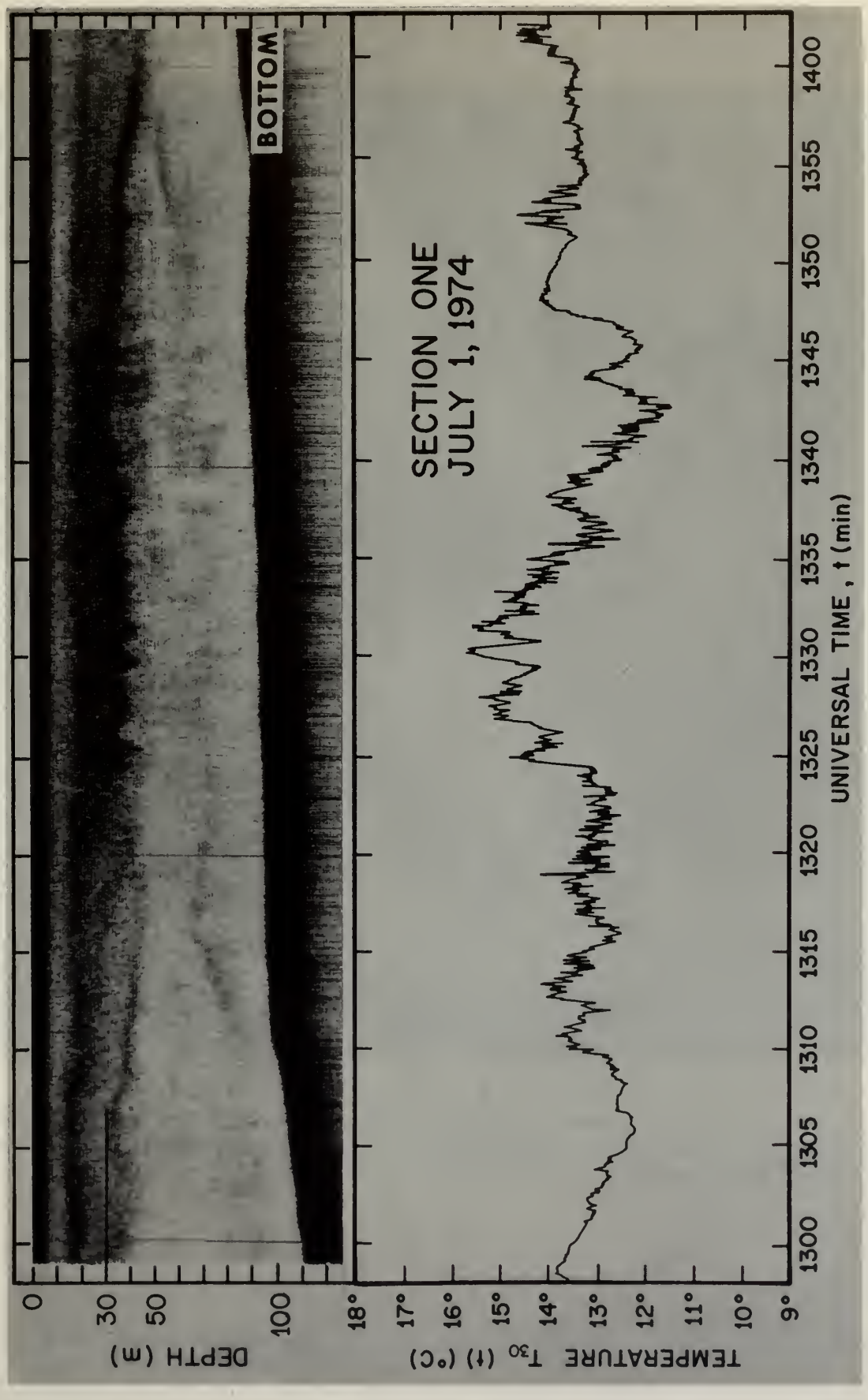

Figure 38. Acoustic (top) and temperature data taken before the triangle maneuver, July 1, 1974. Between 1320 and 1350 UT oscillations are seen that correspond to possible internal-wave packet No. 1, interpreted as a newly developing packet.

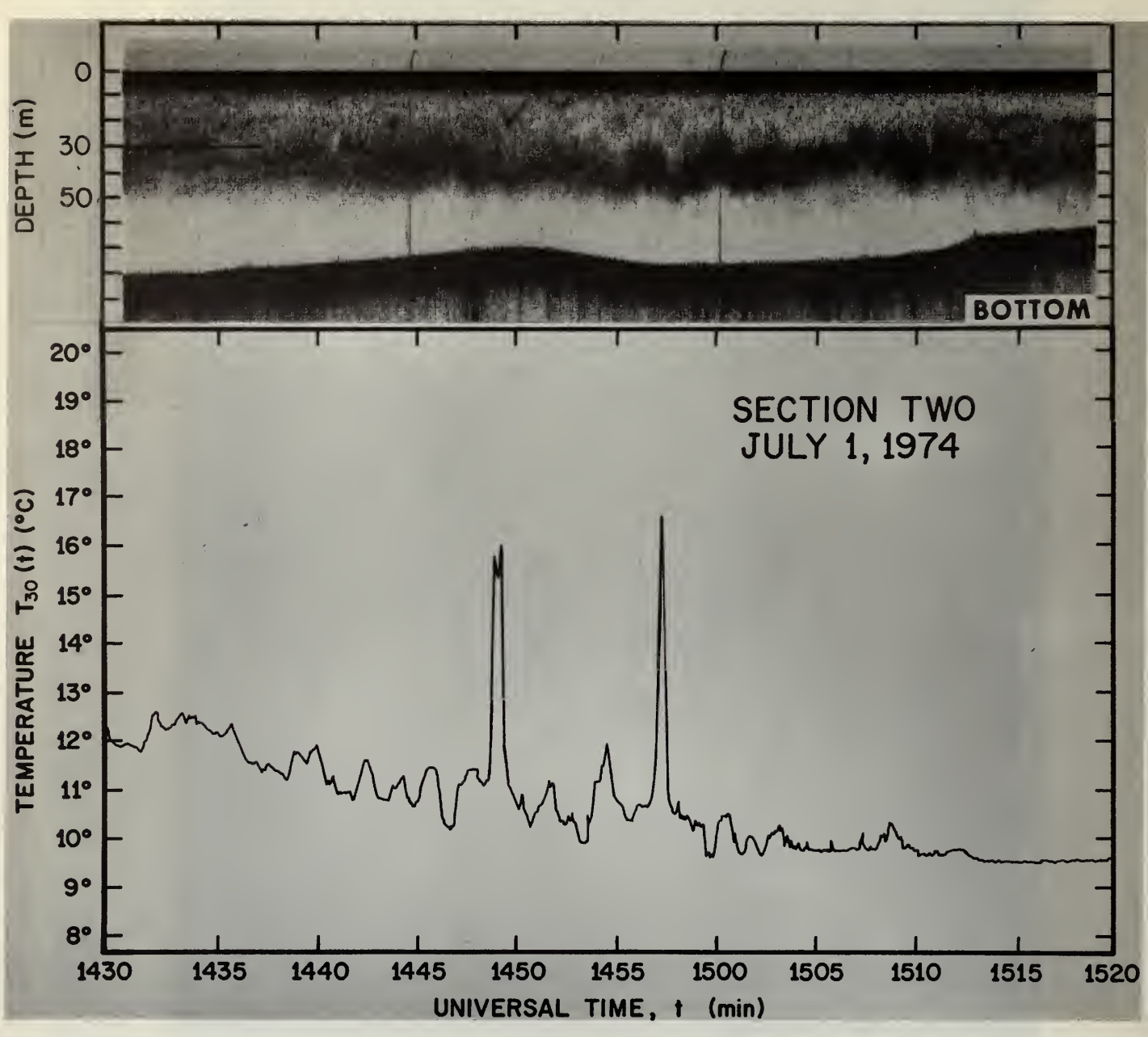

Figure 39. Acoustic (top) and temperature data taken before the triangle maneuver. The temperature spikes at 1448 UT and at 1457 UT may correspond to a poorly developed internal-wave packet.

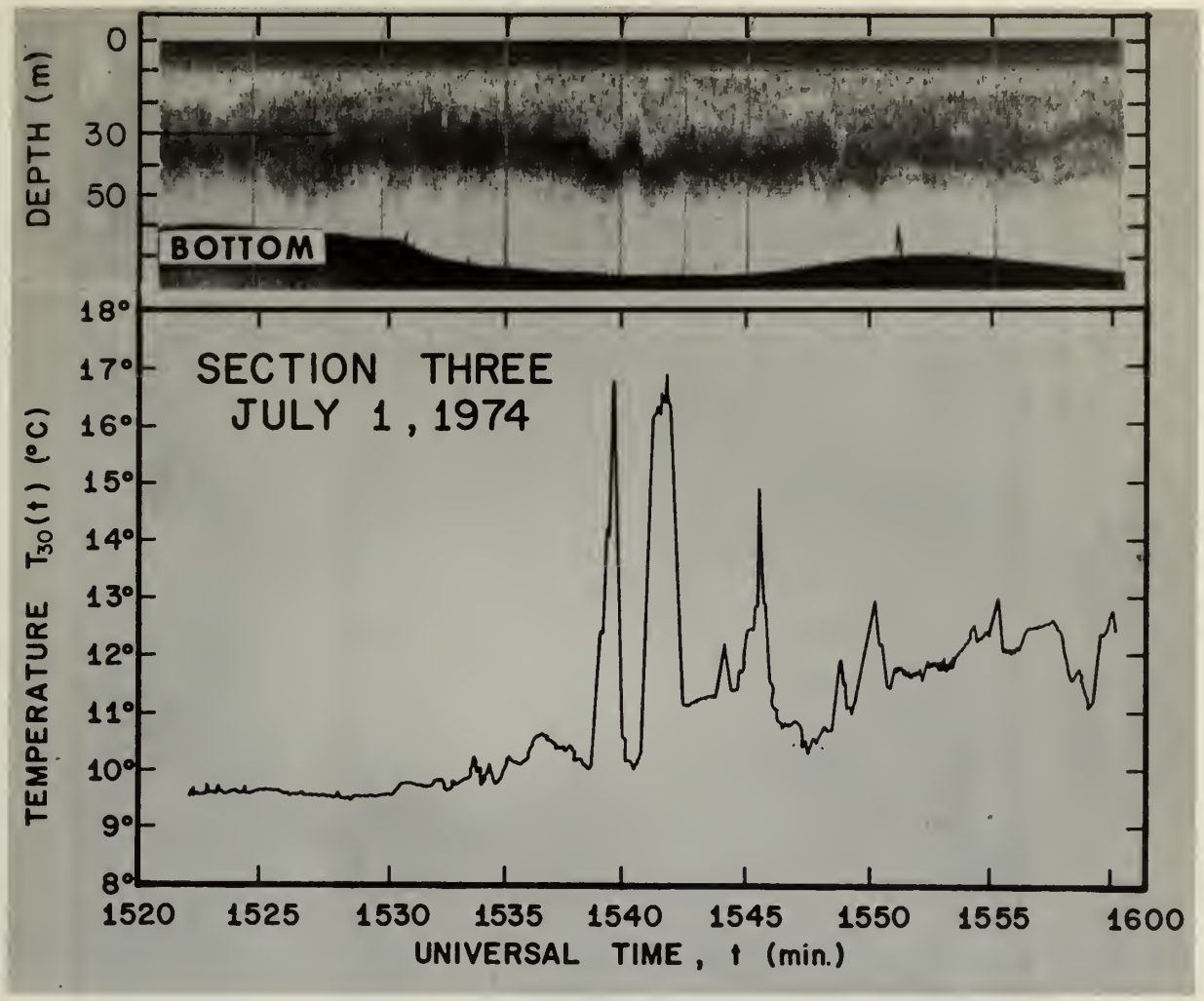

Figure 40. Acoustic (top) and towed-thermistor data for Leg 1 of the triangle maneuver.

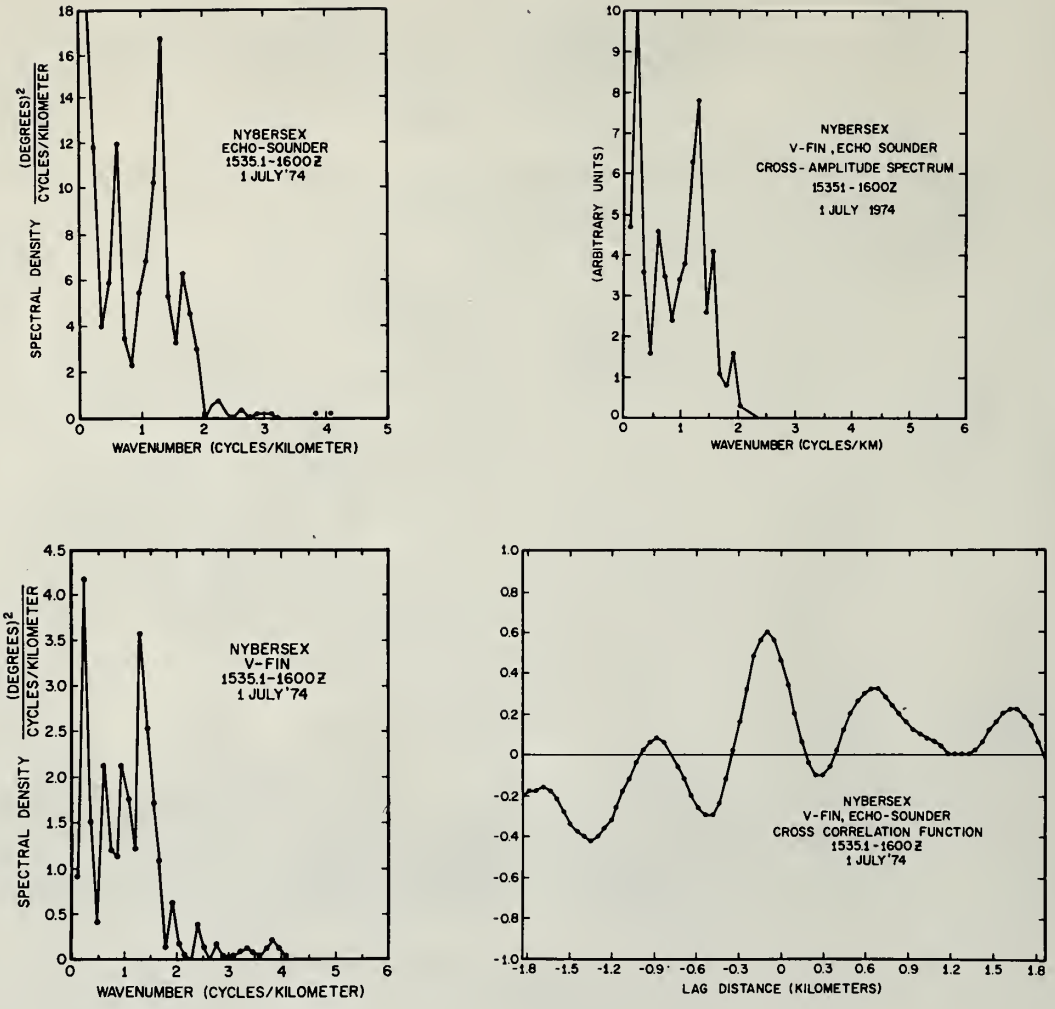

Figure 41. July 1, 1974, Leg 1. Counter-clockwise from upper left: power spectrum for acoustic sounder; power spectrum of temperature; acoustic-temperature cross-correlation; cross-spectrum.

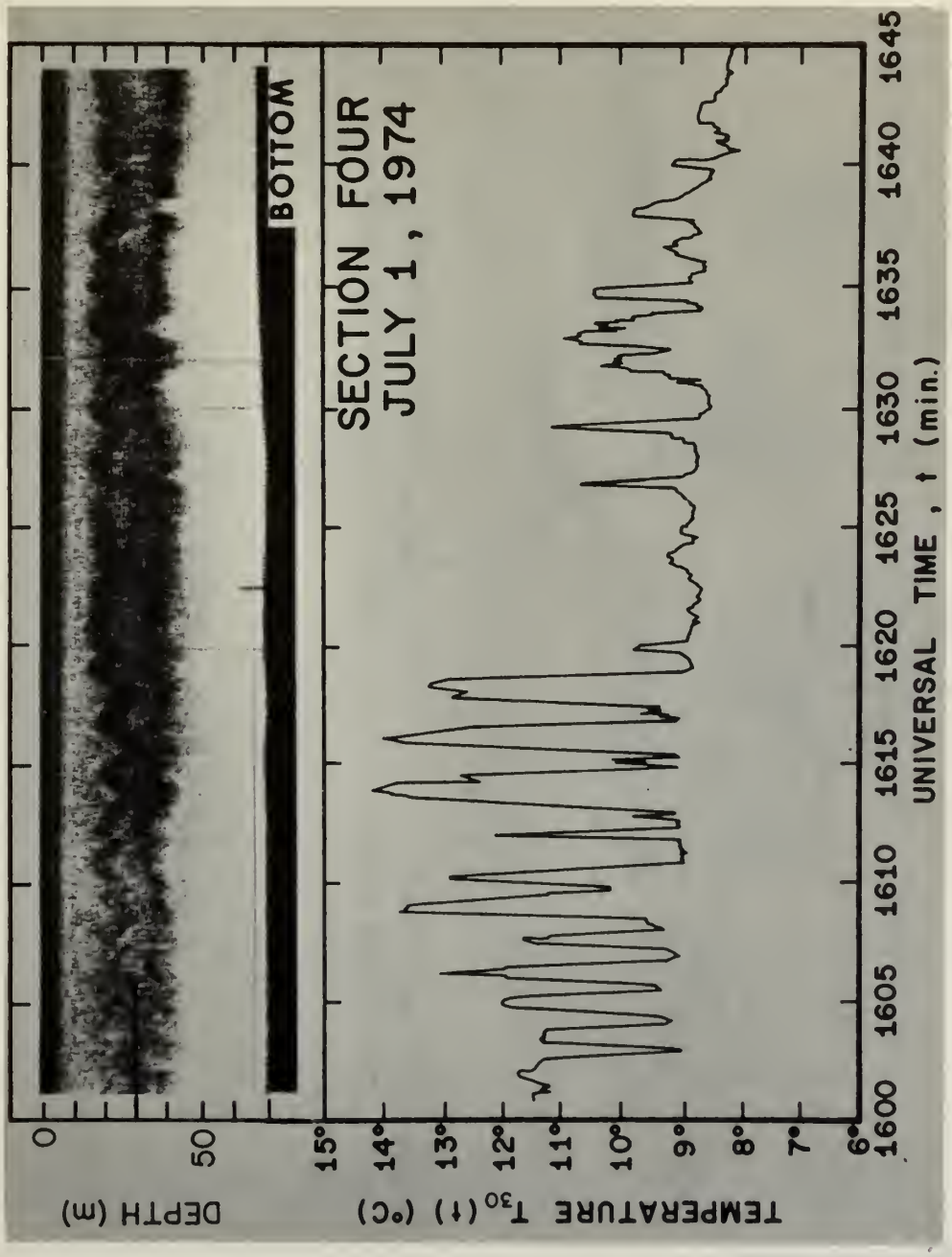

Figure 42. Acoustic and thermistor data taken during Leg 2 of July 1, 1974, triangle maneuver.

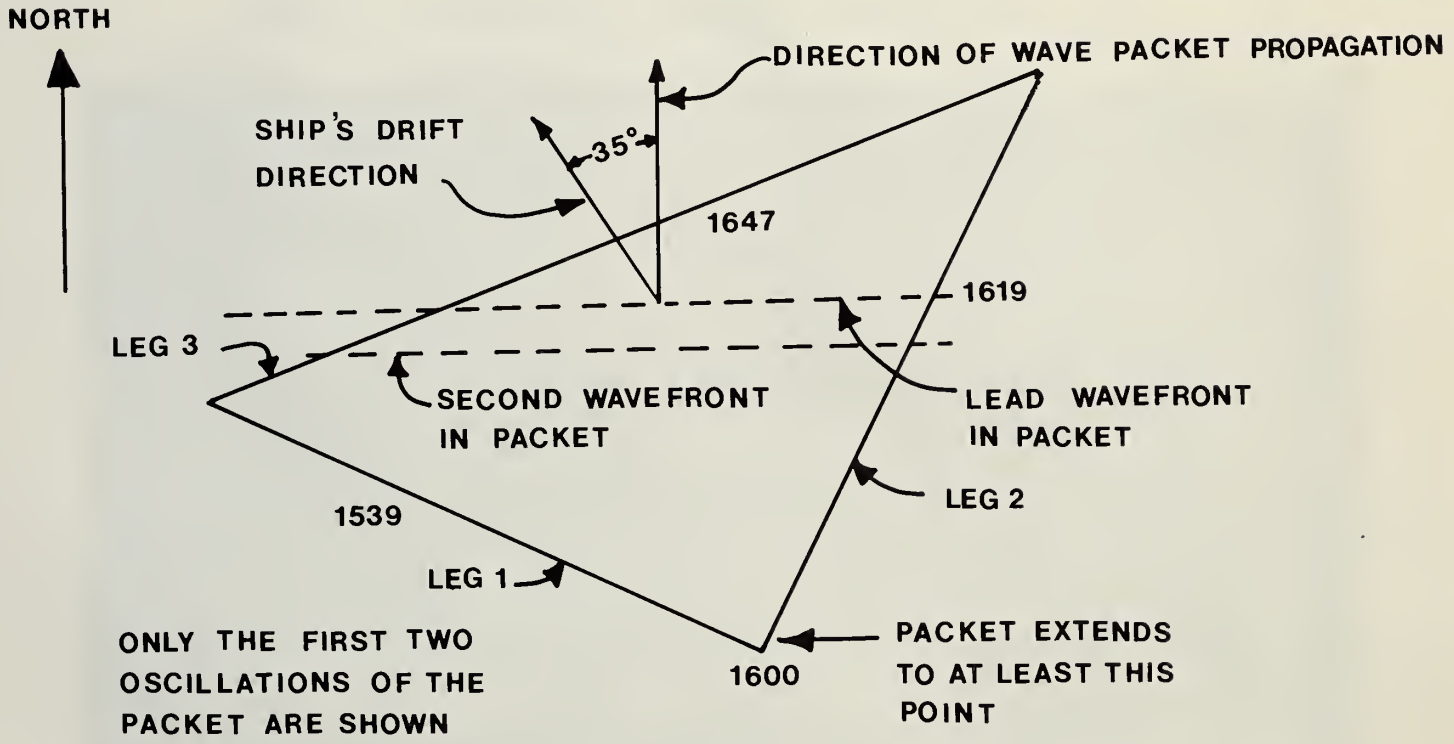

WAVEPACKET GEOMETRY

Figure 43. Geometry of the triangle maneuver and successive encounters with the wavepacket.

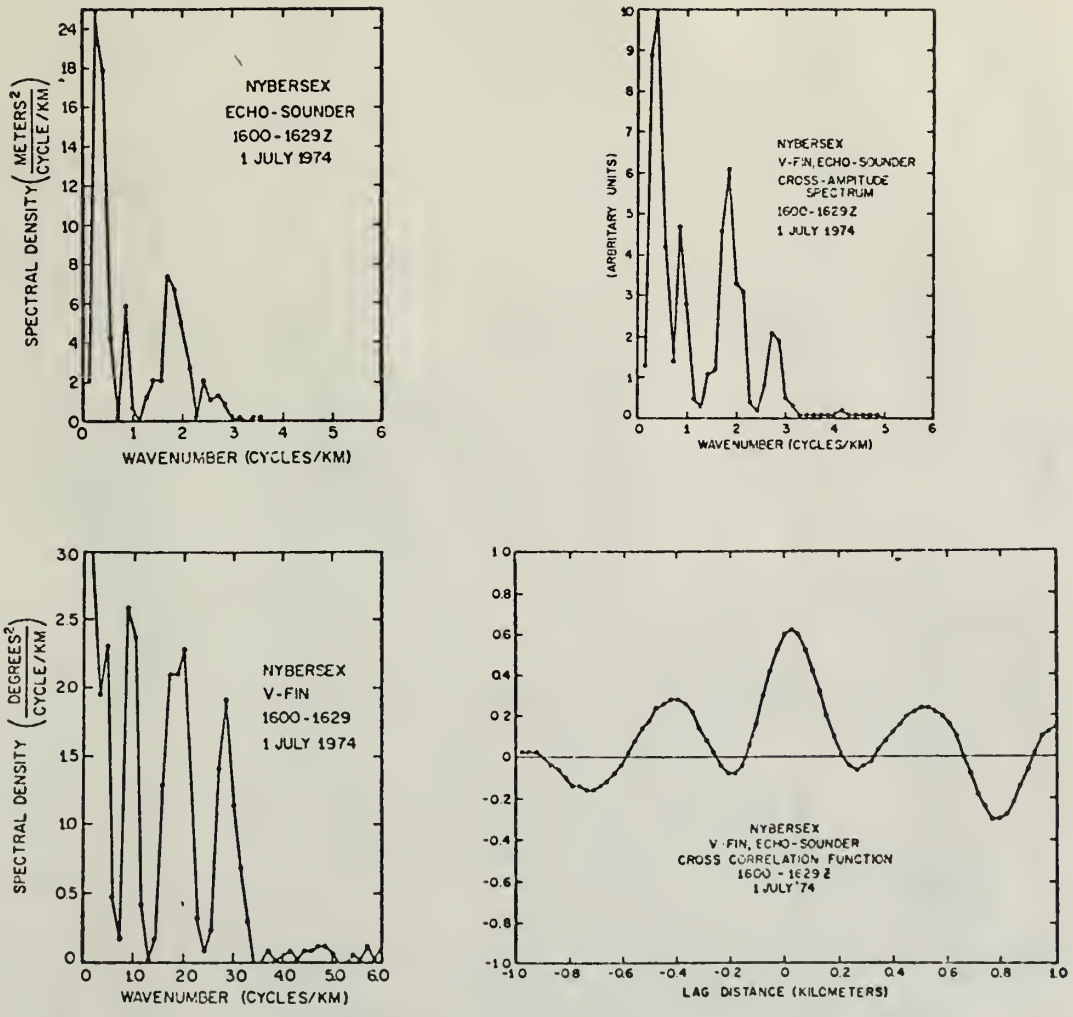

Figure 44. Triangle maneuver, Leg 2, spectral analysis of acoustic and thermistor data, as in figure 41 for Leg 1.

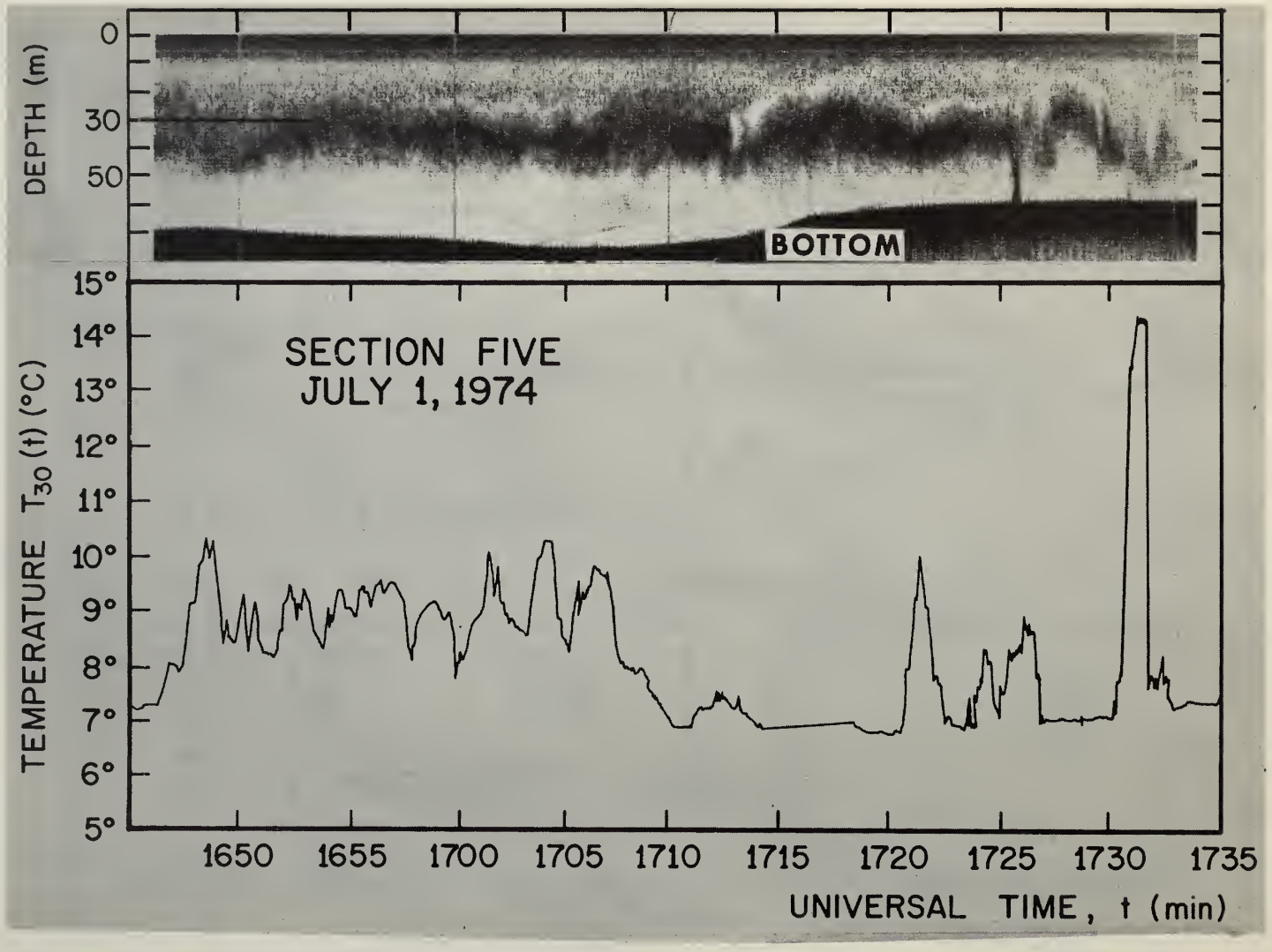

Figure 45. Acoustic and thermistor data for Leg 3 of the triangle maneuver.

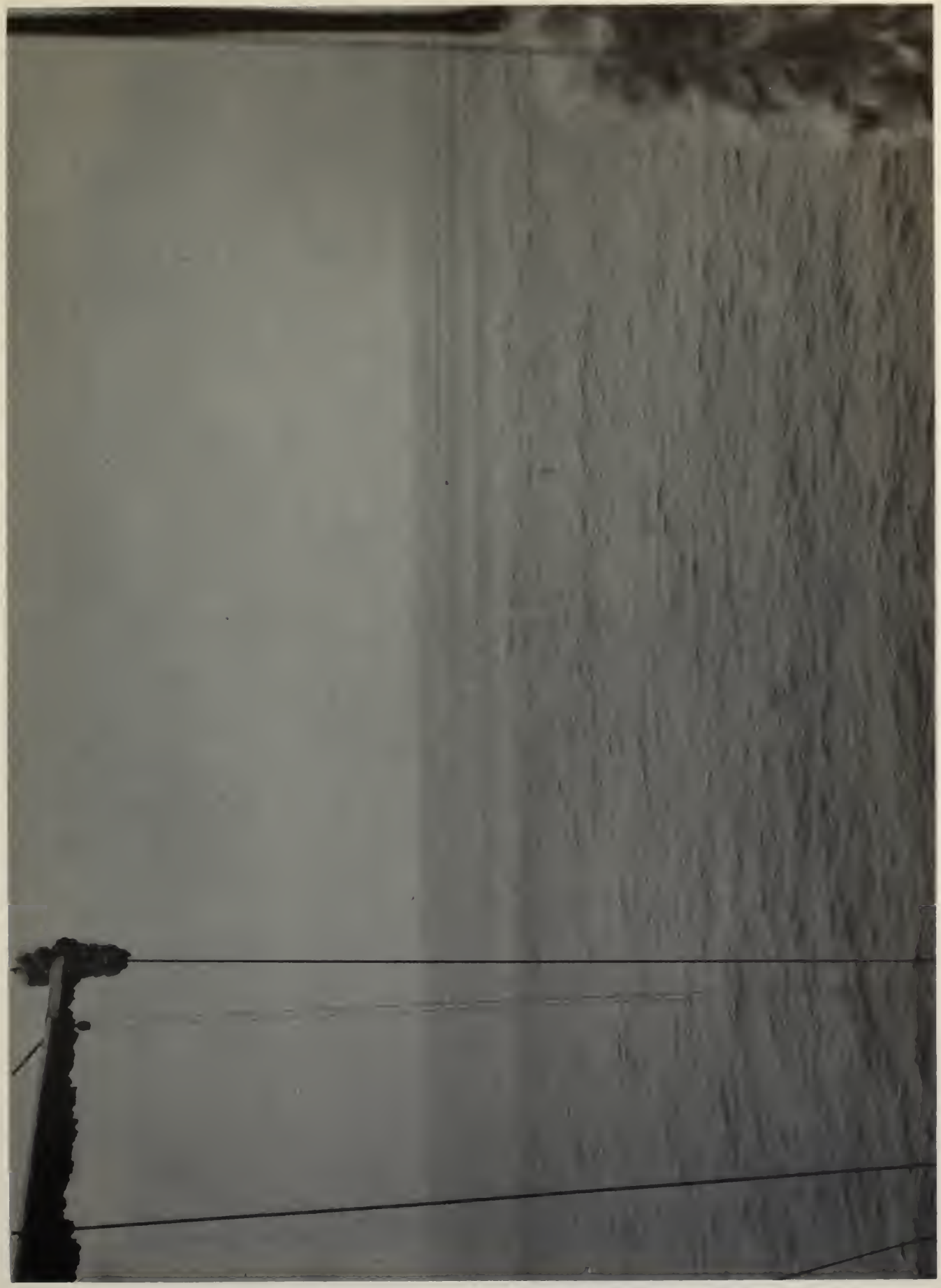

Figure 46. Surface slicks observed from shipboard.

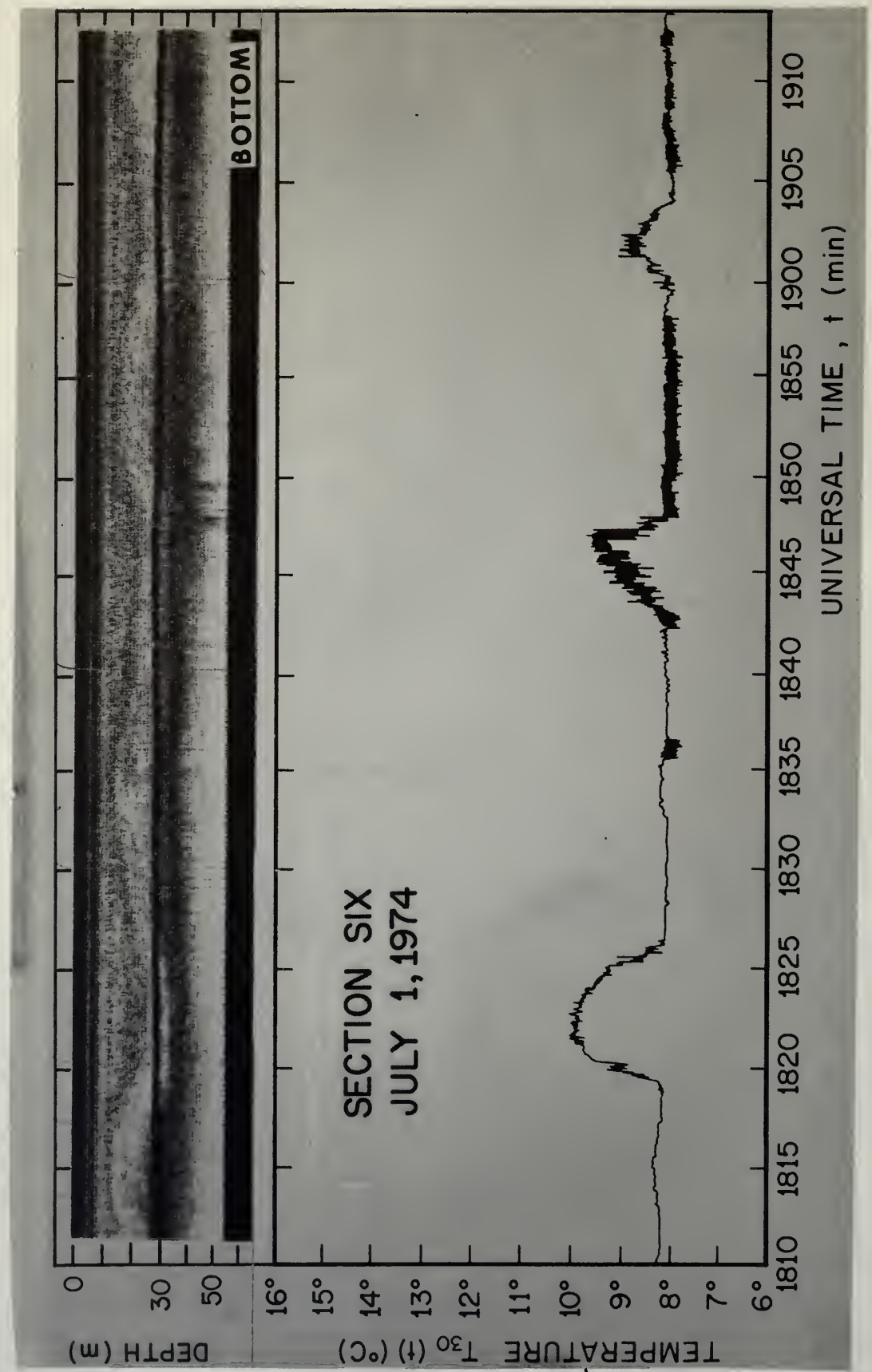

Figure 47. Part of the acoustic and thermistor records during the on-station measurement. The thermistor has dropped to 45 m depth.

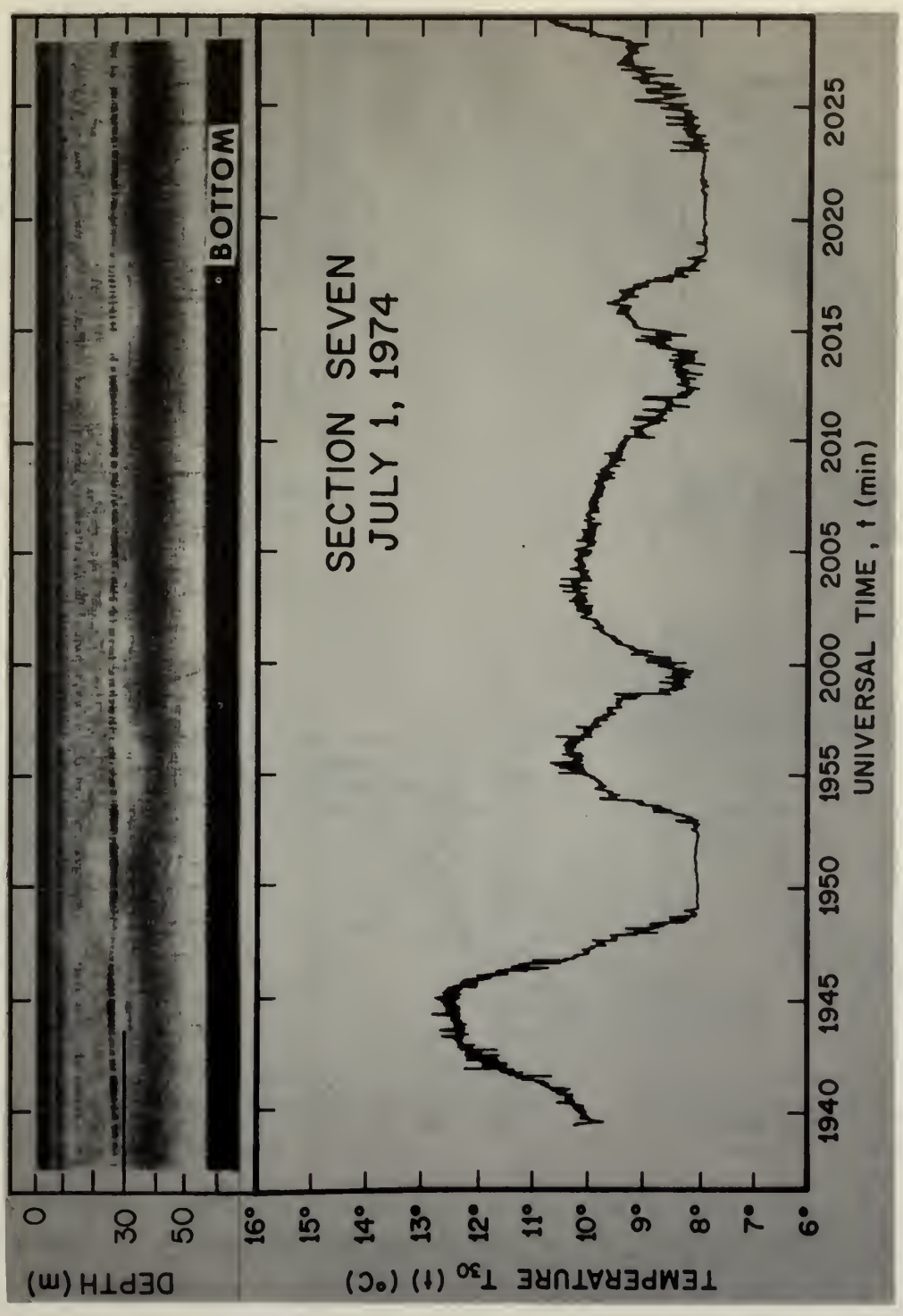

Figure 48. A later part of the on-station measurement of acoustic echo and temperature.

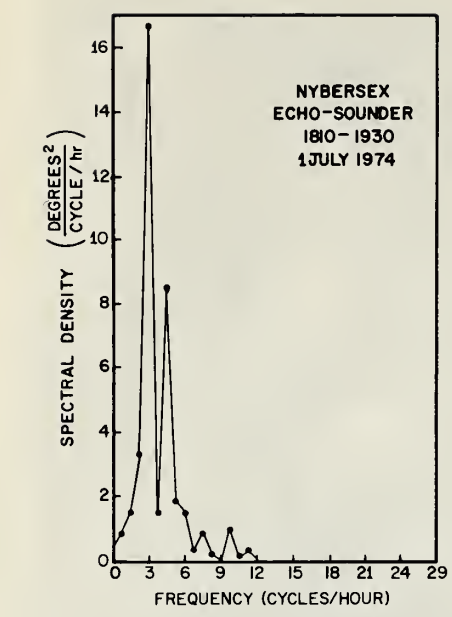

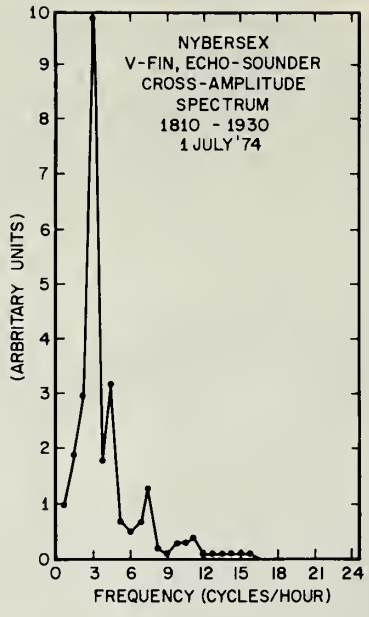

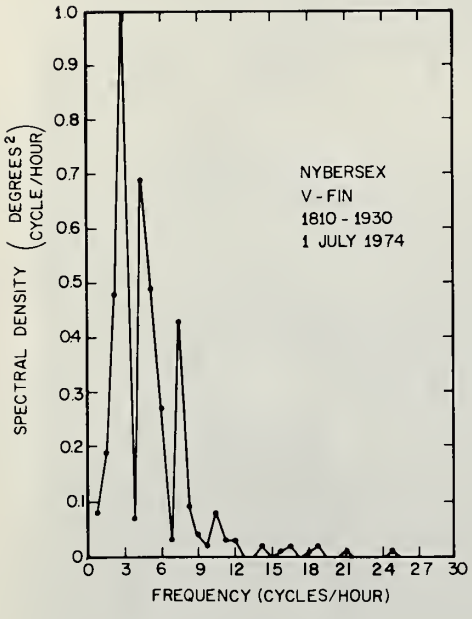

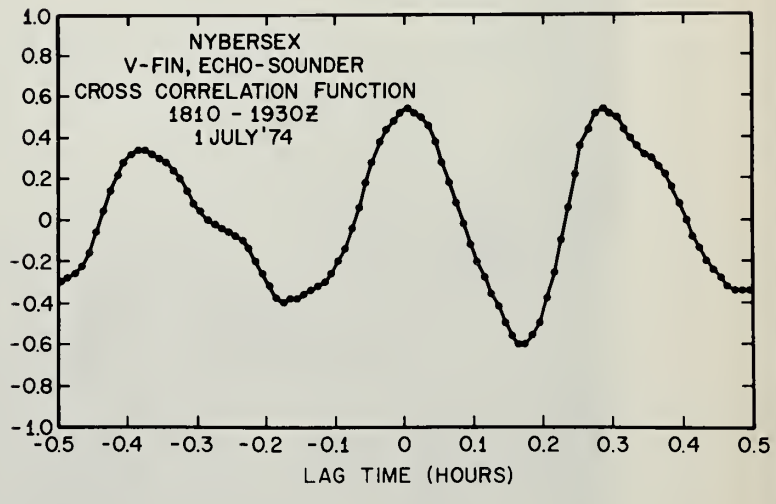

Figure 49. Spectral analysis of the on-station data shown in figure 47.

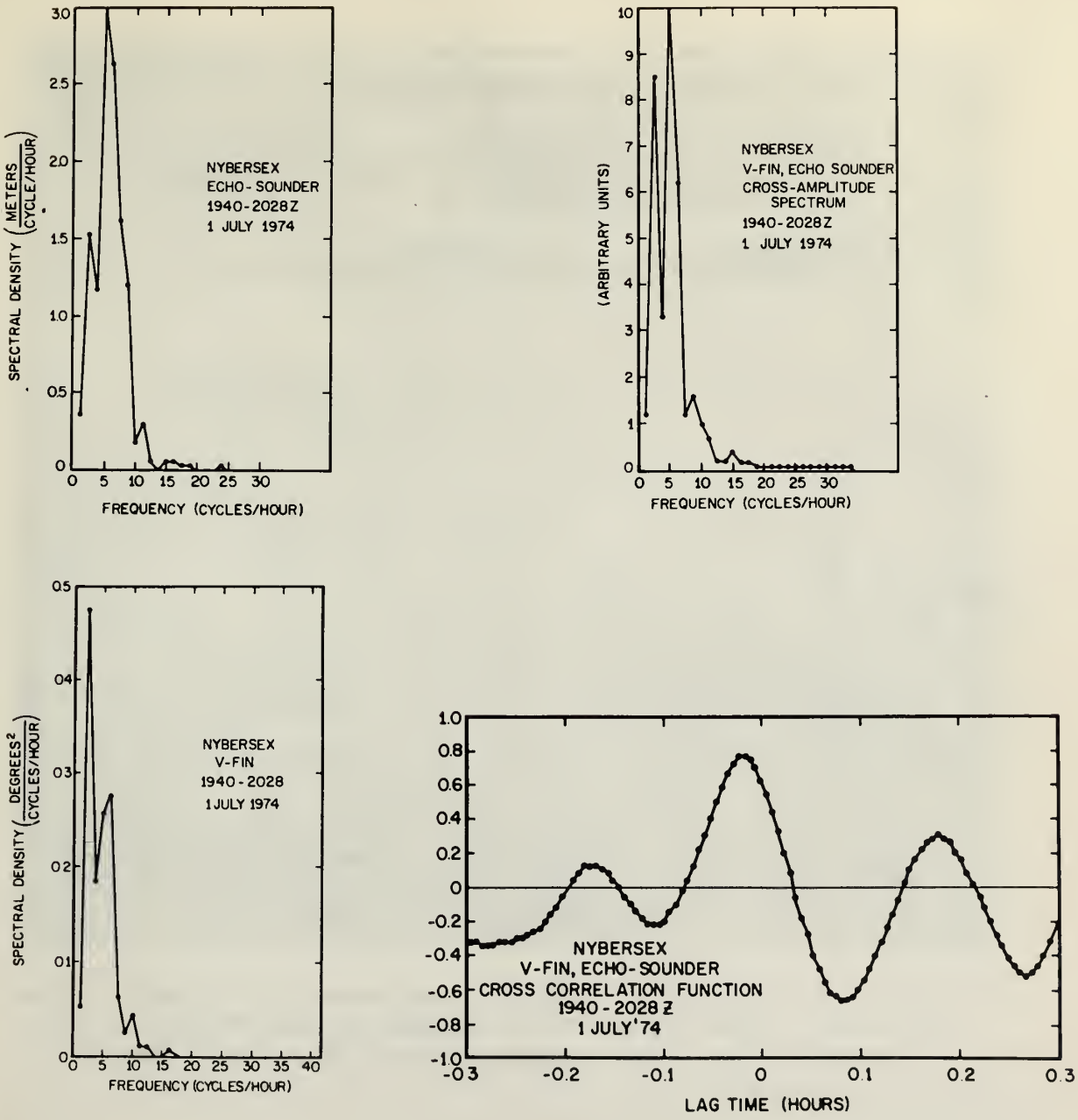

Figure 50. Spectral analyses of the on-station data shown in figure 48.

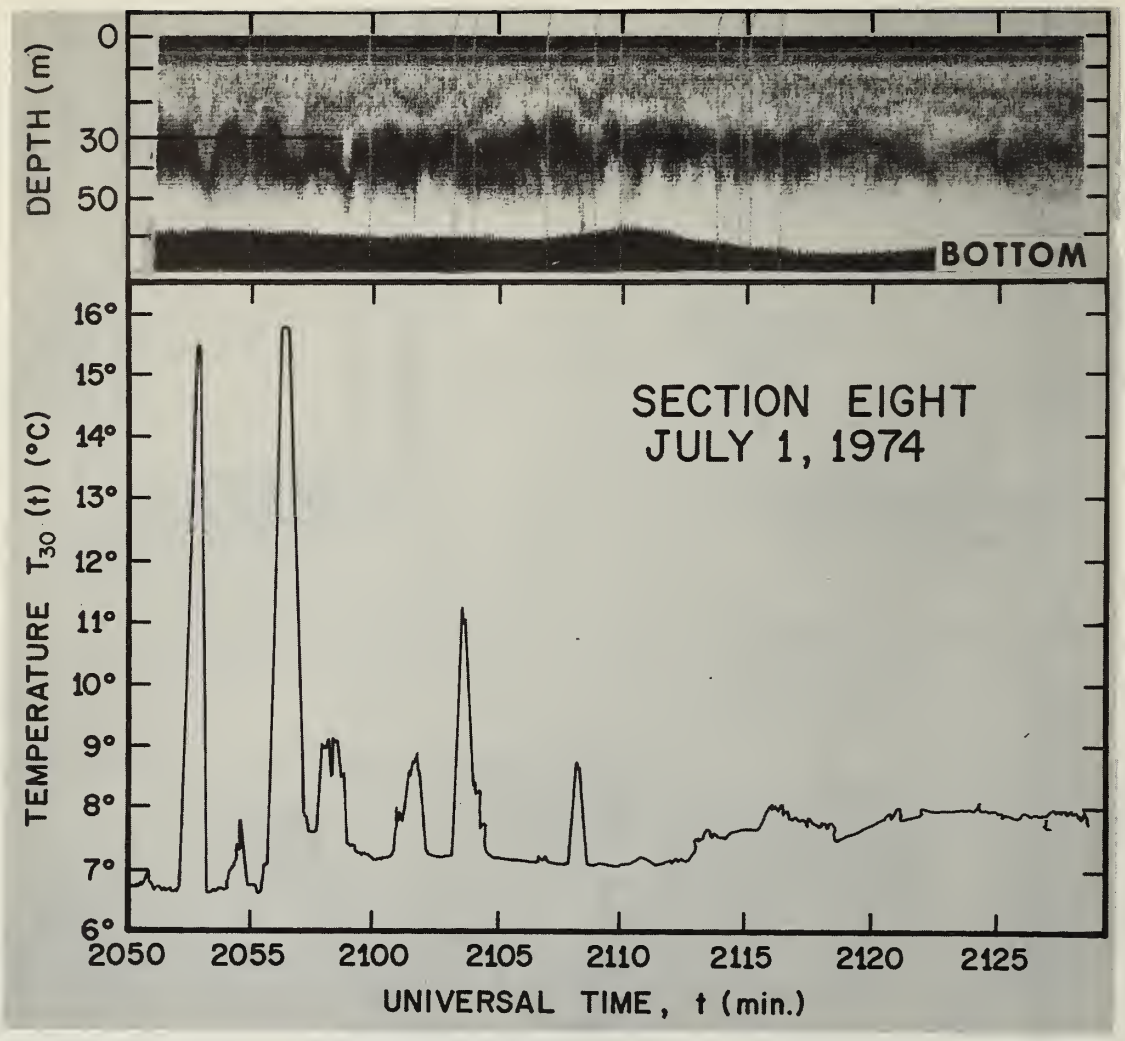

Figure 51. Acoustic and thermistor data related to shipboard siting of slicks. Beginning and end of passage of ship through a slick are marked by the light vertical lines on the acoustic record.

Figure 52. Photographically enhanced image from the satellite Landsat-1.

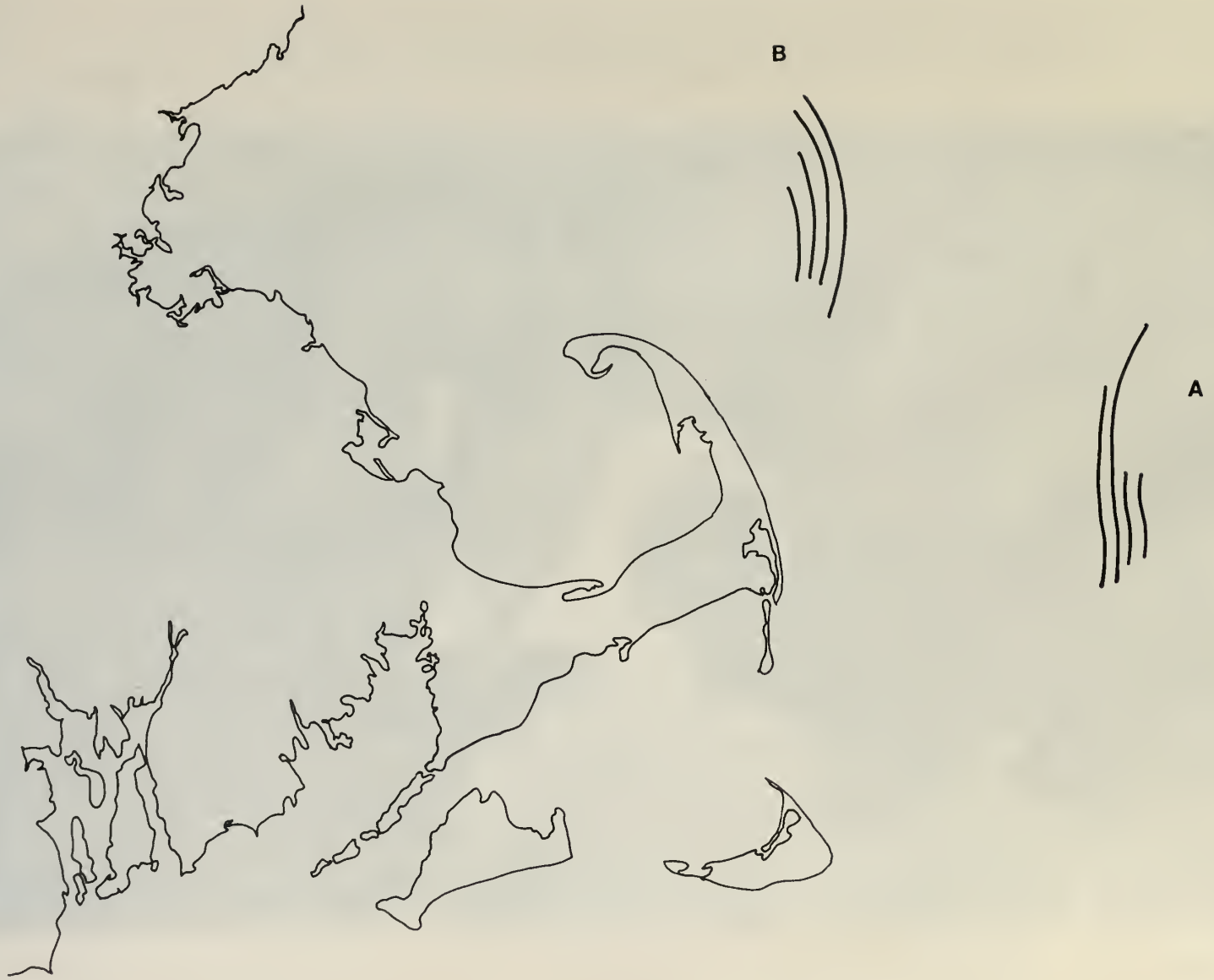

Figure 53. Line drawing locating features discussed in text.

Figure 54. Digitally enhanced images from Landsat-1, including the scene shown in figure 52.

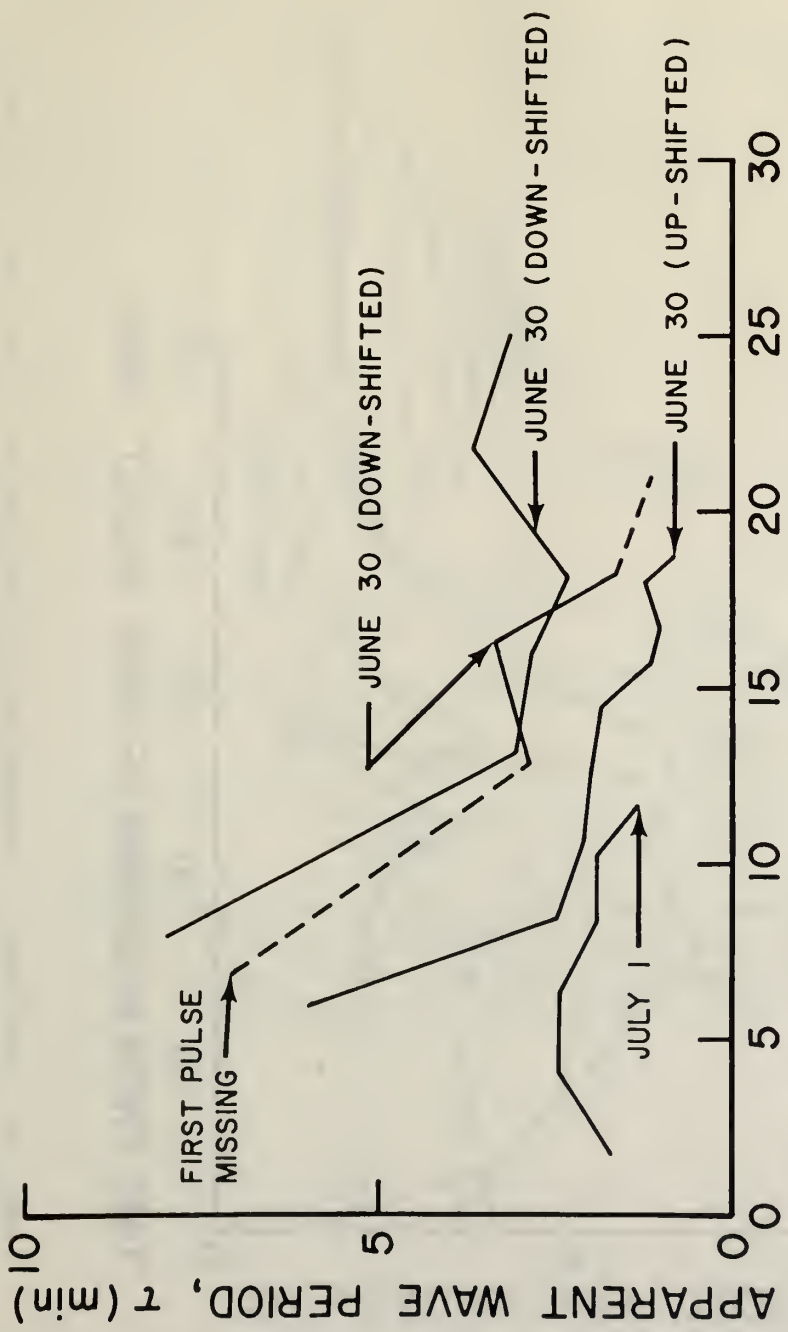

Figure 55. Wave period as a function of time, which can be interpreted as wavelength as a function of distance from the front of the packet.

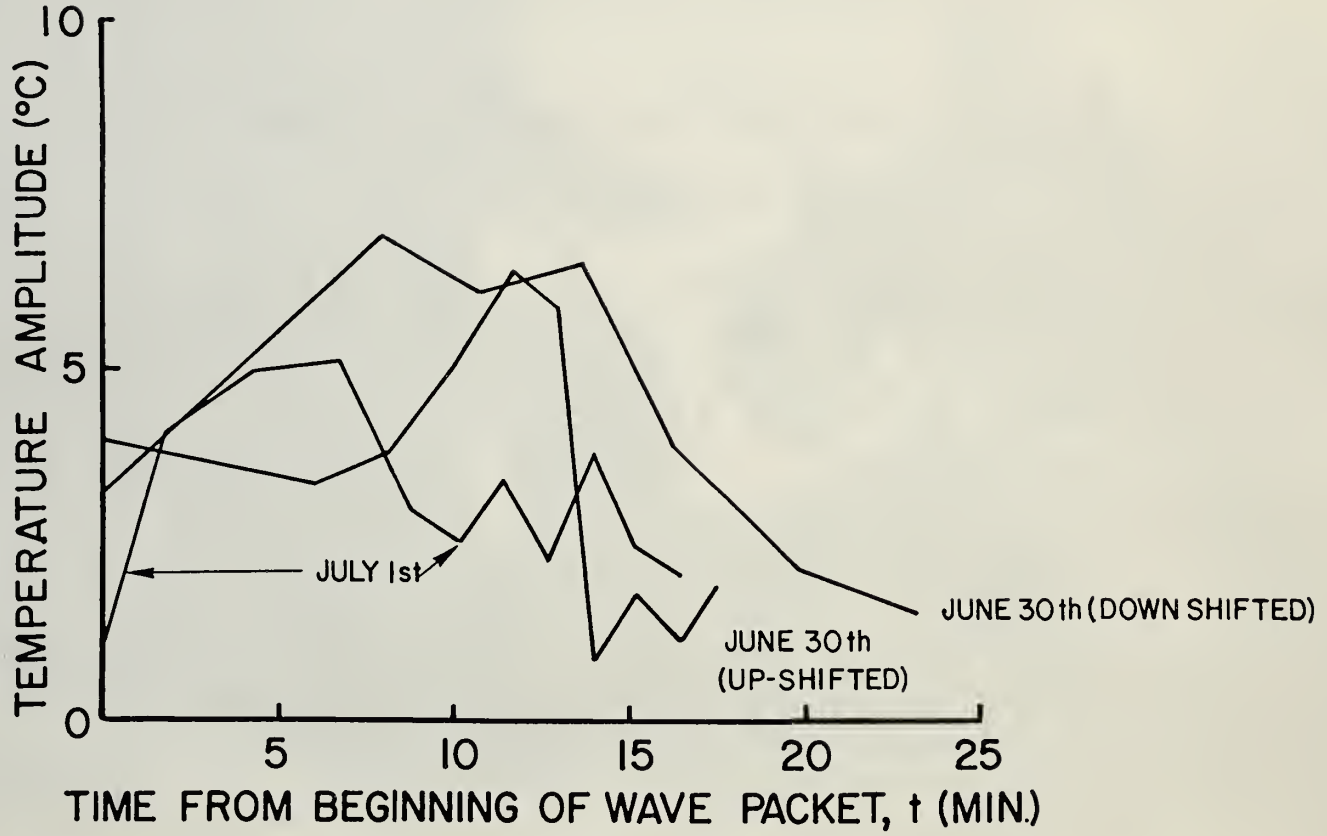

Figure 56. Amplitude of temperature fluctuations as a function of distance from front of packet.

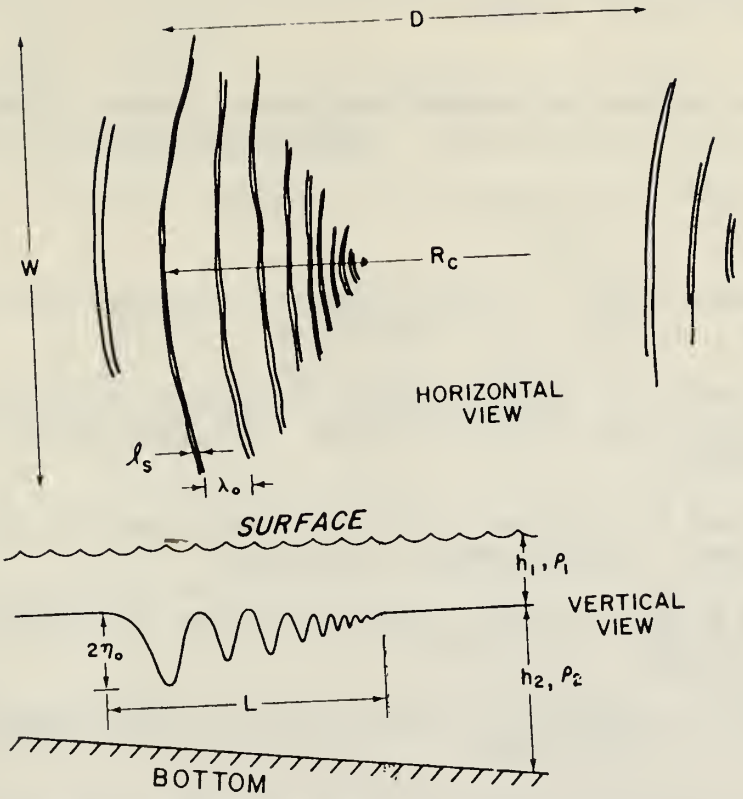

Figure 57. Schematic of internal-wave packet showing characteristic lengths and features; (upper) view from surface; (lower) view in a vertical section (Apel et al., 1976).

REFERENCES

Apel, J. R., H. M. Byrne, J. R. Proni, and R. L. Charnell (1975a): Observations of oceanic internal and surface waves from the Earth resources technology satellite. J. Geophys. Res., 80:865-881.

Apel, J., R. H. M. Byrne, J. R. Proni, and R. L. Sellers (1976): A study of oceanic internal waves using satellite imagery and ship data. Remote Sensing of Environ., 5:125-135.

Apel, J. R., J. R. Proni, H. M. Byrne, and R. L. Sellers (1975b): Near simultaneous observations of intermittent internal waves on the continental shelf from ship and spacecraft. Geophys. Res. Lett., 2:128-131.

Barnes, P. G. (1973): The generation of internal tides by flat-bump topography. Deep-Sea Res., 20:179-205.

Benjamin, T. Brooke (1967): Internal waves of permanent form in fluids of great depth. J. Fluid Mech., 29:559-592.

Bereyin, Y. A., and V. T. Karpman (1967): Nonlinear evolution of disturbance in plasmas and other dispersive media. Sov. Phys. JETP, English Translation, 24:1049.

Gargett, A. E., and B. A. Hughes (1972): On the interaction of surface and internal waves. J. Fluid Mech., 52:179-191.

Garrett, C., and W. Munk (1972): Space-time scales of internal waves. Geophys. Fluid Dyn., 2:225-264.

Halpern, D. (1971): Semidiurnal internal tides in Massachusetts Bay. J. Geophys. Res., 76:6573-6584.

Hunkins, K., and M. Fliegel (1973): Internal undular surges in Seneca Lake: A natural occurrence of solitons. J. Geophys. Res., 78:539-548.

Korteweg, D. J., and G. de Vries (1895): On the change of form of a new type of long stationary waves. Philos. Mag., 39:422.

Lafond, E. C. (1962): Internal waves. In The Sea, Vol. 1, edited by M. N. Hill, Interscience, N. Y., 731-763.

Lee, C., and R. C. Beardsley (1974): The generation of long nonlinear internal waves in a weakly stratified shear flow. J. Geophys. Res., 79:453-462.

Long, R. R. (1955): Some aspects of the flow of stratified fluids: No. 3, Continuous density gradients. Tellus, 7:341-357.

Ostapoff, F., J. R. Proni, and R. L. Sellers (1975): Preliminary analysis of ocean internal wave observations by acoustic soundings. GATE Rep. No. 14, WMO, Geneva, 392-397.

Prinsenberg, S. J., and M. Rattray, Jr. (1975): Effects of continental slope and variable Brunt-Väisälä frequency on the coastal generation of internal tides. Deep-Sea Res., 22:251-263.

Proni, J. R., and J. R. Apel (1975): On the use of high frequency acoustics for the study of internal waves and microstructure. J. Geophys. Res., 80:1147-1151.

Proni, J. R., F. Ostapoff, and R. L. Sellers: Preliminary acoustic observations of high-frequency deep ocean internal wave groups during the GATE (in press).

Shand, J. A. (1953): Internal waves in the Georgia Strait. EOS Trans. Am. Geophys. Union, 34:849-856.

Woods, J. D. (1968): Wave-induced shear instability in the summer thermocline. J. Fluid Mech., 32:791-800.

REMOTE SENSING OF ENVIRONMENT 5, 125-135 (1976)

A Study of Oceanic Internal Waves Using Satellite Imagery and Ship Data

JOHN R. APEL*, H. MICHAEL BYRNE, JOHN R. PRONI, and RONALD SELLERS

Ocean Remote Sensing Laboratory, Atlantic Oceanographic and Meteorological Laboratories, Environmental Research Laboratories, National Oceanic and Atmospheric Administration, Miami, Florida 33149

Surface manifestations of oceanic internal waves have been studied in Landsat-1 and -2 data since 1972. The internal waves appear as periodic, intermittent variations in the surface optical reflectivity and are visible from spacecraft, aircraft, and surface vehicles under certain circumstances. The Landsat data suggest that the source of the waves is semidiurnal and diurnal tidal action at the edge of the continental shelf. A study of the wave characteristics yields considerable insight into the physics of their excitation, propagation, and dissipation. Packets have been observed from the Gulf of Maine to Cape Hatteras and in images taken off the U.S. and African east and west coasts, the Gulf of Mexico and the Caribbean, The Gulf of California, the Sulu Sea, and the Baltic. The internal wave groups show an orderly variation in wavelength from front to rear of the packet, due to a combination of frequency dispersion and nonlinear amplitude effects. An oceanographic cruise was carried out in synchronism with two 18-day Landsat-1 cycles, and data were taken on temperature, density variations, acoustic echoes, and surface slicks accompanying the internal waves. The data were satisfactorily correlated with spacecraft and U-2 imagery taken simultaneously.

I. Introduction

Surface manifestations of oceanic internal waves have been observed by many investigators, and their dependence upon wave-associated surface currents has been recognized for at least a generation (Ewing, 1950). The surface signatures are most evident on a relatively calm sea and take the form of a quasi-periodic, long-length modulation of the capillary-ultragravity wave spectrum; the scale of the modulation is usually of the order of hundreds of meters (Gargett and Hughes, 1972). Visible manifestations on the ocean surface are theorized as being due to at least two mechanisms, either of which modulates the short surface wave structure rather than causing a change in optical reflectivity or absorptivity at depth. The first theory suggests that the high velocity of surface water arising from the large internal wave amplitude sweeps together surface oils and debris to form a slick in regions of surface water convergence, thus *increasing* the specular reflection and decreasing the diffuse scattering over the convergence region. The second theory predicts that the small waves are concentrated in the convergence regions due to wave-current stresses, thereby

*Present address: Pacific Marine Environmental Laboratory, NOAA, Seattle, Washington 98105

decreasing the specular reflection and increasing the scatter over the convergence region.

II. Spacecraft Observations

We have observed these types of periodic features in photographs and imagery taken from various spacecraft over widely separated regions of the world. To date, quasi-periodic features on the ocean surface have been seen on images made from Skylab, the Earth Resources Technology Satellite-1, its successor, Landsat-2, the DMSP meteorological satellite, and the Apollo-Soyuz mission, taken over both the continental shelf and deep ocean areas; they have been observed off the North American and African east and west coasts, in the Gulf of California, the Caribbean, the Baltic, and the Sulu Seas (Apel *et al.*, 1975-a;-b). These features are almost certainly surface manifestations of internal waves discussed above.

A particularly dramatic example of internal waves may be seen in Fig. 1,

FIG. 1. Landsat-1 negative image, computer enhanced, showing internal wave packets south of long Island, New York, on 24 July 1973 (lower right-hand corner).

which is a computer enhanced, negative Landsat-1 image of the ocean south of Long Island, New York (I.D. 1366–15079). The Appendix discusses the enhancement techniques used. The size of the picture is approximately 140 by 140 km^2. The waves are most apparent in the lower right-hand corner as two sets of curved, quasi-periodic variations in brightness having a packet-like behavior, a general north-south orientation, and with phase fronts convex towards the west. The wavelengths are of order 1000 m. In addition to the waves, a light-dark "marbling" pervades the image, probably brought about by light winds advecting oils on the surface and causing more or less random changes in optical reflectivity. Also visible are two acid waste dumping events in the ocean (center-left) near the inner portion of the New York Bight. (Charnell *et al.*, 1974).

Figure 2 is an interpretive line drawing of the internal wave packets taken from Fig. 1 but with the area covered extended farther to the south in order to illustrate the wide extent of the internal wave signatures. The figure also shows bottom bathymetry so as to illustrate the general orientation of the lines of constant wave phase with isobaths, as well as the concentration of wave activity near the Hudson Valley on the continental shelf. Repeated Landsat overpasses show these to be highly persistent characteristics of the waves (Sawyer and Apel, 1976; Apel *et al.*, 1975-a).

Also shown are calculated isophase fronts (dashed lines), arrived at by assuming that a plane internal wave is initially generated nearby and parallel to the edge of the continental shelf, which then propagates on the shelf under the influence of varying water depth and density. The lines are spaced at arbitrary intervals. For convenience the calculation assumes a water column stratified in two layers of thickness h_1 and h_2 and nearly equal densities $\rho_1 \simeq \rho_2 \simeq \rho$. The dispersion equation, $\omega \cong \omega\,(k)$, relating frequency ω and horizontal wave number k, for the two layer system is obtained from Eq. (1) (Lamb, 1932):

$$\omega^4\,(\coth kh_2 \coth kh_1 + 1) - \omega^2\, gk\,(\coth kh_1 + \coth kh_2) + (\Delta\rho/\rho)g^2\, k^2 \cong 0. \quad (1)$$

For a density contrast, $\Delta\rho/\rho \cong 10^{-3}$, a mixed layer depth of 50 m, and a wavelength $2\pi/k \cong 1000$ m, the phase speed ω/k is approximately 0.25 m/s, depending on the water depths shown in Fig. 2. The refraction of the calculated fronts on the shelf is due to the influence of the deeper water over the Hudson Valley. The overall behavior of the model is in reasonable agreement with the spacecraft observations.

A study of Landsat-1 and 2 imagery has been completed for all satellite overpasses occurring during the summers of 1972 to 1974, between Cape Hatteras, N.C., and Nova Scotia, Canada; the results are being assembled in an atlas that will be published in the near future (Sawyer and Apel, 1976). The study shows persistent internal wave activity all along the continental shelf and some limited patterns seaward of the slope. A more detailed analysis shows they have several characteristics which are pervasive enough to be worthy of note:

(1) The waves occur in groups or packets of width L=3 to 5 km, usually

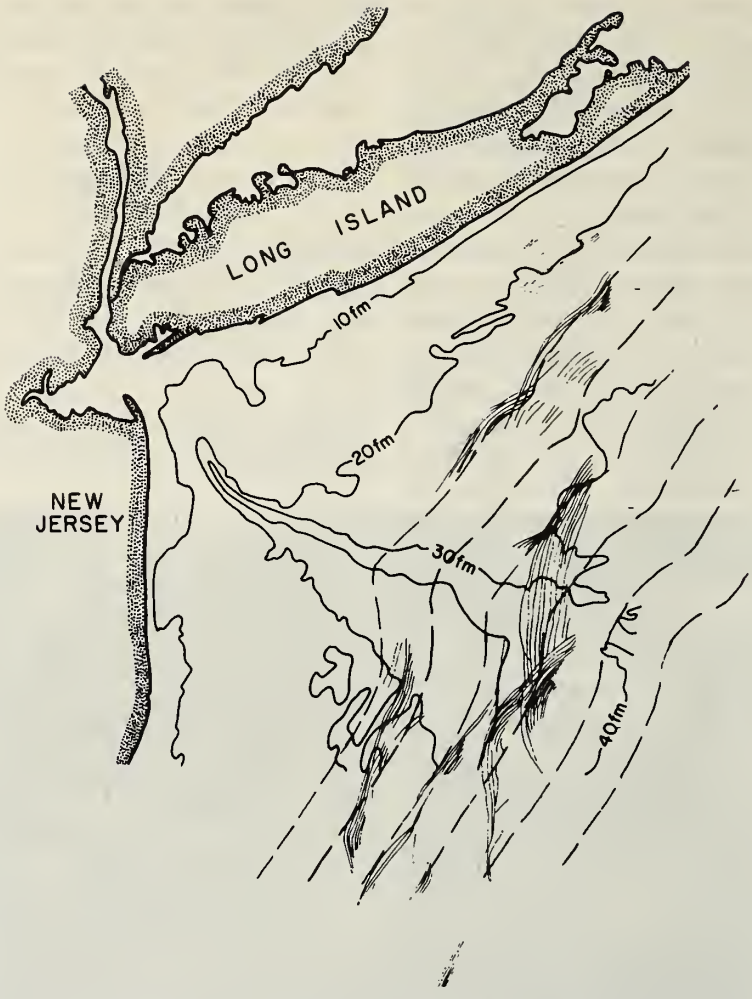

FIG. 2. Geographically corrected line drawing of internal wave fields observed in Fig. 1, superimposed on bottom topography. The dashed lines on the graph show isophase contours as calculated from a two-layer model.

landward of the continental slope and separated by distances, D, which are of the order of either 15 or 30 km; taken together with both the observed and calculated phase velocities, these facts suggest a semidiurnal or a diurnal origin;

(2) the crests are nearly always oriented parallel to the local bottom topography or can be loosely associated with some topographic feature seaward of their observed position, or both;

(3) the wavelengths fall between 200 and 10,000 m, depending on the geographical area; within a given packet,

there is often a monotone decrease in wavelength, varying from λ_o at the front to $\lambda < \lambda_o$ at the back of the group;

(4) the lengths of the crests, W, fall between a very few and perhaps 100 km, with a decrease in crest length occurring from front to back of the group;

(5) the widths of the slicks, l_s, are often small compared to the lead wavelength λ_o:

(6) the crests are curved in a horizontal plane with their convex sides pointed in the direction of propagation; the radii of curvature, R_c, range from essentially infinity to a few kilometers;

(7) as the packet progresses up on the shelf, there is some evidence of a continued increase in the wavelengths throughout; an accounting for this may be had by a combination of linear dispersion and nonlinear effects akin to solitary wave behavior.

Other data off southwest Africa (Apel *et al.*, 1975-a) show six distinct packets apparently radiating from a small source, perhaps a submarine canyon, approximately 150 km offshore, with spacings indicative of once-a-day excitation. If such is the case, these data provide evidence that internal waves may have lifetimes of several days, even on the continental shelf.

III. Shipboard Observations

A cruise with the acronym NYBERSEX: New York-to-Bermuda Remote Sensing Experiment—was undertaken during June and July of 1974 to verify the interpretations offered above; it was scheduled so as to coincide with three consecutive Landsat-1 overpasses of the New York Bight, plus a NASA U-2 flight at the conclusion of the cruise. The ship was instrumented with a salinity-temperature-depth sensor, expendable bathythermographs, thermistors towed in a vee-fin, and a 20 kHz, downward-looking acoustic echo-sounder to delineate internal wave motion at depth (Apel *et al.*, 1975-b; Proni and Apel, 1975). Because of weather, it was not possible to obtain one set of simultaneous observations involving all of the available instrumentation. Nevertheless, an ample quantity of cross-correlated data was gathered to enable us to assert unequivocally that the spacecraft imagery does indeed contain surface manifestations of internal waves. The U-2 also obtained photography and multispectral scanner imagery of internal wave packets in and near the Hudson Canyon; the latter sensor is the prototype for the Nimbus-G Coastal Zone Color Scanner (Hovis, 1975).

Figure 3 is a yellow-filtered, color infrared photograph made with the Vinton 70 mm camera on the U-2 at 20,000 m altitude, showing surface and internal waves and oil slicks in the sun glint patterns at the head of the Canyon on the shelf edge. For this packet, $\lambda_o \cong 500$ m.

Figure 4 illustrates shallow water internal wave data from the echo-sounder (upper) and the towed thermistor (lower), illustrating a packet approximately 150 km due east of Sandy Hook, New Jersey in some 80 m of water. The water was sharply stratified into two layers

FIG. 3. Infrared color photograph made of internal wave surface signatures from the NASA U-2 at 20,000 m altitude. Also visible are surface waves and oil slicks.

having upper and lower temperatures of about 17 ° C, and 8 ° C, separated by a 10 m thick gradient region centered at approximately 30 m depth. Clearly defined surface slicks accompanied the underlying internal wave field. The ship was proceeding at about 2.5 m/s from the rear to the front of the wave group while the data of Fig. 4 were taken.

Two layers of acoustic-reflecting material were concentrated in regions where the macroscopic curvature of the vertical temperature profile, $\partial^2 T/\partial z^2$, was the largest; these layers are clearly seen in Fig. 4. This is in accord with models of acoustic scattering from fluctuations in the acoustic index of refraction (Proni and Apel, 1975). Thus the measurement yields some evidence that, in addition to scattering from biological material—the mechanism that is usually invoked to explain such reflections—, these signals may be partially returned from microstructure and turbulence in the water column. Both the acoustic measurement and the coincident towed thermistor record yield a peak-to-trough amplitude, 2η, of about 15 m; the latter record was used to evaluate $2\eta \simeq (T_u - T_l)\,(\partial T/\partial z)^{-1}$, with T_u and T_l being the maximum and minimum temperatures occurring during an oscillation.

At 1625 UT, a 135 ° turn was executed because the forward edge of the packet, as defined by its slick pattern, had been passed. The wave coherence on the new course is somewhat lower, as may be seen on Fig. 4. A power spectrum for the portion of the echo-sounder record to the left of 1625 UT is shown

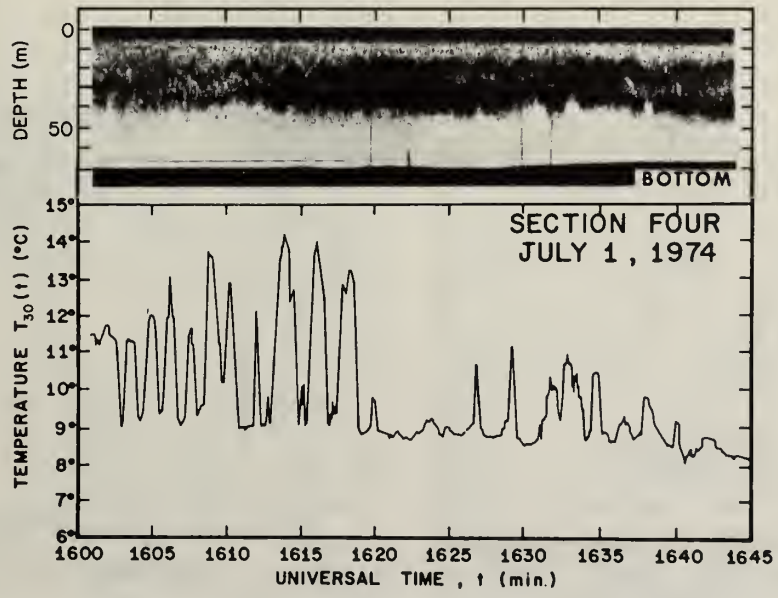

FIG. 4. (Upper) internal wave packet in 80 m water off New Jersey as observed by 20 kHz acoustic echo-sounder; (lower) temperature record from a towed thermistor at 30 m depth. A 135 ° turn was executed shortly after 1625 UT.

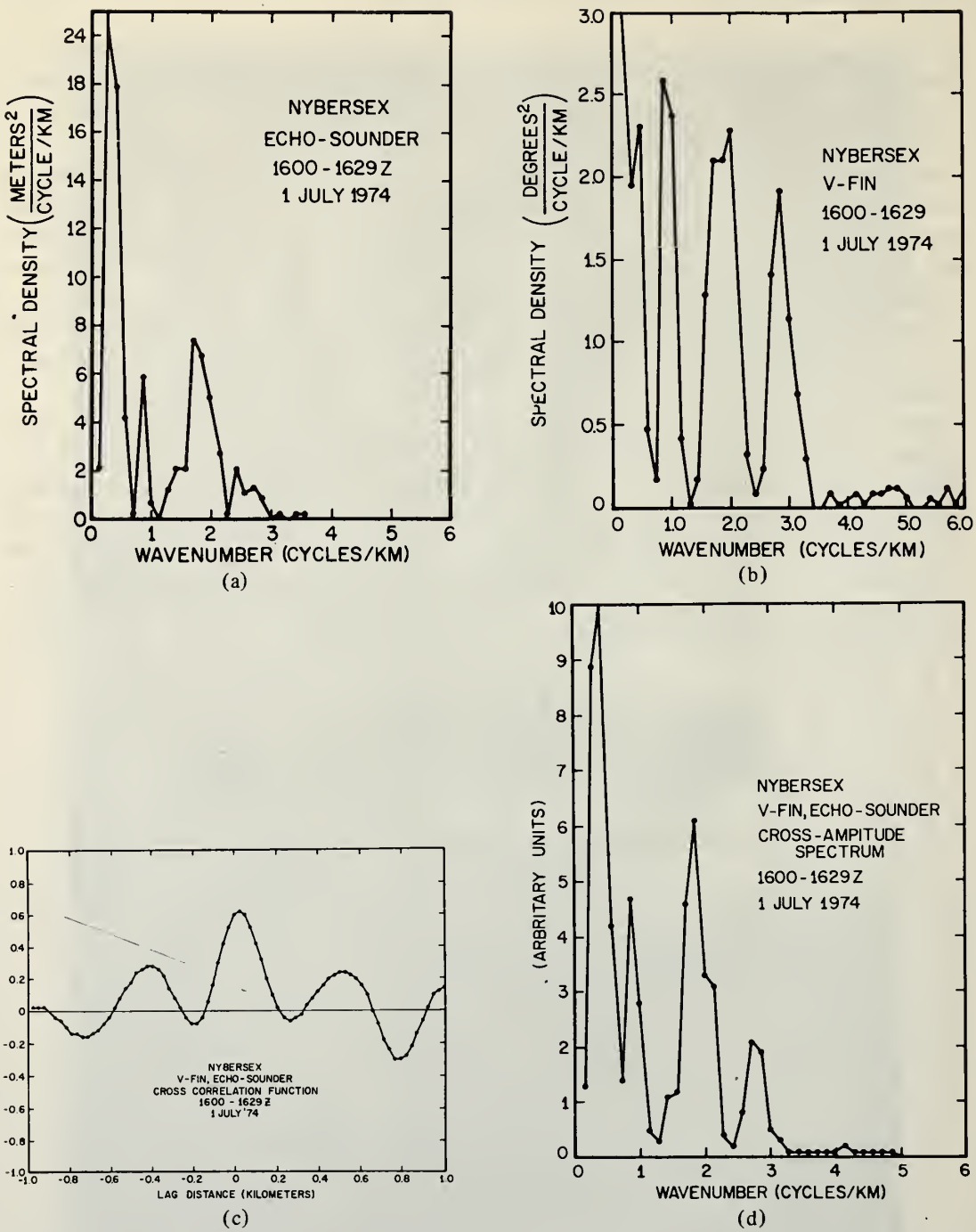

FIG. 5. (a) Power spectrum from the portion of the acoustic echo-sounder record to the left of 1625 UT on Fig. 4; (b) spectrum for the thermistor temperature record from the same interval; (c) acoustic temperature cross-correlation function; (d) acoustic-temperature cross-amplitude spectrum. The dominant spectral component at 2 cycles/km corresponds to the dominant wavelength observed in Fig. 4.

in Fig. 5; the acoustic time series has been demeaned, detrended, and cosine-tapered in order to obtain the spectrum shown. Similarly, vee-fin temperature spectra, and acoustic-temperature cross-correlation functions and cross-spectra have also been evaluated and are reproduced in Fig. 5. These show that the oscillations observed using the acoustic remote sensor are highly correlated with the temperature observations, a more conventional method of internal wave measurements.

There are several significant features to be noted in Fig. 4. First, the oscillations are indeed packet-like, having a sharply defined leading edge, as was observed from the Landsat and U-2 images. Second, the leading oscillation, occurring at about 1618 UT, is downgoing; this is in accord with the solitary wave interpretation mentioned above (Lee and Beardsley, 1974). Third, both the amplitudes and the wavelengths decrease toward the rear of the packet (i.e., earlier times); the decreasing amplitude is consistent with the shorter crest lengths observed in the spacecraft images, since a small amplitude is accompanied by reduced currents, which in turn implies a reduced surface signature. Fourth, the mean depth of the upper mixed layer is lowered during the passage of the wave packet. Fifth, the packets observed from the ship had spacings consistent with a 12 hr generation interval.

Because of clouds or bad weather, no one packet has been simultaneously identified from ship and spacecraft; however, all of the data, including observations of the disappearence of surface effects during winds above 6-8 m/s, are consistent with the picture offered above.

IV. Summary of Packet Characteristics

A schematic diagram that summarizes the salient features of the packets is shown on Fig. 6. This figure defines several quantities used in an empirical mathematical model for the amplitude of the packet, Eq. (2); some of the quantities have been defined above in the list of seven wave characteristics deduced from the satellite imagery. In terms of a moving coordinate system with its origin at the front of the packet and its x-axis increasing toward the rear, an expression for the vertical displacement, η, is given by

$$\eta(\vec{r}) = \eta_o R_c(x,y)\, W(z)\, (x/\ell_1)\, e^{-x/\ell_2} \left\{\sin\left[k_o(1+x/\ell_3)\, x - \pi\right] + z_1\right\}. \tag{2}$$

Here η_o is a normalizing amplitude; $R_c(x,y)$ describes the curvature, R_c, of the crests in the horizontal plane; $W(z)$ is the solution to the linear, vertical-velocity eigenvalue problem for the density profile existing; the function $x\exp(-x)$ together with the constant z_1 and the phase, $-\pi$, give a downgoing initial pulse whose mean depth and envelope decay toward the tail of the packet; and the linearly increasing wave number, $k_o(1+x/l_3)$, accounts for the decreasing wavelength. The l's give scales for the various features described.

This expression, while only a model of the wave behavior, nevertheless contains the important features observed to date. Work is in progress to derive a theory

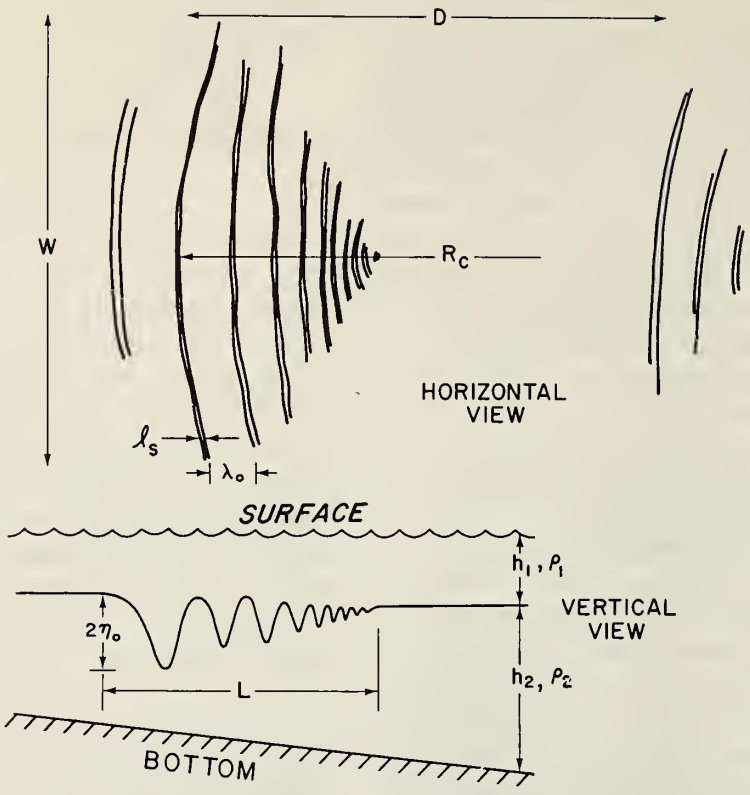

FIG. 6. Schematic of internal wave packet showing characteristic lengths and features; (upper) view from surface; (lower) view in a vertical section.

from a basic viewpoint that contains a more rigorous rendition than this admittedly qualitative behavior.

V. Conclusions

High-resolution satellite imagery has been shown to be useful in studying internal waves on the continental shelf under conditions of clear skies and light winds. Amplitude information can be obtained from acoustic echo-sounding without the necessity for temperature sensors whenever scattering from microstructure or biological material imbedded in the internal wave motion is sufficiently intense. These two remote sensing techniques together constitute a set of new tools for investigations of high-frequency internal waves.

VI. Appendix

Figure 1 is a contrast-enhanced negative image of Landsat-1 image I.D. 1366–15079, Channel MSS-6. This wavelength interval, 700 to 800 nm, shows near-surface effects most readily

of the four MSS Channels. The contrast enhancement was done digitally by applying a linear stretch to the original digital numbers 9-13 (on a scale of 127) so that they occupy the full dynamic range of the film. The optimum stretch appears to be one for which the intensity histogram for the oceanic part of the scene (which is nearly gaussian) has its stretched mean at approximately 64 and has about 3% of the energy falling beyond the limits 0 and 127. Figure 1 is geographically distorted in the east-west direction by a factor of 3600/2400 because of the size of Landsat pixels; nor is it corrected for earth rotation. The interpretive line drawing, Fig. 2, is geographically correct, however.

Maul (1974) has discussed more fully some enhancement techniques for Landsat oceanic images of this type.

A portion of this work was supported by the Defense Advanced Research Projects Agency, which assumes no responsibility for the accuracy of this report. The authors thank the National Aeronautics and Space Administration for special data taking from both Landsat-1 and the NASA U-2.

References

Apel, J. R., H. M. Byrne, J. R. Proni, and R. L. Charnell (a), (1975), Observations of oceanic internal and surface waves from Earth Resources Technology Satellite, *J. Geophys. Res.* **80**, 1147.

Apel, J. R., J. R. Proni, H. M. Byrne, and R. L. Sellers (b), (1975); Near simultaneous observations of intermittent internal waves on the continental shelf from ship and spacecraft, *Geophys. Res. Lett.* 2, 128.

Charnell, R. L., J. R. Apel, W. Manning, III, and R. H. Qualset (1974), Utility of ERTS-1 for coastal ocean observation: The New York Bight Example, *Marine Technol. Soc. J. 8* p.42.

Ewing, G., Slicks (1950), Surface films, internal waves, *J. Mar. Res.* **9**, 161.

Gargett, A. E., and B. A. Hughes (1972), On the interaction of surface and internal waves, *J. Fluid Mech.* 52, 179-191.

Hovis, W. (1975), Ocean color imagery-coastal zone color scanner, *Proc. NASA Earth Resources Survey Symp. VI-c* Houston, Texas, p. 1989.

Lamb, H. (1932), *Hydrodynamics*, Cambridge Univ. Press, London, p. 370.

Lee, C., and R. C. Beardsley (1974), The generation of long nonlinear internal waves in a weakly stratified shear flow, *J. Geophys. Res.* **79**, 453.

Maul, G. A., R. L. Charnell, and R. H. Qualset (1974), Computer enhancement of ERTS-1 images for ocean radiances, *Remote Sensing of Environ.* 3, (3), 237-252.

Proni, J. R., and J. R. Apel (1975), On the use of high-frequency acoustics for the study of internal waves and microstructure, *J. Geophys. Res.* **80**, 1147.

Sawyer, C., and J. R. Apel (to be published), An atlas of internal waves from Landsat, NOAA-ERL Technical Memo.

Received 22 December 1975; revised 11 March 1976

NEAR-SIMULTANEOUS OBSERVATIONS OF INTERMITTENT INTERNAL WAVES ON THE CONTINENTAL SHELF FROM SHIP AND SPACECRAFT

John R. Apel, John R. Proni,
H. Michael Byrne, and Ronald L. Sellers

Ocean Remote Sensing Laboratory
Atlantic Oceanographic and Meteorological Laboratories
Environmental Research Laboratories
National Oceanic and Atmospheric Administration
Miami, Florida 33149

Abstract. Internal waves on the continental shelf off New York have been observed from ship and the ERTS-1 spacecraft, and positive correlations made between surface and subsurface measurements of temperature, acoustic volume reflectivity, and surface slicks. The spacecraft imagery senses the quasi-periodic variations in surface optical reflectivity induced by the internal waves. The waves appear to be tidally generated at the shelf edge and occur intermittently in packets, which propagate shoreward and disappear in water near 50-m depth.

Introduction

Surface manifestations of internal waves have frequently been identified during observations from ships, aircraft, and offshore towers, with "surface slicks" or "regions of enhanced capillary waves" being terms used to describe the state of the sea surface overlying the internal wave field. In a recent publication, we report on what appear to be surface signs of internal waves detected in visible and near-infrared imagery obtained from the multi-spectral scanner on the NASA Earth Resources Technology Satellite, ERTS-1 (Apel et al., 1975). These signs usually take the form of periodic variations in optical reflectivity of the ocean surface; they have wavelengths of order 500 to 5000 m and appear repetitively in several groups, or packets, which are separated by intervals ranging from about 15 to 40 km. The surface manifestations usually occur during conditions of light winds and relatively clear skies.

While the absolute identification of the features in the spacecraft imagery as being due to internal waves had not been attempted until now, it has nevertheless been possible to synthesize a simple, consistent internal wave model that accounts for most of their major characteristics. They appear intermittently on the continental shelf at intervals which suggest their generation by semidiurnal and diurnal tides at the edge of the shelf (Halpern, 1971); they seem to be refractively controlled in phase speed and propagation direction by the mixed layer and water depths and the Brunt-Väisälä profile; and they largely disappear where the mixed layer comes to occupy a substantial fraction of the water column. Nonlinear, dispersive behavior is indicated by certain of their characteristics, including a sharp onset and the frequent appearance of the longest wavelengths at the front of the packet (Lee and Beardsley, 1974).

New York-to-Bermuda Remote Sensing Experiment (NYBERSEX)

A cruise was scheduled during June and July 1974 aboard the R/V Westward, a 30-m auxiliary staysail schooner selected in part for her quiet acoustic characteristics. The experiment was primarily intended to observe internal waves in the New York Bight coincident with three consecutive ERTS-1 overpasses of that region (12 June, 30 June, 18 July), during the early summer, a season when previous ERTS observations of the periodic surface features had been most frequent (Apel et al., 1975).

The ship was instrumented with a salinity-temperature-depth device (STD), expendable bathythermographs (XBT), a horizontally towed underwater hull containing temperature and depth sensors, an echo sounder (20-kHz, 2-ms pulse, $12^{o} \times 15^{o}$ beam) that viewed vertically downward to delineate internal wave motion at depth (Proni and Apel, 1975), and color and infrared films for photographing surface features.

Preliminary Results of the Experiment

Measurements were made during approximately 20 days of ship operation and 16 separate spacecraft overpasses. Because of weather, it was not possible to obtain one set of simultaneous observations involving all of the available instrumentation. Nevertheless, an ample quantity of cross-correlated data was gathered to enable us to assert unequivocally that the spacecraft imagery does indeed contain surface manifestations of internal waves.

Figs. 1(a) & (b) illustrate the geographical area under investigation on 17 July 1974; a portion of the photographically enhanced ERTS-1 negative image (numbered 1724-14475-6) taken in the near-infrared between 700 and 800 nm; and a line drawing interpretation of the periodic surface features. The ship's track is located in the lower left-hand corner of Fig. 1(a), with the circle denoting its position at the time of the satellite overpass--1447.5 GMT--and the triangle the location of a well-defined internal wave field encountered later on, at approximately 2115 GMT. Four packets are visible in the image,

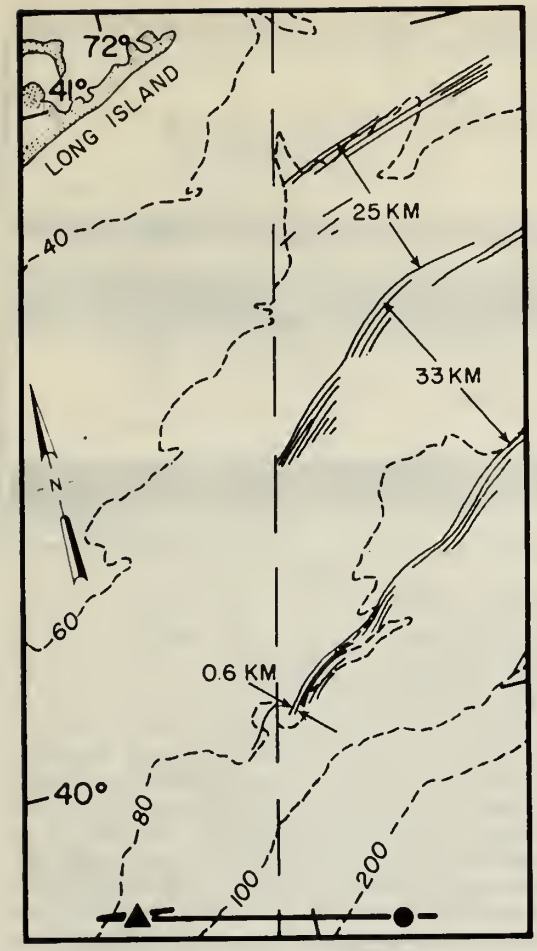

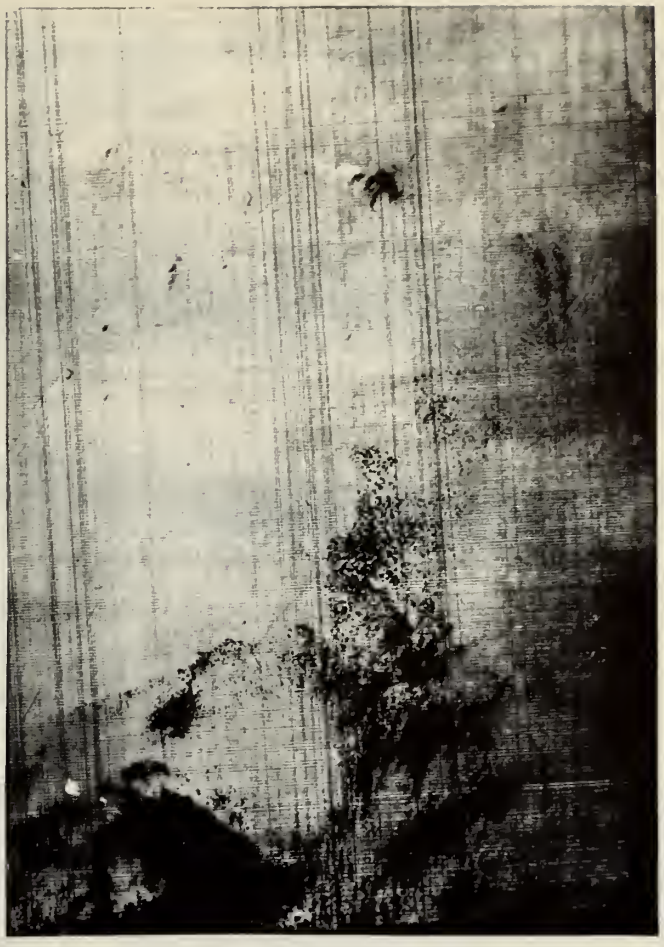

Figure 1(a) (Left). Line drawing showing internal wave packets south of Long Island (solid lines) overlain by isobaths in meters (dotted lines). Ship track at bottom shows position at time of ERTS-1 overpass (dot) and at encounter with internal wave packet (triangle). Vertical dashed line is western edge of spacecraft image. Figure 1(b) (Right). Section of negative image from ERTS showing internal wave field from which Figure 1(a) was derived. Dimensions 154 x 108 km^2. Black areas are clouds.

generally oriented along isobaths and separated by 24 to 33 km. They have wavelengths at the front of the packets ranging from approximately 400 to 1000 m and appear to be propagating shoreward, a view that is substantiated in part by the absence of packets seaward of the shelf break and in part by the observed doppler shifts discussed below.

No surface slicks were visible from the ship at the time of the overpass, nor are there any apparent at that point in the image. Nor would any waves be expected there, since the ship was beyond the edge of the shelf and hence outside of the boundary of the hypothesized generation region. However, at the position where the internal wave field was encountered (at the triangle), slicks were visible from the ship. Color photographs taken from the ship show that the slicks have the color of reflected skylight, in the low winds of 3 to 4 m/s; see Fig. 2.

Figure 3 illustrates temperature and acoustic data gathered during a maneuver involving course reversals that was executed through the region indicated by the triangle on Fig. 1. The upper trace shows the temperature at a depth of 29 m

Figure 2. Photo of internal wave slicks, taken from deck height (photo courtesy of R. L. Hughes).

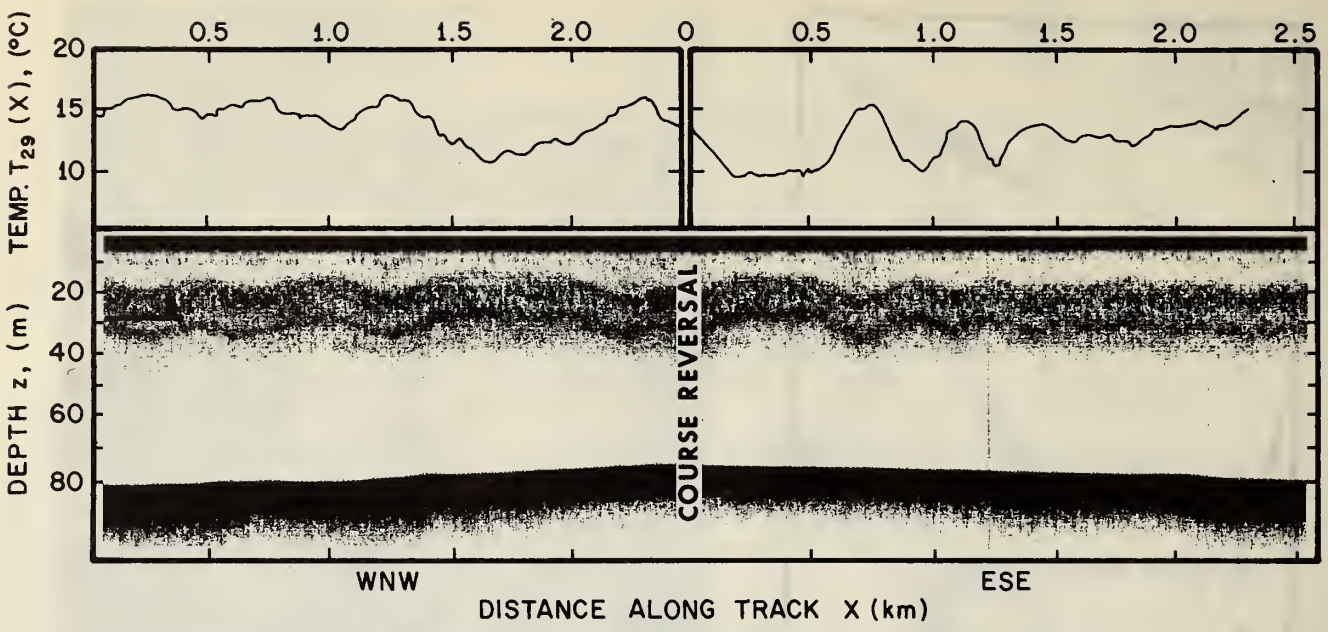

Figure 3 (upper). Temperature trace at 29 m depth taken near triangle on Figure 1; (lower). acoustic reflections from two scattering layers at 20 and 33 m depth, and from bottom at 80 m. Ship course was reversed midway through.

as obtained from the towed thermistor. The left half of the record was obtained during a 2.5-km segment of a west-northwest course, during which the internal wave packet of about 2 km total length was encountered; the right half shows the trace obtained during the reverse course. The left half shows down-shifted and the right half up-shifted oscillations. The maximum temperature excursions were of order 6°C. The lower record was obtained from the 20-kHz echo sounder and clearly shows two acoustic reflecting layers oscillating vertically with peak-to-trough amplitudes of approximately 15 m. The temperature and acoustic records are in very good correlation, with a 180° phase shift and with the troughs of the wave corresponding to downward-moving warm water from the mixed layer and the crests to upward-flowing cold water. An STD cast made approximately one-half hour before the onset of this wave packet showed a temperature profile which, if oscillated vertically by 15 m, would yield approximately the temperature excursions shown in the upper portion of Fig. 3.

This same graph can be used to derive the dominant wavelength, λ, period, T, and the projection of the internal wave phase velocity, $\vec{c}$, along the ship velocity, $\vec{u}$, by assuming negative and positive doppler shifts due to the ship motion on the reciprocal courses. From the down- and up-shifted wavelengths on that figure, one obtains approximately

$$\lambda \approx 500 \text{ m}, \quad T \approx 20 \text{ min}, \quad c \approx 0.35 \text{ m/s},$$

where a ship speed u = 1.5 m/s has been used. The phase and group speeds for a 500-m wavelength are about 0.5 m/s for λ = 500 m, as calculated from the observed density profile, for which $2\pi/N_{max} \tilde{=} 140$ s.

Returning to Fig. 1, the wave packet that is closest to the one shown on Fig. 3 has a wavelength of approximately 600 m and a packet length of about 3 km, values quite near to those observed from the ship. In addition, the isophase lines of the packet appear to be nearly parallel to the isobaths, and it is quite reasonable to assume that the isophase fronts of the wave group marked by "0.6 km" can be extended toward the southwest parallel to the bottom topography, out of the ERTS picture and to the region of ship observation. During the seven-hour time delay between satellite overpass and shipboard measurements, the waves would have propagated only about ten km toward the northwest and could thus be expected at about the location shown. Assuming constant phase and group speeds of 0.35 m/s, the wave packet would progress about 33 km shoreward in 25 hr. This is close to the spatial intervals observed on Fig. 1, which suggests once-daily generation.

Additional spacecraft and shipboard data show weakly developed internal wave striations on 12 June 1974, a calm, moderately clear day. However, on 13 June 1974 no evidence of slicks was visible either on the ERTS image or from the ship; this was a day of fresh, 7-8 m/s northeasterly winds, and slicks apparently do not form under such conditions.

Another experiment (a) established that the echo-sounder was indeed quantitatively observing internal waves; and (b) showed the location of the reflecting layers relative to small-scale temperature gradients. Figure 4(a) (left) shows two XBT traces obtained on 1 July 1974; one was taken at the crest and the other at the trough of an internal wave packet that was propagating past the ship while it was adrift. The packet was accompanied by a well-defined series of slicks. The temperature traces show the thermocline oscillating up and down with approximately a 20-min period by an amount $\eta(z)$ that depends on depth z; by differencing the two traces, one may obtain the displacement, which is shown on the right. The lowest order mode is clearly

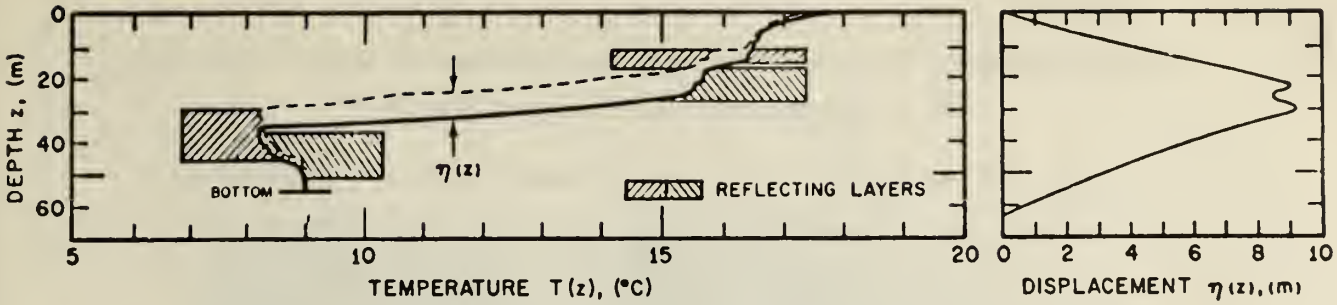

Figure 4 (Left). Temperature profile at internal wave trough (solid line) and crest (dotted line). Cross-hatching shows regions of intense acoustic reflections, as in Figure 3. (Right). Displacement of isotherms shows dominant first-order mode.

the dominant one, but higher order modes are also present. Coincident STD data demonstrate that the water column is statically stable, with the temperature inversion shown being offset by increased salinity in that region.

The coincident towed thermistor and echo-sounder records also yielded data on this internal wave field. These traces (not reproduced here) appear quite similar to those on Fig. 3. The acoustic record shows two reflecting laminae that undergo vertical excursions whose amplitudes and phases are in excellent agreement with those shown on the towed temperature and XBT records. The locations of these reflecting layers are indicated by the hatched regions of Fig. 4(a) and are clearly associated with depths where the macroscopic curvature of the temperature record, $\partial^2 T/\partial z^2$, is the largest. This is in accord with models of acoustic scattering from fluctuations in the index of refraction. Thus the experiment yields some evidence that, in addition to scattering from biological material--the mechanism that is usually invoked to explain such reflections--these signals may be partially returned from microstructure and turbulence in the water column.

Conclusions

The combined measurements of horizontal and vertical temperature variations, density structure, acoustic reflections, and spacecraft imagery have shown that the periodic features seen in ERTS images taken over the New York Bight are indeed surface slicks associated with oceanic internal waves; that such waves appear to be generated at the edge of this part of the continental shelf approximately once a day; that they propagate as intermittent high-frequency packets whose wavelengths, phase speeds, and periods are consistent with the vertical density profiles and depths for the area; and that they are detectable by high-frequency acoustic echo sounders. Thus the combination of spacecraft imagery, which yields synoptic scale data, and echo sounding, which provides amplitude information on a more restricted scale, appears to offer useful tools for investigations of higher-frequency internal waves on the continental shelves.

Acknowledgements. The authors are grateful to NASA for gathering open-ocean ERTS-1 data and to the officers, crew, and apprentices of the Westward for their help. This research was partially supported by funding from the Advanced Research Projects Agency, which assumes no responsibility for the content of this report.

References

Apel, J. R., H. M. Byrne, J. R. Proni, and R. L. Charnell, Observations of oceanic internal and surface waves from the Earth Resources Technology Satellite, J. Geophys. Res., 80, 865, 1975.

Halpern, D., Semidiurnal internal tides in Massachusetts Bay, J. Geophys. Res., 76, 6573, 1971.

Lee, C., and R. C. Beardsley, The generation of long nonlinear internal waves in a weakly stratified shear flow, J. Geophys. Res., 79, 453, 1974.

Proni, J. R., and J. R. Apel, On the use of high-frequency acoustics for the study of internal waves and microstructure, J. Geophys. Res. (to be published), 1975.

(Received November 11, 1974;
accepted March 14, 1975.)

Observations of Oceanic Internal and Surface Waves From the Earth Resources Technology Satellite

JOHN R. APEL, H. MICHAEL BYRNE, JOHN R. PRONI, AND ROBERT L. CHARNELL

Atlantic Oceanographic and Meteorological Laboratories, Environmental Research Laboratories, NOAA Miami, Florida 33149

Periodic features observed on the ocean surface from the Earth Resources Technology Satellite 1 have been interpreted as surface slicks due to internal wave packets. They appear to be generated at the edge of the continental shelf by semidiurnal and diurnal tidal actions and propagate shoreward. Nonlinear effects apparently distort the wave packets as they progress across the shelf. This observational technique constitutes a new tool for delineating two dimensions of the internal wave field under certain limited conditions.

Surface Observations

Visible manifestations of internal waves on the ocean surface may be due to at least two mechanisms, either of which modulates the short surface wave structure rather than causes any change in optical reflectivity or light absorption at depth. The first mechanism suggests that the high velocity of surface water arising from the large internal wave amplitude sweeps together surface oils and materials to form a slick in regions of surface water convergence, and thus the surface reflectivity is increased [*Ewing*, 1950; *Shand*, 1953]. The second mechanism predicts that capillary wave energy is focused in the convergence zones due to surface stress, and thus the small-scale roughness is enhanced and the surface reflectivity is decreased [*Gargett and Hughes*, 1972; *Thompson and West*, 1972]. In either case, quasi-periodic surface features will be produced under light wind conditions, and such effects are very often seen at sea.

Figure 1*a* is a photo taken from an aircraft in the Caribbean during Bomex in 1969 that shows a series of what almost certainly must be internal waves propagating from the left overlaid at nearly right angles by much shorter wind waves (R. B. Grossman, private communication, 1974). A ship wake crosses from left to right. The length of the internal waves is to a very rough approximation near 200 m. Figure 1*b* illustrates internal waves being generated by a tide rip and shows at least three distinct wave trains propagating at different angles [*Lafond*, 1962].

Periodic surface slicks may generally be seen from the air under conditions favorable for viewing oil on the sea, i.e., at low sun angles or in the sun glitter, when light or moderate winds prevail.

Generation Mechanisms

Internal waves can be generated by a wide variety of mechanisms. Wind stress that excites a spectrum of surface waves is one source [*Phillips*, 1966]. In this case, wave-wave scattering between two surface oscillations of wave vectors and frequencies κ_1, κ_2 and ω_1, ω_2, respectively, generates an internal wave whose parameters are set by the conservation rules $\kappa_3 = \kappa_1 - \kappa_2$ and $\omega_3 = \omega_1 - \omega_2$. The amplitude of the internal wave is partially determined by the surface wave amplitudes; the interference pattern decays exponentially with depth with a scale given by $1/|\kappa_3|$ and thus makes itself felt at levels where internal waves may propagate.

A second mechanism for generating internal waves is the scattering of barotropic tidal energy into internal baroclinic tides by bottom roughness or by the discontinuities presented by the edges of continental shelves or island arcs [*Rattray*, 1960; *Halpern*, 1971]. The relative importance of different topographies in transforming tidal motions into internal wave motions is unknown. This phenomenon is difficult to observe in nature; extant evidence suggests that up to ⅓ of the 3×10^{12} W energy dissipation required to account for the lengthening of the day may be ascribed to such scattering [*Hendershott*, 1973]. Thus island arcs, continental shelf edges, and shallow submarine sills become important regions in which to make observations of internal waves.

A third mechanism that can cause internal waves is shear flow instability [*Rattray*, 1960; *Phillips*, 1966]. In regions of the ocean having large baroclinic currents accompanied by horizontal stratification, small fluctuations in depth of a given stratum can grow to large amplitudes in an oscillatory way by mechanisms generally akin to the Kelvin-Helmholtz instability. An indication of the onset of this growth can be obtained by evaluating the gradient Richardson number *Ri*, where $Ri = N^2/(\partial u_0/\partial z)^2$. Here N is the Brunt-Väisälä frequency, and $\partial u_0/\partial z$ is the vertical shear in the horizontal baroclinic current speed $u_0(z)$, which may be due to a mean motion or a tidal current. The onset of the growth generally occurs when *Ri* approaches ¼ (or less). The oscillation amplitude is usually a maximum at some intermediate depth, i.e., is an unstable internal wave. This mechanism may be responsible for the generation of short-period internal waves from baroclinic internal tides of semidiurnal periods or in regions of western boundary currents.

Erts 1 Observations of Internal Waves

Periodic or quasi-periodic features in or on the ocean have been detected on many Erts 1, Skylab, and U.S. Air Force Dapp meteorological satellite images taken over both continental shelf and deep ocean areas; to date we have observed these features off the North American east and west coasts, the Gulf of California, the African east and west coasts, northern South America, the central Pacific, and the Celebes Sea. These features are almost certainly surface manifestations of internal waves that are made visible to the spacecraft by one of the mechanisms described above that serve to 'tag' the waves during winds which are well below whitecapping speeds.

The observations will first be presented, and then arguments will be made to support the internal wave interpretation.

Fig. 1*a*. Aircraft observations of internal waves during Bomex (1969) (latitude 9.5°N, longitude 59.5°W). Also shown are surface waves, a ship wake, and wind rows.

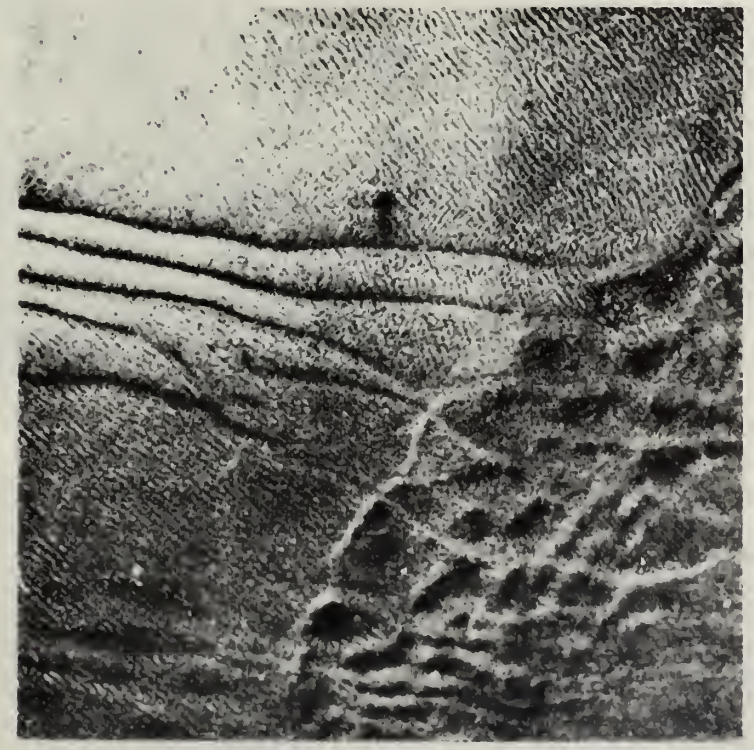

Fig. 1*b*. Additional aircraft photo of internal waves [*Shand*, 1953].

Surface effects on the continental shelves. Figure 2 is a standard Erts image taken with the Erts 1 multispectral scanner southeast of New York; it is printed as a positive image and shows Long Island at the top and New Jersey at the left. The scene dimensions are 184 × 184 km²; north lies approximately 102° counterclockwise from the horizontal edges. The scene was taken in orange-red light between 600- and 700-nm wavelength, at approximately 1007 LT on August 16, 1972. The large white objects in the center of the picture are high-altitude clouds; southeast of the mouth of the Hudson River two U-shaped acid-dumping events are visible; little else of oceanographic interest is apparent.

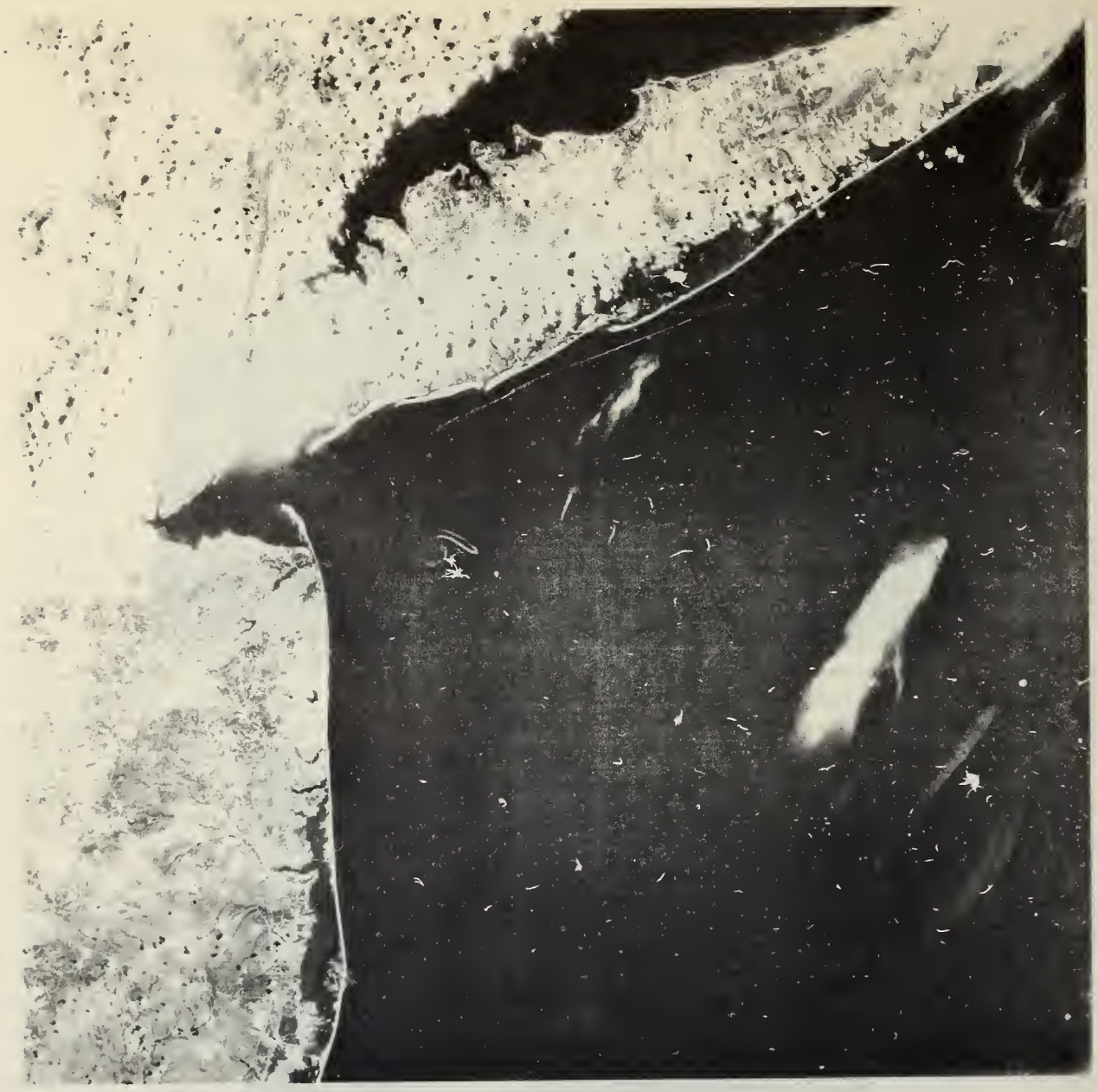

Fig. 2. Standard NASA Erts image. Area shown is the New York bight taken on August 16, 1972.

Figure 3 is a negative print of the same image, computer-enhanced through a process known as contrast stretching, with the land portions sacrificed in favor of ocean information. There is a wealth of data observable, including the Hudson River plume, acid and sewage sludge dumps, color discontinuities, and in the southeast corner, periodic surface slicks. (This figure is also geographically stretched by a factor of 1.4 : 1 in the east-west direction due to computer/photo recorder peculiarities.)

Figures 4, 5, and 6 are similar computer-enhanced images of the New York bight area taken on May 31, July 6, and July 24, 1973; each shows periodic striations in the southeast corner of somewhat similar characteristics. No such features were observed on scenes taken over the same area between August 1972 and May 1973.

Figure 7(*a*, *b*, *c*, and *d*) is a geographically corrected line drawing of the periodic features observed in the four scenes above superimposed over a bathymetric chart of the area. The general orientation of the lines with the local bathymetry and their concentration in the region of the Hudson Valley argues for strong interaction with the bottom topography. We shall return to this figure later.

The nature of these periodic features has recently been verified by direct measurement [*Apel et al.*, 1974], and a simple highly plausible model has been constructed whose predictions are in good quantitative agreement with the observations. It is suggested that the features are surface slicks overlying internal waves that have been generated by scattering of the barotropic tide into baroclinic modes at the edge of the continental shelf, which then propagate up on the shelf, to be absorbed and reflected when the wave breaks on the sloping bottom.

We first eliminate several other possible sources of the periodicities. (1) Atmospheric waves causing the depth of image modulation seen here do exist but would require much more atmospheric water content than is observed in the pictures; nor would atmospheric events reoccur in the same

Fig. 3. Figure 2 after computer enhancement via contrast stretching. Many oceanographic features are now visible including packets of internal waves separated by 12 to 15 km (lower right-hand corner).

geographical location over and over or be so well oriented with respect to the bottom topography. (2) Neither could the features be large surface gravity waves. The observed wavelengths are of the order of 400–1000 m; if these represented surface waves, their periods would be 16–25 s. Even if the slopes were as small as one in 30, the surface wave heights would be of the order of 7–15 m, and such a small rms slope could not account for the one-in-eight brightness change that the features represent on the image. On Figure 3, for example, the observed sea state was World Meteorological Organization code 1–2 with significant wave height, $H_{1/3} \simeq 0.5$ m. Therefore surface waves are eliminated as a possibility. (3) Finally, discussions with NASA Goddard Space Flight Center personnel (W. Hovis, private communication, 1972) have ruled out instrument artifacts as a source because of the somewhat irregular nature and orientation of the periodic variations.

The remaining possibility is that the features are the result of oceanic internal gravity waves. In light seas, such oscillations often have surface slicks associated with them whose origins may be as described above. The result of either mechanism is a periodic variation in surface roughness and hence in optical reflectivity that defines the internal wave field beneath. Such slicks are common at sea [*Shand*, 1953; *LaFond*, 1962].

To support further this hypothesis, refraction calculations have been performed by using published bottom topography and compared with the propagation patterns on Figure 3. A simple two-layer model [*Lamb*, 1932], together with topographic data and density profiles derived from bathythermographs for the area in question (obtained a day after the Erts 1 overflights), was used to compute the progression of a plane wave, originating in deep water, up on the continental shelf in the vicinity of the Hudson Canyon. The predicted phase speed (ω/κ) for conditions extant at the time of overflight is about 0.25 m/s. The wave train was assumed incident normal to the edge of the continental shelf. This is probably not a necessary assumption, since for wavelengths of the order of these, phase orientation due to refraction is so strong that by the time they have progressed to the area of the image, the wave fronts would be rendered nearly parallel to contours of local topography.

Figure 7*a* also shows the results of this calculation by way of a comparison between the observed wave packets and an arbitrarily spaced set of phase fronts (dashed lines) as computed

Fig. 4. The New York bight, May 31, 1973. Note the weak development of an internal wave field in the lower right-hand corner and the large number of ships and ship wakes visible.

from the two-layer dispersion relation. Both theory and observation show the wave fronts advancing more rapidly in the deep water over the Hudson Valley than on the adjacent continental shelf. The overall agreement is quite good.

Thus all the evidence indicates that the periodic features in these Erts 1 photos are internal waves that are being detected by their associated surface slicks. These waves have most likely been generated by tidal action at the shelf edge and are being refracted as they move up onto the shelf.

One pair of Erts 1 images has afforded a possible determina-

Fig. 5. The New York bight, July 6, 1973. Note the more pronounced internal waves compared with those in Figure 4.

tion of both the propagation speed, via time delay measurements, and the generation interval between the internal wave packets. Figure 8 was taken on July 23, 1973, exactly 24 hours before and approximately 110 km to the east of Figure 6. These two images have a good deal of overlap in coverage, allowing observation of the same geographical area. Visible are two sets of packets in the lower center left of Figure 8, separated by 29 to 34 km. Figure 9 is a line drawing showing the packets on Figures 6 and 8. These packets could be standing lee waves created by the bottom topography but more likely are propagating groups of waves. When it is assumed that the packets are propagating, it is possible to arrive at an advance of about 30–33 km for a given packet during 24 hours (solid to dashed). Note as well the aforementioned spatial interval between packets observed on a given day, also about 30 km on both days (solid to solid or dashed to dashed). This near-equality of the between-packet intervals with the distance of advance argues for daily or near-daily generation and implies a phase speed of about 0.35 m/s, which is what one would expect from a 50-m-deep mixed layer with a density contrast $\Delta\rho/\rho \simeq 10^{-3}$ in the depth of water in this region.

Figure 10 shows how the wavelengths on Figure 9 vary with front-to-back position in the packets, as is taken at two separate sectors in the easternmost group on that image. There is clearly a strong tendency observed here and in most other satellite images for a given packet to have longer wavelengths at its front than at its rear. This is probably due to a combination of a nonlinear finite amplitude effect with the dispersive character of the waves, as was recently discussed by *Lee and Beardsley* [1974]. A detailed study of these types of features should yield considerable insight into the physics controlling large amplitude internal wave propagation.

Figure 11, which was made on November 28, 1972, off southwest Africa just north of Cape Town, shows six packets of surface signatures apparently radiating from a small source at the center left. The area visible is about 180 by 250 km. On Figure 12 a line drawing of the packets superimposed on bottom topography is shown, with the depth given in meters. If the interpretation of these signatures as propagating tidally excited internal wave groups is accepted, then the image shows evidence that internal waves may have lifetimes on the shelf of several days. (Density data for this time and place have not yet been obtained, and so no refraction calculations have been made.) Also shown in Figure 11 are the intervals between packets, ranging from 41 to 20 km as shore is approached, as well as the lengths of the leading waves, which increase from 1.6 to 3.5 km as shoal water is reached. The dependence of the

Fig. 6. The New York bight, July 24, 1973. Note the well-developed internal wave fields. In this picture there is a ship wake longer than 40 km.

packet separations and length of leading wavelength as a function of distance and water depth is shown in Figure 13. This curious behavior, wherein the overall packet suffers retardation as the depth decreases while the leading edge portion is apparently accelerated, may be an anomaly, or it may be a highly significant dynamic effect. More study and additional data are obviously required.

A summary of the important characteristics of the surface slick patterns in continental shelf regions follows:

1. The waves occur in groups, or packets, separated by distances that are of the order of either 15 or 30 km, which, together with the calculated phase velocities, suggest a semidiurnal or diurnal tidal origin.

2. They are nearly always oriented parallel to the local bottom contours, as is expected of shallow water waves.

3. None have yet been found in Erts images during the winter or spring in the areas investigated to date.

4. A repeated concentration of energy occurs in the Hudson Valley in the vicinity of 60- to 80- m depth, probably owing to generation and focusing of waves by the headlands near the Hudson Canyon at the edge of the shelf.

5. The wavelengths fall between 300 and 4000 m and have

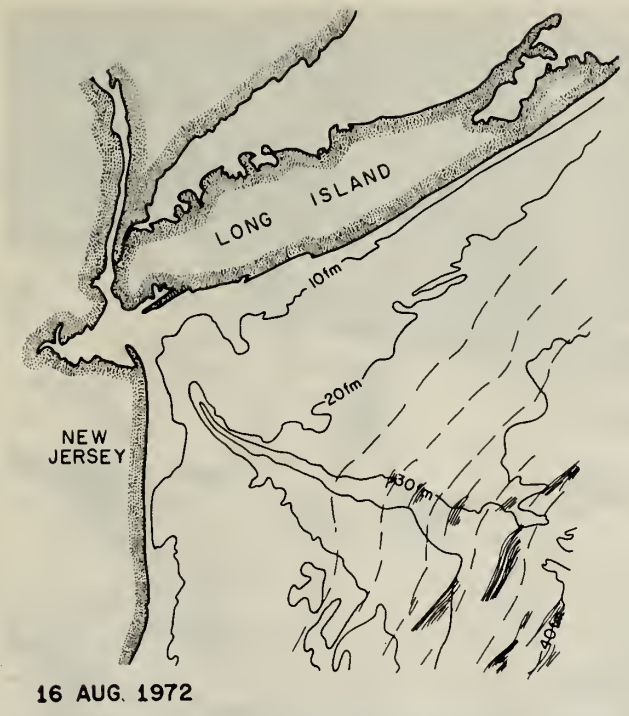

Fig. 7a.

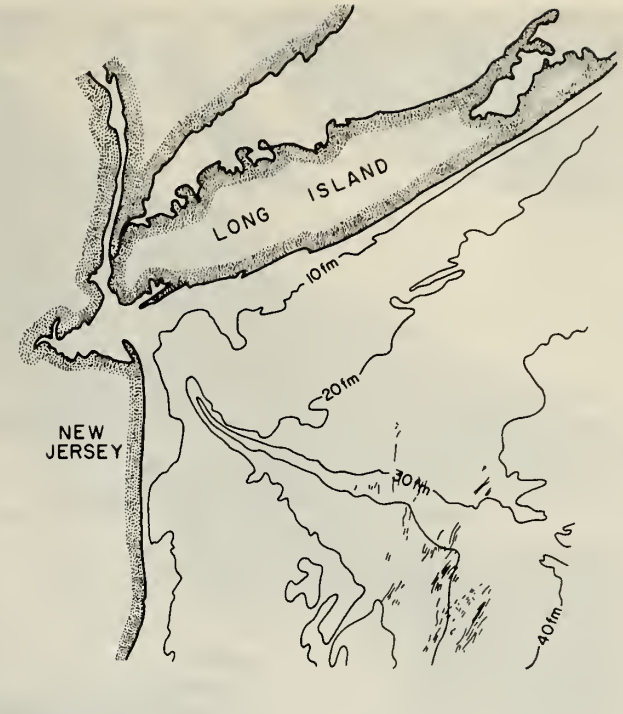

Fig. 7b.

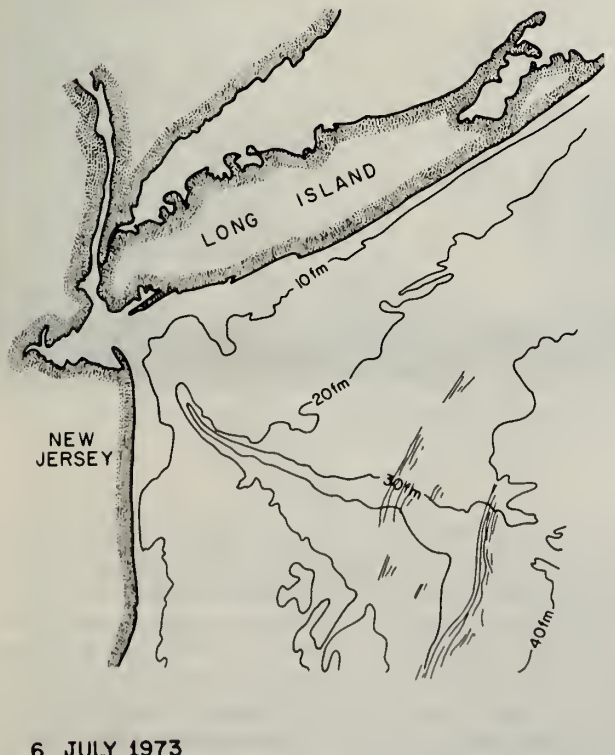

Fig. 7c.

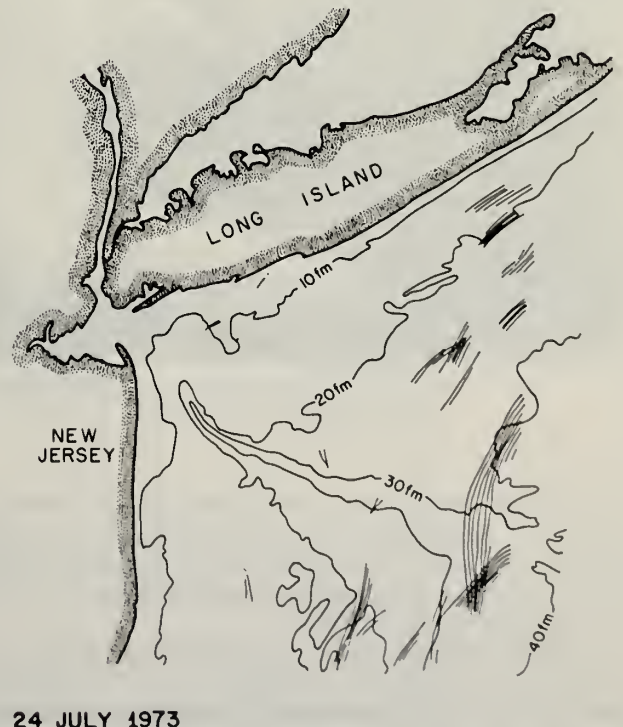

Fig. 7d.

Fig. 7. Geographically corrected line drawing of the internal wave fields observed in Figures 3, 4, 5, and 6 superimposed on the bottom topography. The dashed lines on (*a*) show isophase contours as calculated from a simple internal wave model

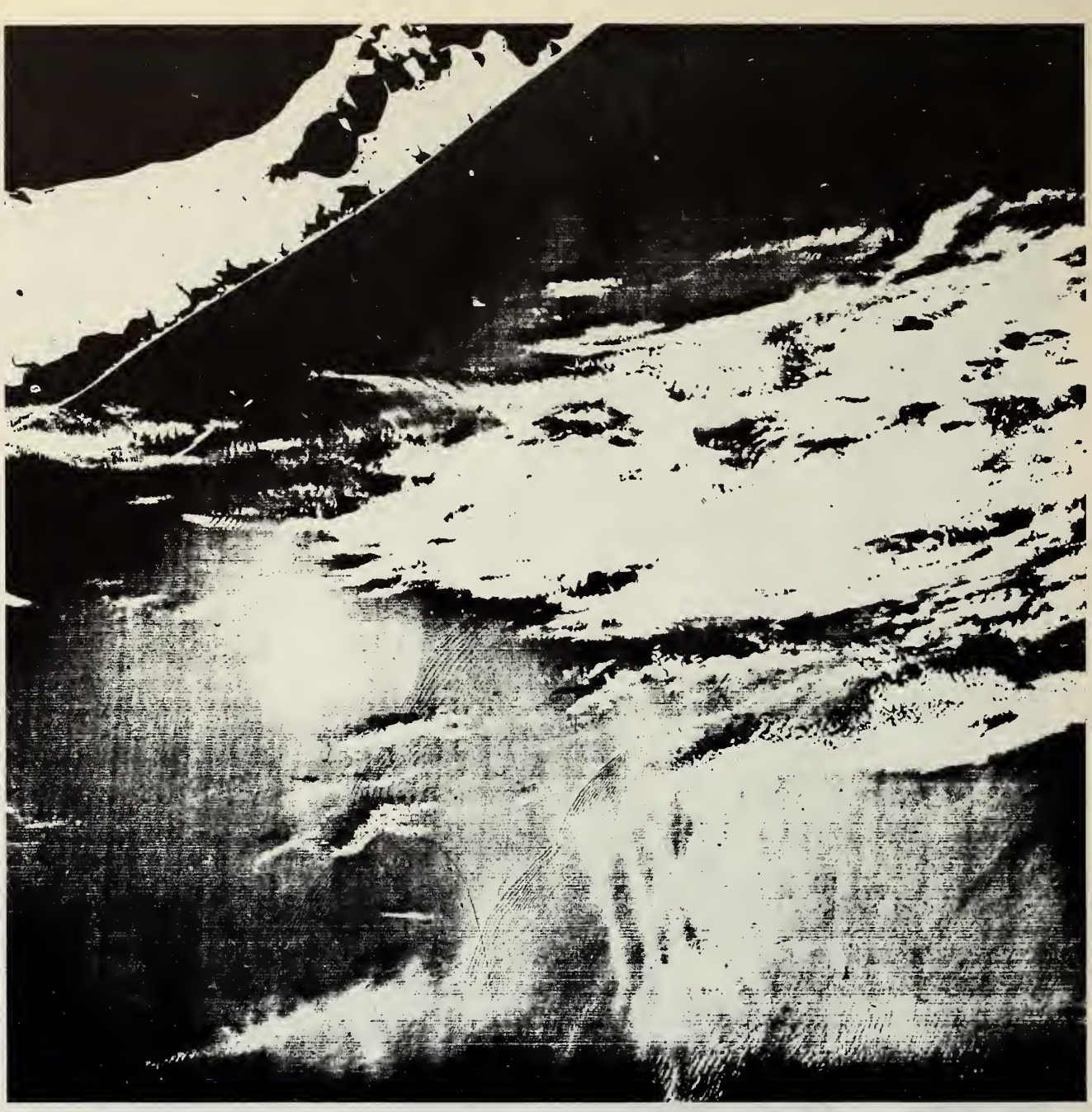

Fig. 8. Eastern Long Island area, July 23, 1973 (photographically enhanced), 24 hours prior to and 110 km to the east of the area shown in Figure 6. Note packets separated by about 30 km in lower left center.

phase speeds near 0.25 m/s, with a longer distance between crests and a greater extent of the packet occurring on the inshore side and shorter wavelengths and smaller packet extent on the offshore side; the reasons for some of these characteristics are not yet clear.

6. There is some evidence of a continued lengthening of the distance between crests, especially in the front of the packets, as the group progresses up on the shelf; an accounting for this may be had by a combination of finite amplitude and dispersive effects.

Surface effects observed in deep water. The data shown thus far have been taken on or near continental shelves, in water depths less than about 500 m. Very limited numbers of Erts 1 images have been taken over deep water in the open ocean, of which two scenes are shown in Figures 14 and 15. Figure 14 illustrates a photographically enhanced image of a portion of the deep Indian Ocean taken on December 4, 1972; equatorial east Africa is visible on the left. The continental shelf in this part of Africa extends only a few tens of kilometers off the coast. Quasi-periodic structures are apparent in the cloud-free center portion of the scene having a scale of 2–4 km and relatively little coherence. In the lower right there is a definite change in the orientation of the structure. These features lie approximately in the southward-flowing Somali current; the image was taken at a time of year when the current in the region usually undergoes sharp spatial and temporal

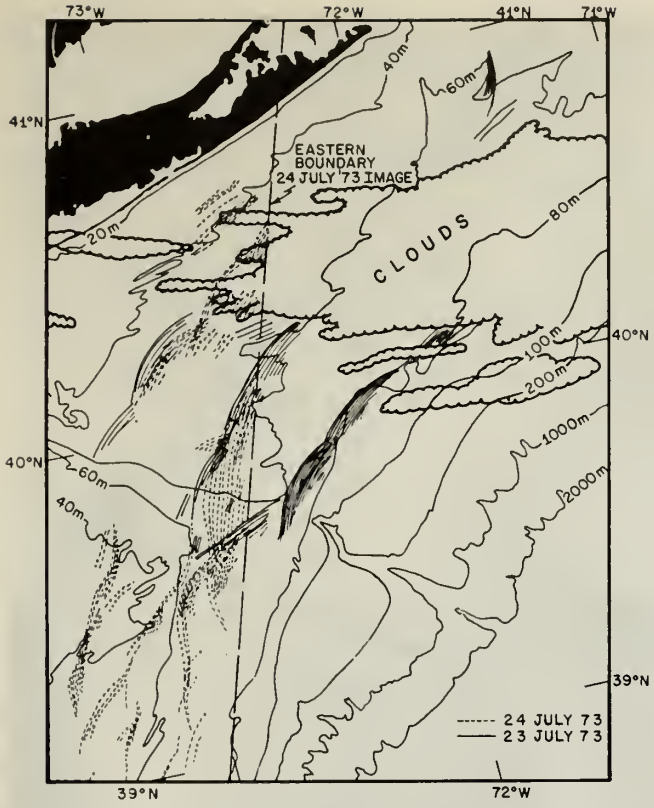

Fig. 9. Geographically corrected line drawing showing wave packets from Figures 6 and 8.

variations due to the shifting monsoon. It is thought that the structure in question may be a surface signature of deep water internal waves; however, no sea truth is available for this area, and so such an interpretation must remain speculative.

Another ocean scene is shown on Figures 15 and 16. These Erts 1 data were taken in the North Pacific at about 40°N, 160°W in September 1973. Figure 15 has dimensions of 92 × 184 km² and is a computer-enhanced negative print showing cumulus clouds in the south and a peculiar surface mottling in the north having a scale of a few kilometers. In this latter region, a microscopic examination shows an expanse of surface waves approximately 200 m in length propagating toward the southeast away from a low pressure cell several hundred kilometers away, having wind speeds of 10 to 15 m/s.

A more detailed look at a 13 × 18 km sector of this region is shown on Figure 16*a*, which clearly illustrates two trains of surface gravity waves of nearly equal wavelength intersecting at approximately 15°, as well as the mottling mentioned above; the latter is seen to be very roughly periodic with an average 'wavelength' of about 2.5 km and approximately a north-south orientation. Figure 16*b* is the logarithm of the two-dimensional Fourier transform of Figure 16*a* and shows the spatial frequency components of the mottling near the origin and those of the surface waves as two concentrations of energy separated by about 15° at nearly equal wave numbers. Under the suspicion that the origin of the mottling might be found either in (1) surface wave interference effects or (2) in the kind of internal wave generation process arising from wave-wave scattering that was discussed earlier, we have applied the wave vector conservation rule $\kappa_1 - \kappa_2 = \kappa_3$ to the scene. The magnitude of κ_3 agrees with that of κ_{mott}, the wave vector of the mottling, to within 10%; its angle, which is nearly at 90° to the mean value of κ_1 and κ_2, agrees to within 20°. Such agreement does not prove that either of the above processes suggested are at work, of course, but such interpretations are at least consistent with the data. Obviously, further controlled experiments are required.

The surface stress hypothesis might explain the visibility of internal waves on the surface of a moderately rough ocean having a wind blowing over it [*Gargett and Hughes*, 1972]. The horizontal surface currents associated with internal waves are large, being of the same order as the phase velocity of the waves themselves; they are oriented approximately either parallel or antiparallel to the direction of propagation and have opposite directions in parts of the wave separated in phase by $(2n - 1)\pi$. A wind field superimposed on the currents will excite a capillary/ultragravity wave spectrum that is steeper where the wind opposes the internal wave current than where it is parallel to it. This periodic variation in the slope spectrum would lead to periodic variations in the optical reflectivity that might serve to delineate the internal wave in the deep sea to high-altitude sensors, much as surface slicks serve to do in continental shelf waters. The difference in the two cases is that the slick cannot maintain its integrity at wind

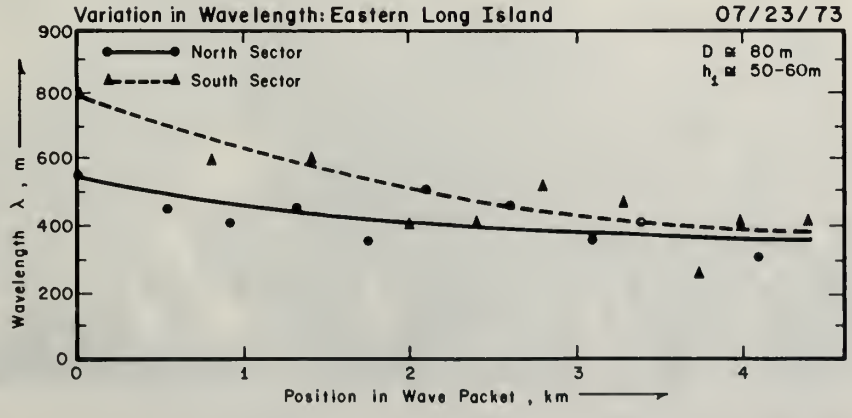

Fig. 10. Variation in internal wavelength as a function of distance from the front of the upper and lower packets seen on Figure 8.

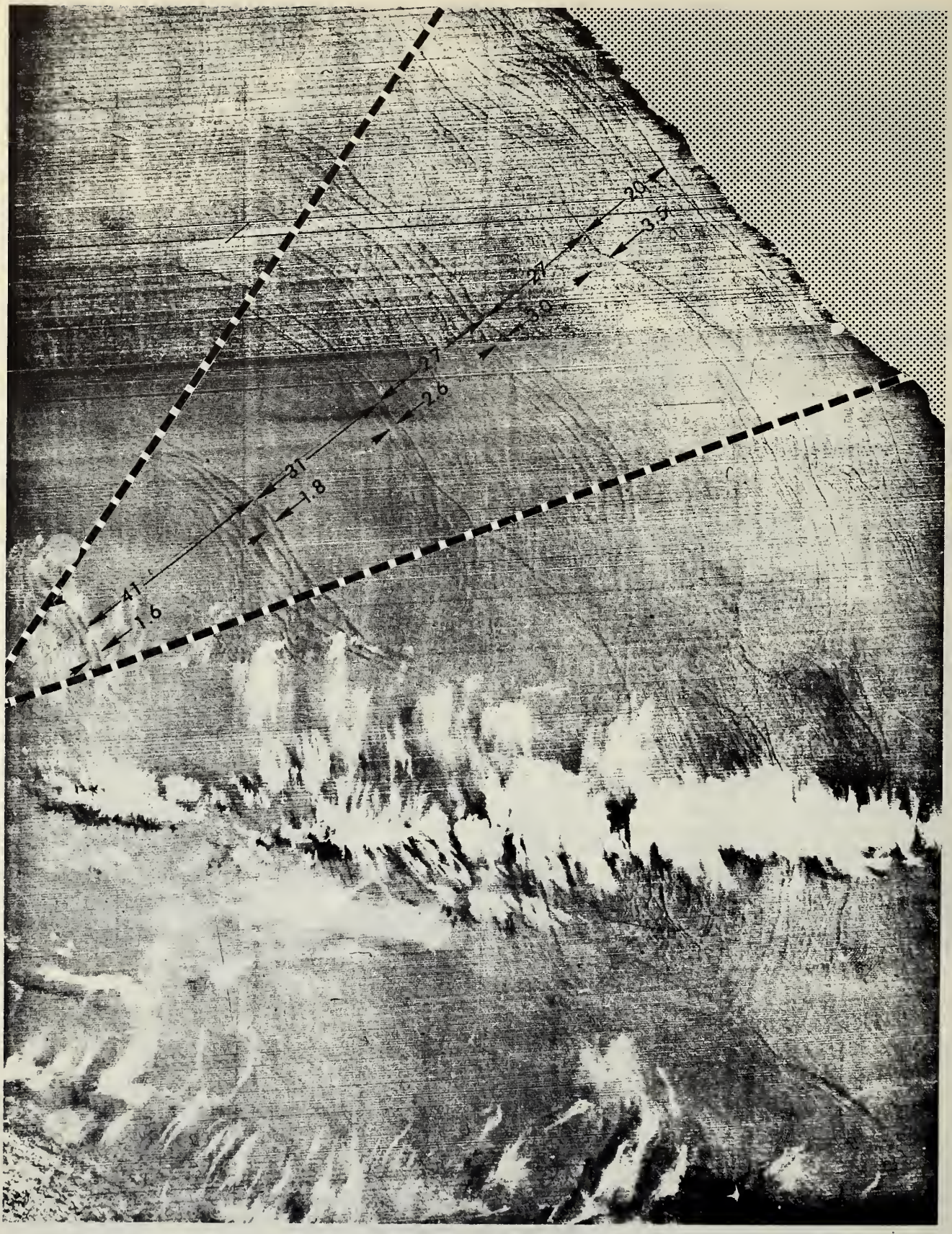

Fig. 11. Enhanced Erts photo made on November 28, 1972, off southwest Africa just north of Cape Town, showing six packets of surface slicks apparently radiating from a small source at the center left. This photo suggests internal waves may have lifetimes on the shelf of several days.

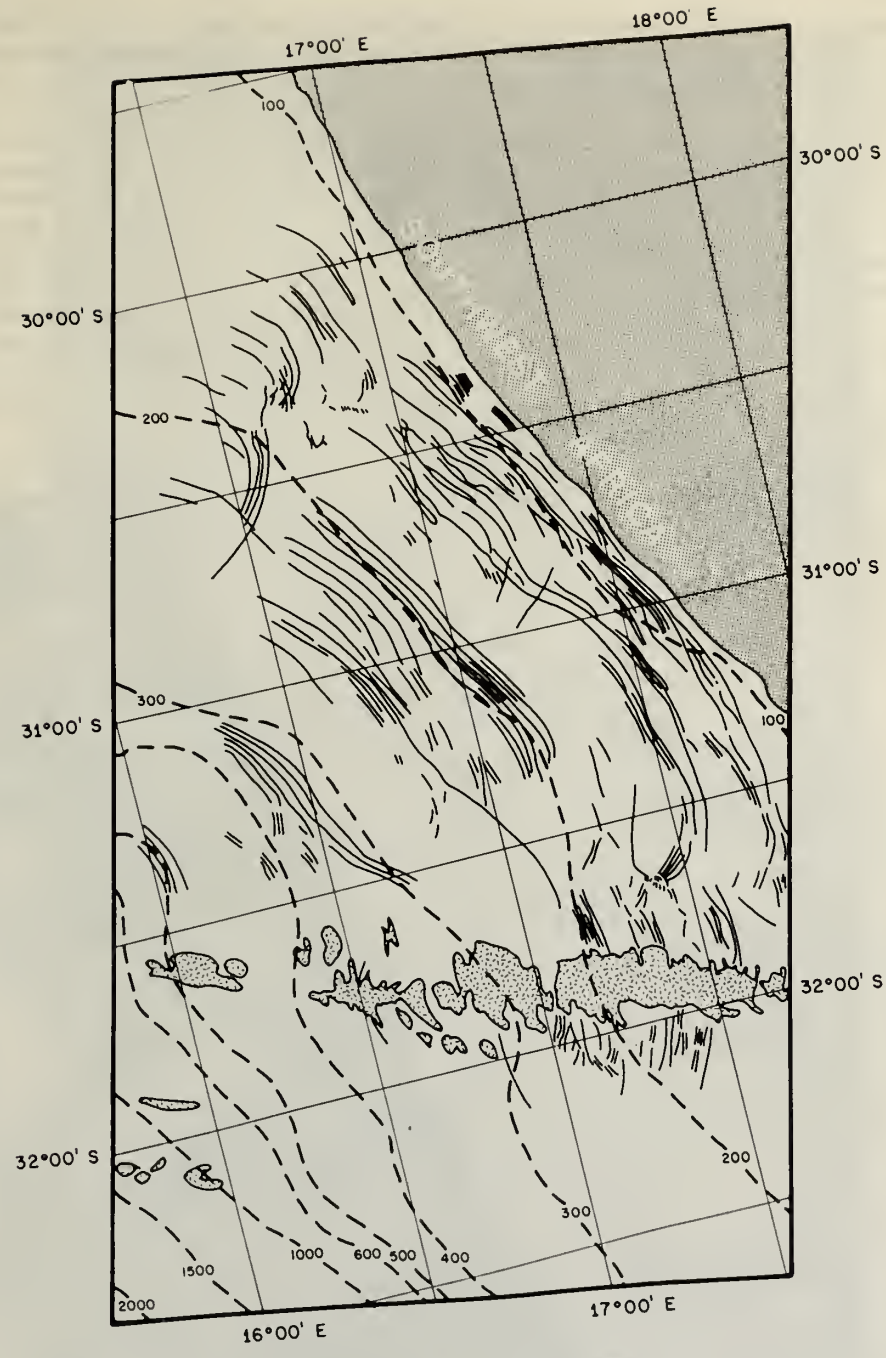

Fig. 12. Line drawing of packets of Figure 11 together with bottom topography.

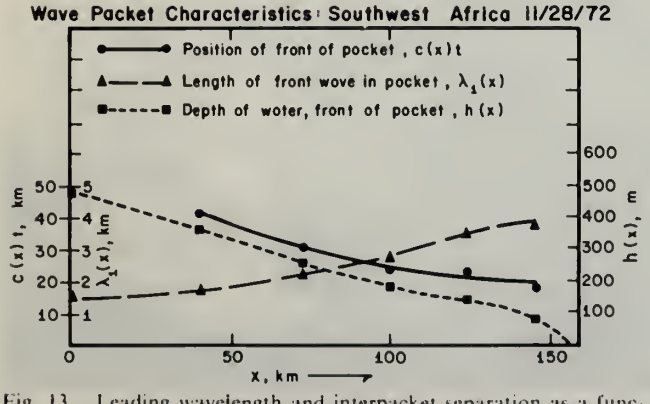

Fig. 13. Leading wavelength and interpacket separation as a function of distance; from Figures 11 and 12.

velocities above whitecapping speeds, whereas the above mechanism may.

Surface effects in the Florida current. Figure 17 is presented as a final example of possible internal waves observed from Erts 1. This is a contrast-stretched negative image of the Florida current made on August 18, 1972, with Miami located near the upper portion of the photograph. At the bottom center near the mean axis of the current is a group of periodic striations oriented roughly northwest-southeast and extending approximately 30 km along the direction of mean flow. The distance between stripes is about 800 m. It is thought that these are surface signs of internal waves excited by and propagating along the Florida current. Periodic surface slicks in this general region are common at sea, and acoustic echo-sounding from ships has indicated that internal waves often underlie

such slicks [*Proni and Apel,* 1975]. The mechanism for their generation is quite possibly a shear flow instability. On the westward side of the current in the region of cyclonic horizontal velocity shear the vertical velocity and density gradients are sometimes such that the Richardson number for the flow approaches ¼. *Düing*'s [1973] data give values for *Ri* that indicate incipient instabilities may occur. Once again, the theoretical conditions that indicate the existence of a mechanism for generating internal waves have to be verified by simultaneous field and satellite measurements.

SUMMARY AND CONCLUSIONS

Convincing proof of the assertions that (1) the periodicities observed on Erts 1 images are surface slicks and (2) the slicks tag internal waves under conditions of light winds has been obtained by the authors in a recent cruise between New York and Bermuda. The data are only partially analyzed and will be published in the near future [*Apel et al.,* 1974].

The limitations of the satellite technique appear to be as follows: light wind and clear sky conditions must prevail, high-frequency internal waves on the shelf are most visible, and coverage is limited by satellite dynamics and sensor characteristics. No amplitude information is currently derivable from the spacecraft images. However, as the accompanying paper shows [*Proni and Apel,* 1975], this missing dimension to the internal wave field may be partially obtained via acoustic echo sounding, so that a more nearly complete picture of the three-dimensional field may be obtained.

Fig. 14. Photographically enhanced Erts image of a portion of the deep Indian Ocean off equatorial east Africa taken on December 4, 1972.

Fig. 15. Enhanced Erts image (negative) taken over the North Pacific at 40°N, 160°W in September 1973. Image dimensions are 92 × 184 km². Note the peculiar surface mottling and surface wave field.

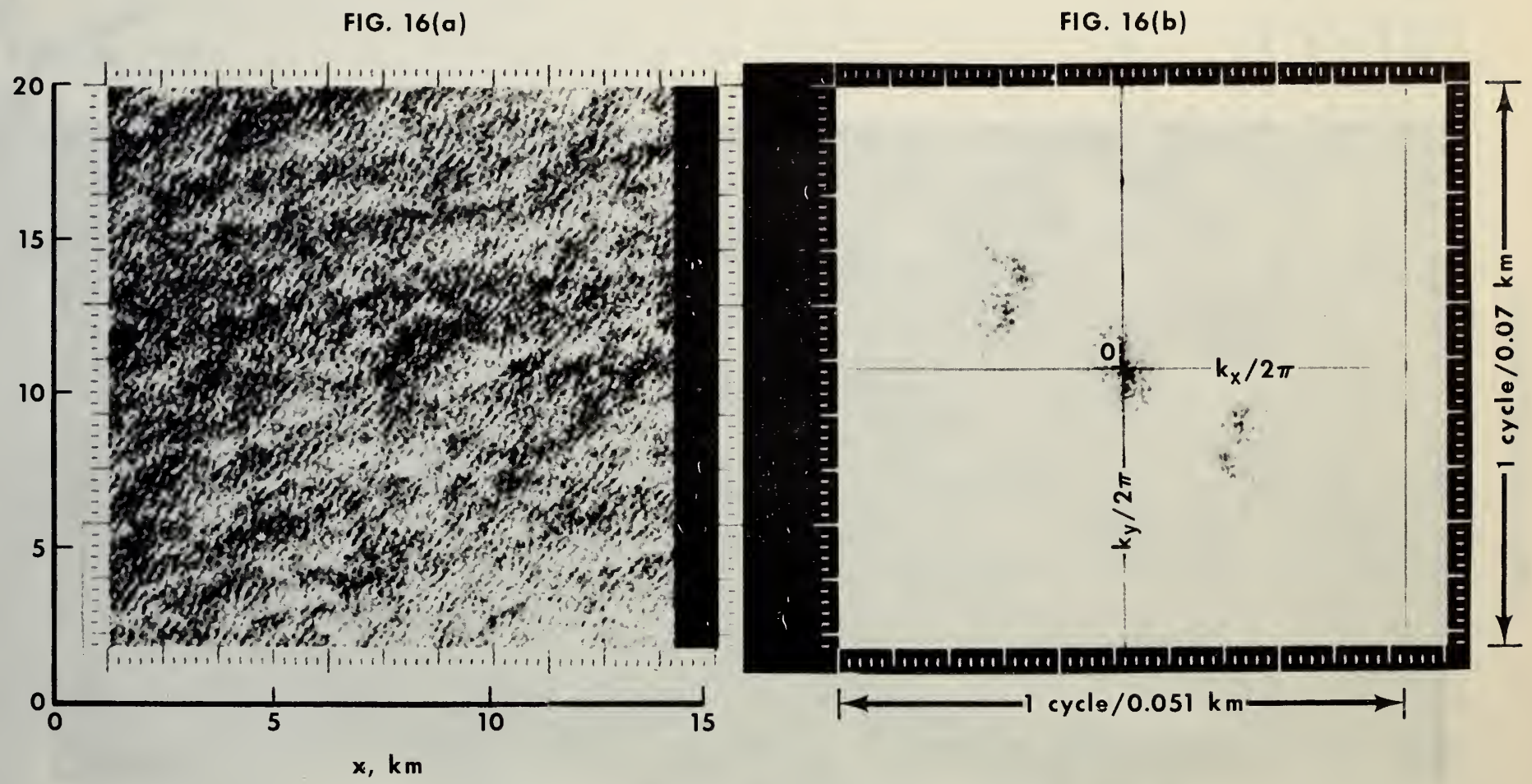

Fig. 16. (*a*) Detail of an 18 × 13 km² sector of Figure 15. Clearly visible are two surface wave trains as well as the peculiar mottling mentioned in the text. (*b*) Logarithm of the two-dimensional Fourier transform of (*a*). This figure shows the frequency components of the mottling (near the origin) and those of the surface waves (as two concentrations of energy separated by about 15° at nearly equal wave numbers).

Fig. 17. Contrast stretched negative Erts image of the Florida current made on August 18, 1972. Note the periodic striations present at the bottom center of the image.

Acknowledgment. This project was partially supported by funds from the Advanced Research Projects Agency, which assumes no responsibility for the correctness of the results.

REFERENCES

Apel, J. R., J. R. Proni, H. M. Byrne, and R. L. Sellers, Near-simultaneous observations of intermittent internal waves from ship and spacecraft, submitted to *Geophys. Res. Lett.*, 1974.

Düing, W., Observations and first results from Project Synop 71, *Sci. Rep. UM-RSMAS 73010,* Univ. of Miami, Miami, Fla., 1973.

Ewing, G., Slicks, surface films and internal waves, *J. Mar. Res., 9,* 161, 1950.

Gargett, A. E., and B. A. Hughes, On the interaction of surface and internal waves, *J. Fluid Mech., 52,* 179–191, 1972.

Halpern, D., Semidiurnal internal tides in Massachusetts Bay, *J. Geophys. Res., 76,* 6573–6584, 1971.

Hendershott, M., Ocean tides, *Eos Trans. AGU, 54,* 76–86, 1973.

Lafond, E. C., Internal waves, in *The Sea,* vol. 1, edited by M. N. Hill, pp. 731–763, Interscience, New York, 1962.

Lamb, H., *Hydrodynamics,* p. 370, Cambridge University Press, London, 1932.

Lee, C., and R. C. Beardsley, The generation of long nonlinear internal waves in a weakly stratified shear flow, *J. Geophys. Res., 79*(3), 453–462, 1974.

Phillips, O. M., *The Dynamics of the Upper Ocean,* pp. 161–197, Cambridge University Press, London, 1966.

Proni, J. R., and J. R. Apel, On the use of high-frequency acoustics for the study of internal waves and microstructure, *J. Geophys. Res., 80,* in press, 1975.

Rattray, M., On the coastal generation of internal tides, *Tellus, 12,* 54–62, 1960.

Shand, J. A., Internal waves in the Georgia Strait, *Eos. Trans. AGU, 34,* 849–856, 1953.

Thomson, A. J., and B. J. West, Interaction of non-saturated surface gravity waves with internal waves, *Tech. Rep. RADC-TR-72-280,* Phys. Dyn. Inc., Berkeley, Calif., (ARPA order 1649), October 1972.

(Received July 24, 1974;
accepted November 6, 1974.)

☆ GPO: 1978—796-417/116-10